Laminate Blending Demonstrator

A buckling experimental campaign of a physical laminate blending demonstrator

M. Gomaa

Delft University of Technology

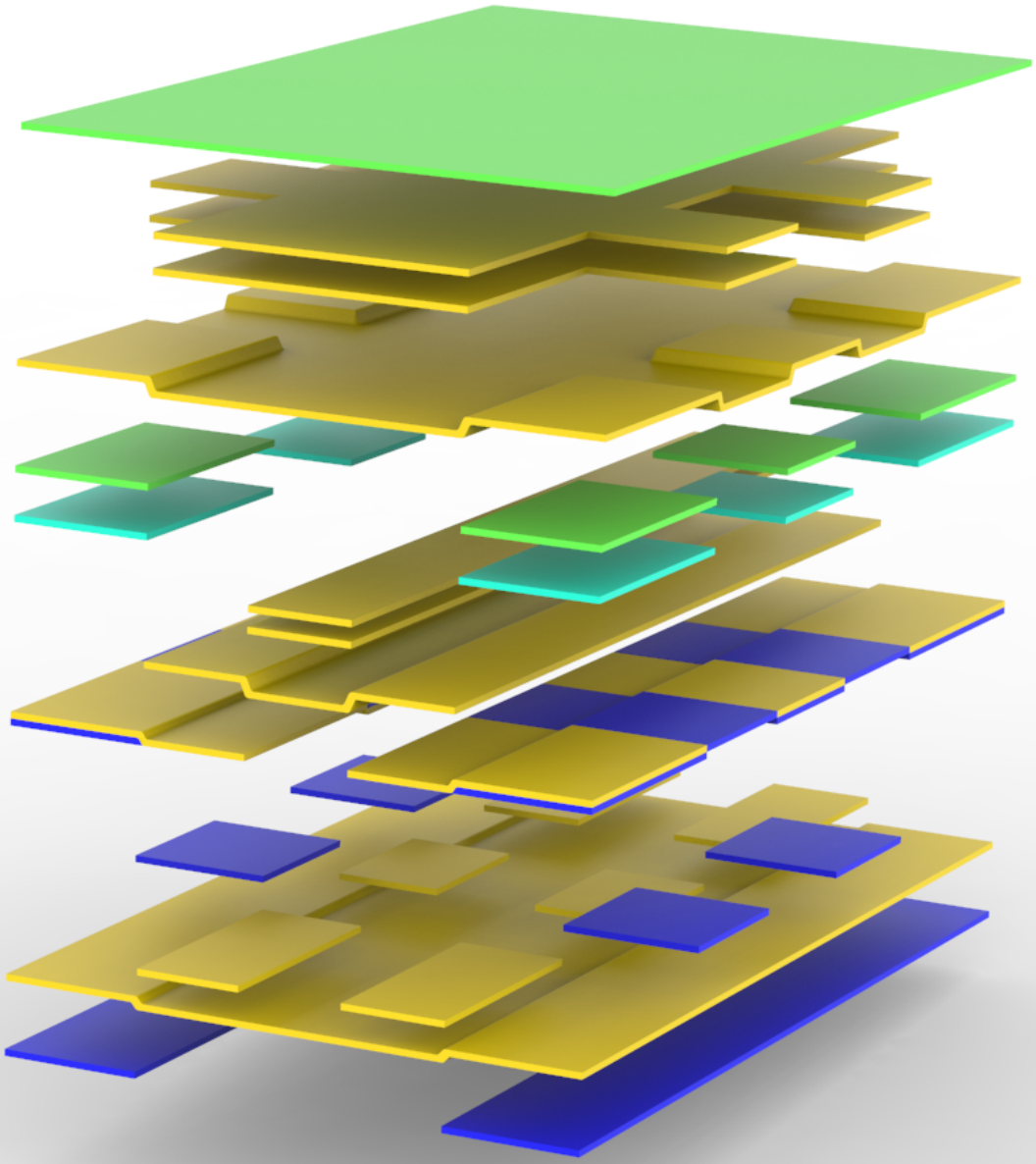

TU Delft Delft University of Technology

Laminate Blending Demonstrator

A buckling experimental campaign of a physical laminate blending demonstrator

by

M. Gomaa

to obtain the degree of Master of Science in Aerospace Engineering
at the Delft University of Technology,
to be defended publicly on Friday, August 23, 2019 at 10:00 AM.

Student number: 4363744
Project duration: December, 2018 – August, 2019
Thesis supervisor: Dr. ir. J.M.J.F. van Campen, TU Delft, Lecturer

TU Delft Delft University of Technology

Delft University of Technology
Faculty of Aerospace Engineering
Department of Aerospace Structures and Materials

GRADUATION COMMITTEE

Dated: August 23, 2019

Chair holder:

Prof. Dr. C. Kassapoglou

Committee members:

Dr. ir. J.M.J.F. van Campen

Prof. C.A. Dransfeld

Dr. B. Chen

Acknowledgments

Writing these acknowledgments hurts, as it means my time in Delft is reaching an end. This beautiful journey officially started in August 2014. I will forever be grateful to everything this city had to offer me. I am very thankful to my supervisor Dr. ir. J.M.J.F. van Campen for his constant support and guidance throughout the time I spent working on this thesis. His feedback was a key factor to the completion of the work presented here. In addition to that, our cooperation was always very pleasant and efficient. I would also like to thank my assessment committee members, Prof. Dr. C. Kassapoglou, Prof. C.A. Dransfeld, and Dr. B. Chen for taking the time to review my work and give me feedback. I would also like to thank all the technicians in the Delft Aerospace Structures and Materials Laboratory (DASML) who helped me achieve the promising results of this work. Also, how can I forget Weronika Dziarnowska, thank you for all the hours, stress and sweat you put in helping me build these laminates.

Delft did not just give me knowledge and life lessons, but it also gave me two extra brothers, Nicolas Gartland and Ayoub Malkoui, thank you guys for all the good times.

I will always be indebted to my mum and dad for their unquantifiable love and support, without which I would not be where I am today. I am also grateful to my aunt Z. Helmy and her Husband M. Elbady for all the positive influence they had on my life growing up. I am very thankful to my cousins, Omar, Yousef, Ali, and Adam, you know very well what you mean to me. I am also thankful to have my brothers, Alhussein and Yassin, and my sister Maryam. This thesis is for all of you.

Finally and most importantly, I would like to thank Mr. W. Coutry, a very close family friend and a source of inspiration who supported me by all means throughout my career. Thank you for all the good times and conversations.

M. Gomaa
Delft, August 2019

Abstract

The use of fiber-reinforced composites in the aerospace industry has increased over the past couple of decades because of their high specific properties and the tailoring capability they offer. Furthermore, composite laminates -both curved and flat- are important structural elements in this industry. They are used to make wing skin panels, fuselage shells, floor panels, etc. The composite materials used to build these laminates offer engineers the possibility to optimize the stacking sequence to satisfy the stiffness and strength requirements. However, engineers are currently limited to a set of fiber orientation angles of which they choose the laminate stacking sequence. Such a conventional design would have a constant stiffness and does not utilize the full potential of fiber-reinforced composites. An innovative approach would be to segment the laminate into smaller sections and optimize the stacking sequence of each section depending on the local stiffness and strength requirements. However, the result of following such an approach would be a theoretical optimum laminate with severe incompatibilities between its sections. This lack of continuity between the different segments in the laminate would have a negative consequence on its structural integrity because of the stress concentrations they generate. This highlights the importance of laminate blending, which is a term given to the process of locally optimizing a laminate while enforcing continuity rules between the sections, and therefore also manufacturability and structural integrity.

The laminate blending problem suffers from a very large design space, especially when the number of sections in a laminate increases. This causes the computational cost of the optimization problem to increase exponentially. To solve this issue, researchers have been working on developing more efficient blending strategies and definitions. Very recently, a Genetic Algorithm (GA) and a Cellular Automaton (CA) based blending method was proposed at the Delft University of Technology by Van den Oord. The novel method offers a blending solution for laminate with a large number of sections while implementing a blending definition which allows for the maximum utility of the design space.

The objective of this thesis is to validate the theoretical findings of Van den Oord by actually designing and building a blended laminate demonstrator using their proposed blending algorithm, and then testing it in an experimental campaign. The manufactured demonstrator is the first-ever discrete variable stiffness laminate to be manufactured and satisfies the relaxed generalized blending definition. It will also serve as a new benchmark for the laminate blending problem.

The blended demonstrator was optimized for its critical buckling load under a uniaxial loading scenario. In addition to that, a conventional constant stiffness laminate was also designed and manufactured to be used as a reference during the experimental campaign. The local optima of the blended laminate were obtained using the lamination parameters (LP) based GA optimizer of Van Campen. Then, the blended configuration was achieved using the CA blending algorithm of Van den Oord and a manual global patch interpretation step to ensure manufacturability. The modification steps performed on the local optima to achieve a blended configuration have a knock-down effect on the laminate's buckling performance. Therefore, finite element (FE) models of both laminate types were constructed and used to predict their buckling performance. A total of three blended laminates and two conventional laminates were manufactured and tested. The experimental results of the blended demonstrator in terms of stiffness and buckling load were then compared to the results of the conventional reference. The experimental results of both laminates were also compared to the predictions of the FE models constructed.

Contents

Nomenclature

Abbreviations

CA	Cellular Automaton
CS	Constant Stiffness
AFP	Automated Fiber Placement
AR	Aspect Ratio
BL	Blended Laminate
CL	Conventional Laminate
CLT	Classical Laminate Theory
DASML	Delft Aerospace Structures and Materials Laboratory
DIC	Digital Image Correlation
FE	Finite Element
GA	Genetic Algorithm
LP	Lamination Parameters
LVDT	Linear Variable Differential Transformer
UD	Uni-directional
VS	Variable Stiffness

Latin symbols

a	Laminate length
A_{ij}	Components of the in-plane stiffness matrix
b	Laminate width
B_{ij}	Components of the bending extension coupling stiffness matrix
C	Size of the design problem
D_{ij}	Components of the bending stiffness matrix
E	Longitudinal modulus
h	Total laminate thickness
G	Shear modulus
g_{min}	Buckling constraint
L	Number of plies
m	Number of half waves in the longitudinal direction of the laminate
m_a	Slope of algorithm
m_b	Slope of baseline
n	Number of half waves in the transverse direction of the laminate
n	Number of sections
N_o	Critical buckling load per unit length
N_x	Longitudinal compressive force
N_y	Transverse compressive force
Q_{ij}	Components of the reduced lamina stiffness matrix
T	Computational time
t_{ply}	Ply thickness
U_i	Material invariant
V_i^A	In-plane lamination parameters
V_i^B	Coupling lamination parameters
V_i^D	Flexural lamination parameters
W	Weight
z	Through-the-thickness coordinate

Greek symbols

β	Penalty parameter for fitness function
Γ	Material invariant matrices used to define the stiffness matrices
γ	Shear strain
ε	In-plane strain
ε	Bonus parameter for fitness function
θ	Fiber orientation angle
θ	Fitness value
κ	Curvature
λ	Parameter used to satisfy boundary conditions
ν	Poisson's ratio
σ	In-plane normal stress
τ	In-plane shear stress

1

Introduction

The structural weight of an aircraft is one of the main factors that affect its operational costs. A heavier aircraft must generate more lift to maintain a steady-state flight. Furthermore, the drag experienced by an aircraft is a function of its lift [1]. This means that increasing the structural weight of an aircraft also increases the drag vector acting on it, which requires the aircraft to generate more thrust to compensate for this increased resistance. More thrust translates to higher fuel consumption and consequently more expensive operations. A lighter aircraft can therefore carry the same payload for longer distances, or can carry a heavier payload for the same range, or even carry the same payload across the same range for a reduced cost.

As part of the efforts to reduce the structural weight of aircraft, the industry is witnessing a transition from all-metal to all-composite aircraft. This transition was motivated by the advantages of fiber-reinforced composites in terms of their strength-to-weight ratio and stiffness-to-weight ratio. In addition to that, these materials are anisotropic and thus, they offer designers the ability to tailor their mechanical properties to satisfy the stiffness and strength requirements. For instance, an engineer can build a laminate by stacking up different layers of that material at different orientations and different stacking sequences to achieve the optimum design for the given loading scenario. However, all these advantages are offset by the increased complexity in their design, manufacturing, and maintenance processes. In the following paragraphs, one of the design challenges of fiber-reinforced composites is introduced. In addition to that, the objective of the work conducted in this thesis is presented.

A conservative approach to design a composite laminate that is subjected to a varying load would be to optimize its stacking sequence for the highest load acting on it. However, this results in an over-designed structure that does not fully utilize the tailoring capability of composite materials. An alternative strategy would involve dividing the laminate into sections and then optimize the stacking sequence of each one according to the local stiffness and strength requirements. The main issue with this method is that incompatibilities between the sections are inevitable. These incompatibilities do not only affect the possibility to manufacture the laminate but also cause stress concentrations along the section boundaries, which significantly reduce its structural integrity. This is why this optimization problem must take the continuity constrains and design rules into account to ensure manufacturability and structural integrity. This combinatory optimization problem is most commonly referred to as laminate blending. Another way to look at the blending problem is to imagine the two extreme results of a multi-sectional laminate optimization problem. The first is that of minimum weight, where the stacking sequence of every section was optimized to meet the local stiffness and strength requirements. The second is that of a laminate where the stacking sequence is completely dictated by the most critical section. Between these two extremes, there exists a design solution weighing close to the minimum weight but still possess sufficient continuity characteristics.

Over the years, researchers have been developing new blending strategies. The latest of which is a cellular automaton (CA) based blending algorithm proposed by Van den Oord [2]. This algorithm can blend a multi-sectional laminate with a large number of sections while satisfying the relaxed general-

ized blending definition introduced by Van Campen *et al.* [3]. This definition states that a laminate is considered blended and therefore manufacturable if the transitions between its sections are free of any butted edges. Van den Oord [2] also compared the results of their proposed method with the results of the stat-of-the-art blending methods using the current horseshoe pattern benchmark. The 18 panel horseshoe benchmark is a completely theoretical benchmark that has been used by researchers to compare the effectivity of their blending algorithm. However, that benchmark was limited in its number of sections, and the loads per section were pre-defined. Therefore, it does not take into account the load redistribution that results from altering any of the sections.

The objective of this research is to validate the theoretical findings of Van den Oord [2] by designing a blended laminate demonstrator using their proposed method and testing it in an experimental campaign. The problem definition used to design the blended demonstrator should then serve as the new benchmark for the laminate blending problem.

1.1. Reader's guide

This thesis report is structured into three main parts. The first part, namely literature survey covers the background of laminate blending and its definitions which are described in chapter 2. In the same part, but in chapter 3, the innovative blending method proposed by Van den Oord [2] is described and compared to the other state-of-the-art blending methods. The first part of the report is concluded by chapter 4, where the objective and hypotheses of this research are discussed, and the research questions that had to be answered are presented.

In the second part of the report is called thesis work. As the name suggests, this is where the core work of the thesis is described. Firstly, the problem definition and methodologies followed during the experimental campaign are elaborated upon in chapter 5. Secondly, the laminate design results are presented in chapter 6. Subsequently, the laminates manufacturing process is described in chapter 7. The results of the experimental campaign are presented and discussed in chapter 8. Finally, the conclusions and the recommendations of the conducted research can be found in chapter 9.

The final part of this report is a compilation of appendices that provide insight into some of the complementary work done during this research.

I

Literature survey

2

Background

Fiber-reinforced composite materials are known for their high stiffness-to-weight and strength-to-weight ratios, especially when compared to most metals. This and the fact the most aerospace structures are thin shells meant that fiber-reinforced laminates are highly applicable in the industry. Furthermore, these materials are anisotropic which means that their mechanical properties are very directional. This directionality gives the designer more freedom to tailor the mechanical properties of the laminate. However, it also means that fiber-reinforced composites require different and more complex design and analysis methods. The complexity is further amplified when the composite structure at hand is subjected to a varying load case.

In this chapter, background information on composite laminates and their design and analysis are reviewed. Firstly fiber-reinforced composite laminates are discussed in section 2.1. The classical laminate theory is explained in section 2.2. In addition to that, the lamination parameters (LP) are briefly explained in section 2.3. Finally, laminate blending and the different blending definitions are presented and explained in section 2.4.

2.1. Fiber-reinforced composite laminates

Composite laminates are made up of multiple plies that are sequentially stacked on top of each other in different orientations to achieve final desired properties. Each composite ply (also called a lamina) is a fiber-reinforced polymeric composite material. The reinforcement fibers are usually unidirectional (all fibers are in one direction), or in a woven form embedded in a resin system [4]. The resin system which can be a thermoset or a thermoplastic also hold the lamina together to form the final laminate. A schematic representation of a composite laminate can be seen in Figure 2.1 as depicted by Kassapoglou [4]. The x-y axes resemble the laminate global coordinate system, and the 1-2 axes resemble the local ply coordinate system. The 1-axis is always parallel to the direction of the fibers.

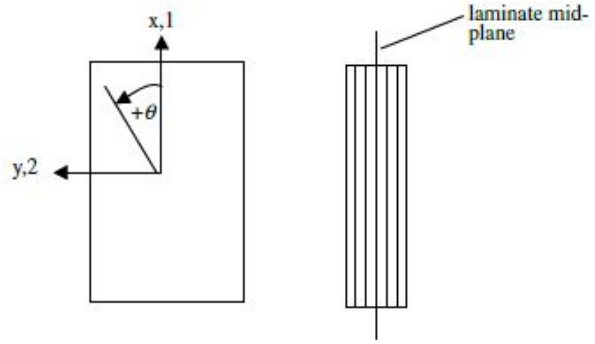

Figure 2.1: Laminate axes and the positive θ orientation [4]

2.1.1. Laminate notation and types

The layup of a composite laminate is usually descried in literature by the following notation:

$$[\theta_1/\theta_2/\theta_3...]$$

Where $\theta_i,\ i = 1, 2, 3...$ are the fiber orientation angles of the plies in a laminate starting from the top outermost ply of the laminate. Furthermore, there are several types of laminates that are commonly used in practice, and their importance is highlighted later in the chapter after the mechanical properties of composite laminates are discussed. These laminate types are [4]:

- Symmetric
  A symmetric laminate will have a symmetric stacking sequence with respect to its mid-plane in terms of materials thickness and fiber orientation angle.
- Balanced
  A balanced laminate will have a $-\theta$ ply for every $+\theta$ ply in its stacking sequence.
- Cross-ply
  A cross-ply laminate will only have plies of fiber orientations $0°$ and $90°$.
- Quasi-isotropic
  A quasi-isotropic laminate will have the same stiffness in any of its in-plane directions.

2.1.2. Conventional composite laminates

Unlike most metals which are isotropic, composite laminates are physically anisotropic, and thus their mechanical properties are very dependent on the loading direction. Every ply in a composite laminate is orthotropic, which means that it has different mechanical properties along three mutually orthogonal axes [4]. This gives laminated composites an advantage over their metal counterparts, as designers are not only limited to changing the shape and the size of the desired structure but also manipulate the properties of the material. This is commonly known as tailoring of composite materials. In general, the optimization problem of a composite laminate has three main design variables, which are the number of plies in the laminate, the orientation of each ply with respect to a fixed global laminate reference system and the through-thickness order of the different plies. Traditionally, each ply in a laminate is assigned a specific fiber orientation angle, which yields a constant stiffness laminate. These fiber orientation angles are also limited to the following conventional set:

$$\{0°, \pm 45°, 90°\}$$

The thickness of each ply is also usually predetermined by the manufacturers. Such composite layups are also called conventional laminates, and up to this day, they make up the majority of the laminates used in the aerospace industry. This is because they are easier to certify, and their gained trust in the industry because of the availability of validated test data.

2.1.3. Non-conventional composite laminates

With conventional laminates, the design possibilities are very limited and therefore the full potential of tailoring composite materials is not utilized. Nowadays, both the composite optimization and manufacturing techniques have advanced so much to allow for non-conventional solutions that utilize a bigger portion of the very large design space composites have to offer. Tailoring non-conventional laminates can be achieved by doing one or a combination of the following:

1. Relaxing the set of fiber orientation angles per ply
   This means that the fiber orientation angles are not restricted to any specific set but still remains constant per ply. Laminates with this feature can be called a ”constant stiffness non-conventional laminate”.
2. Fiber steering
   In this approach, the fiber orientation angle per ply is spatially varying, and therefore the stiffness properties are continuously changing throughout the laminate. Such laminates are commonly known as ”variable stiffness non-conventional laminates”. The effectiveness of stiffness tailoring using fiber steering was demonstrated by Jegley *et al.* [5].

3. Laminate blending
   Another approach is to divide the laminate into smaller sections, and then optimize the stacking sequence of each one individually. However, this has a negative impact on the integrity of the structure as the continuity constraints across the laminate are violated. The problem of locally optimizing each section while satisfying the continuity constraints, or to restore continuity after the local optimization process is known as laminate blending [6]. The stiffness of blended laminates varies discretely from one section to the other, and therefore they are also called "variable stiffness non-conventional laminates". Since laminate blending is the main topic of this literature survey, it is discussed in more details in section 2.4.

2.2. The classical laminate theory

This section sheds some light on the Classical Laminate Theory (CLT), which is an analytical method used to describe the external loads acting on a composite laminate in terms of its deformations. The CLT assumes that a laminate consists of a number of orthotropic plies perfectly bonded together by a non-deformable bond line of negligible thickness [4]. The theory also adapts the Kirchhoff–Love plate theory assumption for laminates under bending, which states that plane sections remain plane and perpendicular to the neutral axis during deformation [4]. Furthermore, the theory considers that a laminate is homogeneous with smeared properties of its fiber-matrix mixture [4]. All the aforementioned assumptions are used to derive an expression for the in-plane stresses in the k^{th} ply of a laminate in terms of its mid-plane strains and curvature, this is given by Equation 2.1. In this formulation z is the through-thickness location of the k^{th} ply as shown in Figure 2.3, and $\overline{Q}_k$ is its transformed stiffness matrix which is a function of the fiber orientation angle θ and the material invariants U_i as demonstrated by Equation 2.2 [7].

$$\begin{Bmatrix} \sigma_x \\ \sigma_y \\ \tau_{xy} \end{Bmatrix}_k = \begin{bmatrix} \overline{Q}_{11} & \overline{Q}_{12} & \overline{Q}_{16} \\ \overline{Q}_{21} & \overline{Q}_{22} & \overline{Q}_{26} \\ \overline{Q}_{61} & \overline{Q}_{62} & \overline{Q}_{66} \end{bmatrix}_k \begin{Bmatrix} \varepsilon_{x0} + z\kappa_x \\ \varepsilon_{y0} + z\kappa_{xy} \\ \gamma_{xy0} + z\kappa_{xy} \end{Bmatrix} \quad \text{where} \quad z_{k-1} < z < z_k \tag{2.1}$$

$$\begin{aligned} \overline{Q}_{11} &= U_1 + U_2 \cos 2\theta + U_3 \cos 4\theta & \overline{Q}_{12} &= U_4 - U_3 \cos 4\theta \\ \overline{Q}_{22} &= U_1 - U_2 \cos 2\theta + U_3 \cos 4\theta & \overline{Q}_{66} &= U_5 - U_3 \cos 4\theta \\ \overline{Q}_{16} &= \frac{1}{2} U_2 \sin 2\theta + U_3 \sin 4\theta & \overline{Q}_{26} &= \frac{1}{2} U_2 \sin 2\theta - U_3 \sin 4\theta \end{aligned} \tag{2.2}$$

Since the transformed stiffness matrix is dependent on the fiber orientation angle and material properties, the stress distribution along the cross-section of a laminate with plies of different fiber orientation angles will not be constant, nor will it vary linearly. The stresses will vary in a discrete manner across the boundaries between plies of different fiber orientation angles. The force and moment resultants acting on a laminate due to the internal stresses are visualized in Figure 2.2, and are computed using Equation 2.3. In these relations, the stresses are integrated along the thickness of the laminate while assuming constant stresses only along the thickness of a single ply.

$$\begin{aligned} N_x &= \int_{-\frac{h}{2}}^{\frac{h}{2}} \sigma_x dz & N_y &= \int_{-\frac{h}{2}}^{\frac{h}{2}} \sigma_y dz & N_{xy} &= \int_{-\frac{h}{2}}^{\frac{h}{2}} \tau_{xy} dz \\ M_x &= \int_{-\frac{h}{2}}^{\frac{h}{2}} \sigma_x z dz & M_y &= \int_{-\frac{h}{2}}^{\frac{h}{2}} \sigma_y z dz & M_{xy} &= \int_{-\frac{h}{2}}^{\frac{h}{2}} \tau_{xy} z dz \end{aligned} \tag{2.3}$$

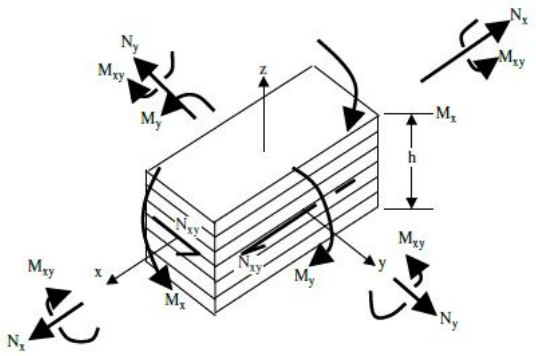

Figure 2.2: Forces and moments acting on a laminate [4].

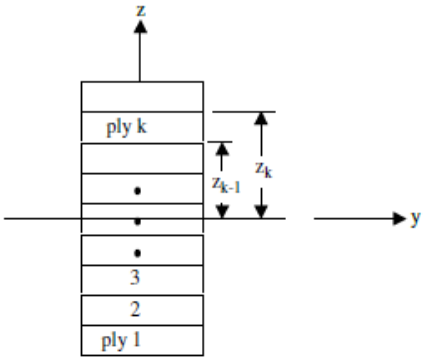

Figure 2.3: Ply numbering system [4].

The stresses in each ply of the laminate given by Equation 2.1 are then substituted in Equation 2.3 to obtain the general constitutive relations of the laminate, which are also known as the ABD-matrix, and are shown by Equation 2.4 [4]. The individual terms of the ABD-matrix are computed using Equation 2.5.

$$\begin{Bmatrix} N_x \\ N_y \\ N_{xy} \\ M_x \\ M_y \\ M_{xy} \end{Bmatrix} = \begin{bmatrix} A_{11} & A_{12} & A_{16} & B_{11} & B_{12} & B_{16} \\ A_{12} & A_{22} & A_{26} & B_{12} & B_{22} & B_{26} \\ A_{16} & A_{26} & A_{66} & B_{16} & B_{26} & B_{66} \\ B_{11} & B_{12} & B_{16} & D_{11} & D_{12} & D_{16} \\ B_{12} & B_{22} & B_{26} & D_{12} & D_{22} & D_{26} \\ B_{16} & B_{26} & B_{66} & D_{16} & D_{26} & D_{66} \end{bmatrix} \begin{Bmatrix} \varepsilon_{x0} \\ \varepsilon_{y0} \\ \gamma_{xy0} \\ \kappa_x \\ \kappa_y \\ \kappa_{xy} \end{Bmatrix} \tag{2.4}$$

$$A_{ij} = \sum_{k=1}^{n} \overline{Q}_{ij} (z_k - z_{k-1}) \qquad B_{ij} = \sum_{k=1}^{n} \frac{\overline{Q}_{ij}}{2} \left(z_k^2 - z_{k-1}^2\right) \qquad D_{ij} = \sum_{k=1}^{n} \frac{\overline{Q}_{ij}}{3} \left(z_k^3 - z_{k-1}^3\right) \tag{2.5}$$

The first entry of the ABD-matrix is the A-matrix, which is the extension-stiffness matrix, and couples the in-plane strains of the laminate with its resultant in-plane forces. However, it is independent of the laminate's stacking sequence and is simply computed by summing the transformed stiffness matrices of all plies weighted by their thicknesses. The B-matrix is bending-extension coupling matrix of the laminate and links the curvature of the laminate with its in-plane forces, and the in-plane strains of the laminate with the moment resultants. The D-matrix is the bending-stiffness matrix, and couples the curvature of the laminate with its moment resultants. Unlike the A-matrix, the B-matrix and the D-matrix are dependent on the stacking sequence of the laminate.

2.3. Lamination parameters

The lamination parameters were first introduced by Tsai and Pagano [8] and Tsai and Hahn [9] to compactly describe the stiffness properties of a laminate in terms of 12 continuous variables as shown in Equation 2.6. Where the $V_i^{A,B,D}$, $i = 1...4$ are the lamination parameters, and $\bar{z}$ is the normalized through thickness dimension.

$$\begin{aligned}
\left(V_1^A, V_2^A, V_3^A, V_4^A\right) &= \int_{-\frac{1}{2}}^{\frac{1}{2}} \left(\cos 2\theta, \sin 2\theta, \cos 4\theta, \sin 4\theta\right) d\bar{z} \\
\left(V_1^B, V_2^B, V_3^B, V_4^B\right) &= 4\int_{-\frac{1}{2}}^{\frac{1}{2}} \bar{z}\left(\cos 2\theta, \sin 2\theta, \cos 4\theta, \sin 4\theta\right) d\bar{z} \\
\left(V_1^D, V_2^D, V_3^D, V_4^D\right) &= 12\int_{-\frac{1}{2}}^{\frac{1}{2}} \bar{z}^2\left(\cos 2\theta, \sin 2\theta, \cos 4\theta, \sin 4\theta\right) d\bar{z}
\end{aligned} \tag{2.6}$$

The A, B and D terms of the ABD-matrix can be written in terms of the lamination parameters as shown in Equation 2.7. The $\Gamma_i,\ i = 1...4$ are matrices in terms of laminate's material invariants, and h is the total thickness of the laminate.

$$\begin{aligned}
A &= h\left(\Gamma_0 + \Gamma_1 V_1^A + \Gamma_2 V_2^A + \Gamma_3 V_3^A + \Gamma_4 V_4^A\right) \\
B &= \frac{h^2}{4}\left(\Gamma_1 V_1^B + \Gamma_2 V_2^B + \Gamma_3 V_3^B + \Gamma_4 V_4^B\right) \\
D &= \frac{h^3}{12}\left(\Gamma_0 + \Gamma_1 V_1^D + \Gamma_2 V_2^D + \Gamma_3 V_3^D + \Gamma_4 V_4^D\right)
\end{aligned} \tag{2.7}$$

The continuous nature of these parameters makes them very suitable to be laminate design variables that could be used to describe and optimize the stiffness properties of a laminate without the need to know its original stacking sequence [8, 9]. Furthermore, they reduce the number of design variables to a maximum of 12, regardless of the number of layers in a laminate. If the laminate under consideration is balanced and symmetric, the number of design variables is reduced even further since the $V_2^A, V_4^A, V_1^B, V_2^B, V_3^B$ and V_4^B drop out. Also, the terms V_2^D and V_4^D could be assumed negligible. Even though using these parameters reduce the number of design variables of the problem and simplifies the analysis, post-processing is still required to recover the stacking sequence of the laminate, which is the main challenge of working with them as design variables.

2.4. Laminate blending

The term blending was first introduced by Zabinsky [6] to take into account the manufacturability and structural integrity of a multi-sectional composite laminate that is being locally optimized. Uniform load distribution over a laminate is rarely ever the case. In reality, laminated structures such as wings are subjected to load cases that vary along their spans, and as a result, the stiffness and strength requirements also vary. Therefore, the use of conventional laminates in such scenarios often results in over-conservative and heavy designs. A more rigorous approach is to divide the laminated structure into smaller sections, and then optimize the stacking sequence of every section individually to meet the local stiffness and strength requirements. However, the resulted design will lack structural integrity, and might even be non-manufacturable because of the stacking sequence incompatibles between the different sections[6]. To tackle this issue, continuity, robustness, and manufacturing constraints have to be considered during the optimization process which is commonly known in the literature as laminate blending. In this section, the currently existing blending definitions are discussed in subsection 2.4.1, this is followed by an overview of the dimensionality of fiber blending that is presented in subsection 2.4.2. Subsequently, guidelines to obtain a blended laminate are presented in subsection 2.4.3

2.4.1. Blending definitions

In this subsection, the degrees of stacking sequences incompatibilities that can exist in a multi-sectional laminate are discussed. Then, the allowable degrees of incompatibilities that are found in the literature are presented in the form of blending definitions which are visualized in Figure 2.4. If two sections in a laminate share the same stacking sequence such as sections XIV and section III, they are considered perfectly blended. Sections I and section II almost share the same stacking sequence except that the outermost ply has been dropped in section II. This is usually acceptable when the loads are low enough and should be avoided when they are high as it can result in premature failure [10]. On the other hand,

it is preferable if plies are dropped as close to the laminate's mid-plane as possible because the risk of delamination becomes smaller [10]. An example of such a ply drop can be seen between sections III and IV. Another undesired incompatibility is the discontinuity of the fiber orientation angles in the same layer of the laminate, which may lead to stress concentrations [10]. An example of this exists between sections IV and V. The worst incompatibility example would be the complete mismatch in the stacking sequence of sections V and VI which would lead to a complete loss of structural integrity.

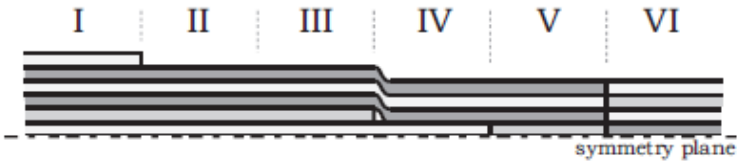

Figure 2.4: An example of a multi-sectional laminate [10].

Inner and outer blending

Inner and outer blending of laminates were introduced by Adams *et al.* [11] while also addressing the high computational cost of the blending problem by introducing guide-based blending. Inner and outer blending are achieved by dropping contiguous sets of plies from either the outside or the inside of the guide laminate respectively. A schematic illustration of both blending definitions can be seen in Figure 2.5. Section I with the most number of plies can be considered as the guide laminate, and as demonstrated in the figure, in the case of the inner blended laminate, the outermost ply of the guide laminate was dropped in sections II and IV. Also, the two outermost plies were dropped in section III. In the case of the outer blended laminate, the opposite is done by allowing the outermost plies to continue into neighboring sections, and the inner plies are dropped.

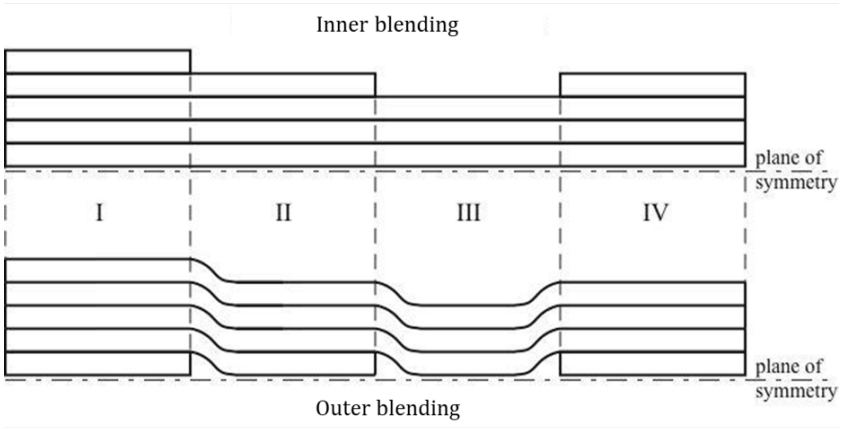

Figure 2.5: Examples of inner (outwardly) and outer (inwardly) blended laminates as depicted by Adams *et al.* [11].

Generalized blending

The main problem with the two previous guide-based blending definitions is that they limit the design space significantly. This is because they only allow the outer or inner plies to be dropped. For instance, "laminate a" in Figure 2.6 is considered to be blended according to the definitions of inner and outer blending. However, "laminate b" does not satisfy these definitions, although it is perfectly manufacturable. Therefore, Van Campen *et al.* [3] introduced the generalized blending definition, which states that "two sections in a laminate are completely blended if all the plies from the thinner section continue into the thicker one, across the entire thickness of the laminate".

Relaxed generalized blending

If two of the laminates that are blended according to the previously mentioned definitions are placed against each other, as shown in Figure 2.7, then the final laminate does not satisfy any of the blending

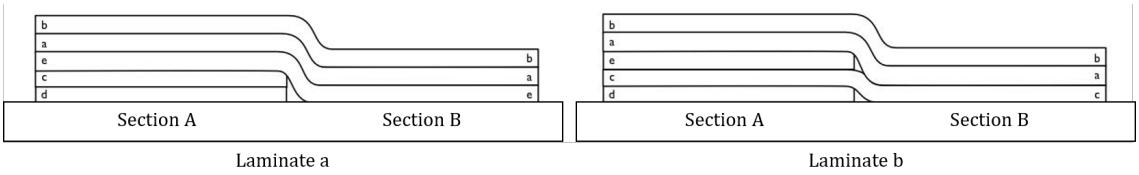

Figure 2.6: Two blended laminates that satisfy the generalized blending definition [3].

definitions discussed so far. Even though that is the case, this laminate is fully manufacturable, and therefore Van Campen *et al.* [3] further relaxed the generalized blending definition and introduced the relaxed generalized blending definition. The new blending definition states that "a laminate is considered completely blended if there are no dropped edges in physical contact between its segments".

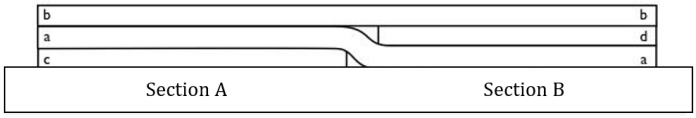

Figure 2.7: A blended laminated that satisfies the relaxed generalized blending definition [3].

2.4.2. Dimensionality of laminate blending

In this subsection, the dimensionality of the laminate blending problem is demonstrated. A composite laminate of N sections is shown in Figure 2.8 as depicted by Van den Oord [2], where L_{min} is the minimum allowed number of plies for a specific section, and L_{max} is the maximum allowed number of plies for all sections. The L_{min} is usually derived from the local optima, and the L_{max} is set to limit the design space of the blending problem.

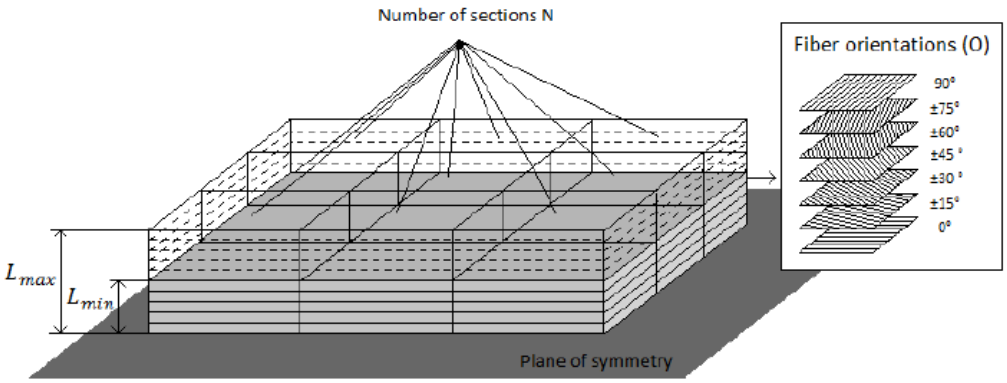

Figure 2.8: A schematic representation of a laminate of N section [2].

The number of possible fiber orientation angles O is usually limited due to manufacturing constraints, and therefore the amount of possible stacking sequences per section can be calculated by:

$$\sum_{i=L_{min}}^{L_{max}} O^i$$

The number of possible laminate designs is then the combination of all possible stacking sequences of all sections and given by:

$$\prod_{i=1}^{L_{max}} \text{Section i possibilities}$$

To put this into perspective, a laminate with 9 sections, where L_{min} is 5, and L_{max} is 10 with 7 possible fiber orientations has a total of $4.587059 \cdot 10^{76}$ possible design solutions. This number increases exponentially with increasing the number of sections in the laminate, and therefore, the laminate blending problem suffers from the "curse of dimensionality".

2.4.3. Laminate design guidelines summary

Designing a composite laminate for a certain application requires one to follow a set of guidelines. Assuming that the laminate being designed is under a uniform loading, the allowed ply angles are usually limited to $0°, \pm 15°, \pm 30°, \pm 45°, \pm 60°, \pm 75°$ and $\pm 90°$, due to manufacturing constraints. During the optimization process of the laminate stacking sequence, there are six main guidelines to be followed [12, 13]:

1. A laminate shall be symmetric about its mid-plane. This will get rid of the bending-extension coupling, and the B-matrix of the laminate will be zero.
2. A laminate shall be balanced when possible. This will get rid of extension-shear coupling.
3. A laminate shall follow contiguity, which means that there should not be more than a given number of plies of the same orientation stacked on top of each other.
4. Two consecutive plies in a laminate shall not have a difference of more than $45°$.
5. A laminate shall have a minimum of 10% of its plies oriented in each of the $0°, \pm 45°$ and $\pm 90°$.
6. A laminate shall not have $0°$ plies placed as the outermost surfaces.

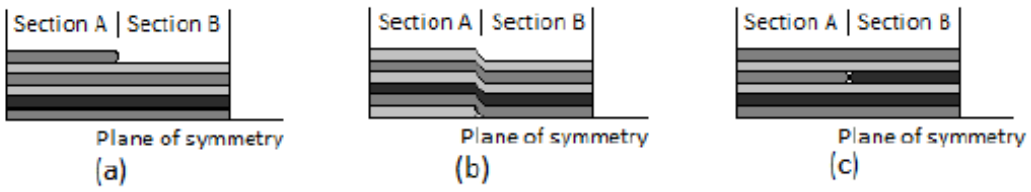

Figure 2.9: (a) External ply drop, (b) Inner ply drop, (c) Butted edges [2].

In the case of composite laminate subjected to a varying load case, the laminate is divided into smaller sections, and their stacking sequences are optimized. Such a multi-sectional laminate might require plies to be dropped in the stacking sequence of any of its sections. These ply drops have to adhere to a certain set of design rules. These rules help avoid delaminations and stress concentrations [13], as well as ensuring a manufacturable design. The main ply-drop rules are [12, 13]:

1. External plies shall not be dropped as they are susceptible to delaminations, especially when the laminate is subjected to a high load. These ply drops are depicted in Figure 2.9.
2. The number of ply drops at the same thickness increment shall be limited, as they are a source of inter-laminar stresses.
3. Butted edges, as depicted in Figure 2.9, shall be avoided as they cause stress concentrations. In addition to that, butted edges require an added manufacturing accuracy and therefore should be avoided from a manufacturing point of view [10].

3

A GA-CA-based blending method

Van den Oord [2] proposed an innovative multi-step blending strategy to overcome the curse of dimensionality in composite laminate blending. The proposed method is suitable for composite laminates with a large number of sections and adapts the relaxed generalized blending definition which guarantees a wider design space. Van den Oord [2] also proposed a new square benchmark and a method to measure the effectivity of laminate blending algorithms.

In this chapter, an overview of the proposed method is firstly described in section 3.1. The novel cellular automaton (CA) used to enforce blending is described in section 3.2. The new square laminate benchmark and the method proposed by Van den Oord [2] to test the effectivity of blending algorithms are presented in section 3.4 and section 3.5 respectively. Finally, the chapter is concluded and discussed in section 3.6.

3.1. Method Overview

An illustrative flowchart of the proposed algorithm is presented in Figure 3.1. The proposed algorithm combines a GA and a CA to blend a multi-section laminated composite with a varying load distribution. The GA was utilized to optimize the stacking sequence of each section in the laminate depending on the local loading conditions. The output local optima of the GA then proceed as input to the CA which is going to evolve the different sections towards a blended transition with their neighbors. Although the CA tries to reach a blended design by applying the least amount of modifications, during that process, sections might still evolve to violate the imposed mechanical constraints. Therefore, after a blended configuration is achieved, all sections of the blended laminate are tested for constraints compliance. If any of the sections fail the test, a layer is added to its stacking sequence, which is then handed over back to the GA to recompute the local optima. After the GA is done revising the local optima, all sections are then directed to the CA. This iterative process is repeated until all sections in the blended configuration comply with the mechanical constraints. The output configuration of this GA-CA-based method is locally blended, and therefore a global patch interpretation is always needed to establish a global patch configuration for manufacturing.

3.2. CA-based blending

The basic feature of a CA paradigm is to divide the domain of interest into a large number of sections. A cell in the domain is then evolved or optimized while only taking into account its state and the state of its neighboring cells. This basic feature makes the paradigm very suitable and effective to homogeneously evolve the local optima in a laminate into a blended configuration [14]. The CA proposed by Van den Oord [2] blends the local optima with a minimum number of modifications to preserve as much of the GA optimization as possible. The CA algorithm translates the blending constraints and rules into local dependencies which are used to evolve the sections accordingly. However, the dependencies between the sections and their neighbors prohibit the simultaneous evolution. Van den Oord [2] tackled this by utilizing a chessboard pattern to obtain a homogeneous evolution while preventing the simultaneous

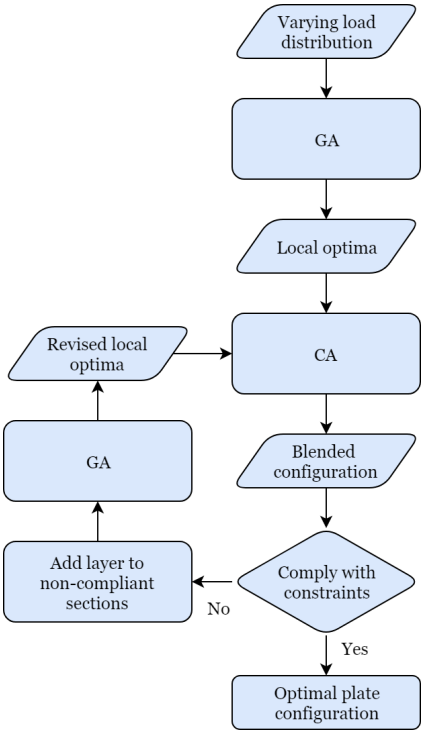

Figure 3.1: Flowchart of the GA-CA-based blending method proposed by Van den Oord [2].

evolution between interconnected sections. The blending process is conducted in three main stages that are shown in Figure 3.2. Each stage has a main objective and a set of rules to be followed to satisfy this objective. In the end, a laminate is considered locally blended if all sections satisfy the objectives of all three blending stages. In the remainder of this section, the three blending steps of the CA are discussed.

3.2.1. Preliminary patches

Defining preliminary patches is the first stage of the proposed CA algorithm, and its main objective is to create patches of interconnected plies that have the same fiber orientation and exist within the same layer of the laminate. To be able to achieve that, the stacking sequence of a cell is compared to that of its neighbors. A genotype, which is a representation of the stacking sequence of the cell being analyzed and its neighbors is then created and used to determine which ply in a cell has the modification priority. Every evolution cycle, only one ply per cell is allowed to be modified, a modification consists of one orientation step either in the positive or negative direction. This stage of the evolution process is considered complete when all isolated plies are eliminated.

3.2.2. Minimum patch size

After the first stage of the evolutionary process, all plies in the laminate are now part of a preliminary patch. The diversity of fiber orientation on the local optima dictates the shape and size of the preliminary patches. When there is a high diversity of fiber orientations in the local optima, smaller preliminary patches and extremities will be generated. Therefore, in this stage, patches that do not comply with the minimum patch size constraint are merged with surrounding patches. The minimum patch size can be considered as a manufacturing constraint, it could be regarded as the minimum cross-sectional length of the placed patches.

3.2.3. Elimination of butted edges

The proposed algorithm implements the relaxed generalized blending definition, and therefore, all butted edges have to be identified and eliminated. As explained by Van den Oord [2], three layers are the minimum amount of layers required to identify a butted edge and differentiate it from a covered

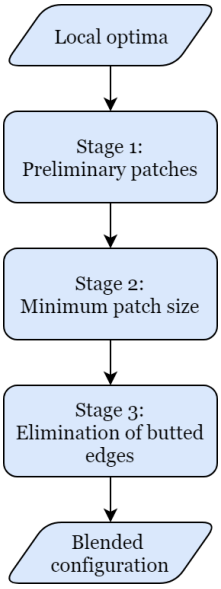

Figure 3.2: Flowchart of the CA algorithm used by Van den Oord [2].

edge. During the elimination of butted edges, patches are allowed to continue in the same layer or adjacent layers. For the proof of concept, Van den Oord [2] implemented the minimum required number of layers. However, this means that the maximum amount of allowed ply drops at the same location will be one. Increasing the range of layers can be beneficial for weight minimization, but it also increases the complexity of the algorithm [2].

3.3. Horseshoe benchmark case

Van den Oord [2] tested the proposed algorithm and compared its results with the results found in the literature using the horseshoe benchmark. The comparative example together with its objective are discussed in Appendix E. An illustration of the stacking sequences of the horseshoe benchmark before and after blending are shown in Figure 3.3 as depicted by Van den Oord [2]. The algorithm managed to achieve the blended results after three iterations between the GA and the CA [2]. The results of the GA-CA-based blending method is comparable to the results of the other methods in the literature in terms of weight. However, the number of patches is higher (this means more expensive and complex manufacturing), and that is because of the small amount of sections and the irregular layout of the horseshoe.

3.4. The proposed benchmark

The proposed blending method is aimed for laminates with a large number of sections but the horseshoe benchmark case is only limited to 18 sections, and therefore, it failed to demonstrate the capability of the proposed method to do so. For that reason, Van den Oord [2] proposed a new benchmark, which is a square laminate under uni-axial compression loading. This benchmark was also used to demonstrate the effectivity of the proposed blending method, this is discussed in section 3.5. For this benchmark, the GA in the proposed algorithm was not used to find the local optima, they were obtained from [10] instead and were based on the lamination parameters distribution. By do so, Van den Oord [2] assumed that the effect of the blending modifications is very minor on the critical buckling load of the laminate. The argument to the validity of this assumption was that the stacking sequences gradually change from one section to the other in a laminate with large number of sections, and therefore the number of blending modifications was minimal [2].

3.5. Effectivity of the proposed blending algorithm

Van den Oord [2] proposed a method to measure the effectiveness of a blending algorithm for a laminate with a varying large number of sections, which is described in this section, and then used to

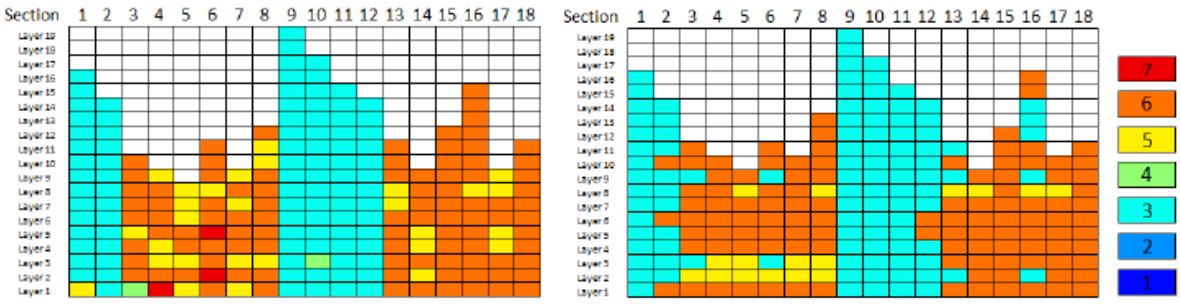

(a) Local optima

(b) Final blended configuration

Figure 3.3: The stacking sequences of the horseshoe benchmark as depicted by Van den Oord [2].

demonstrate the effectivity of the proposed blending algorithm. During the effectivity demonstration of the proposed blending method, the third step regarding the minimum patch size was not implemented. This is because it would distort the results due to the varying size of the sections [2].

3.5.1. Effectivity measurement method

The following method is proposed by Van den Oord [2] to measure the effectivity of a blending method using the size of the design problem C and the computational time T of the algorithm to reach a blended configuration. The size of the design problem is calculated using the same approach described in chapter 2. A baseline is then established, which is an extrapolation of the required computational time for the smallest design problem. In chapter 2 it was explained that the computational time increases exponentially with increasing the problem size, and therefore a logarithmic scale is applied. The computational time is normalized using the time of the smallest design problem and plotted against the size of the design problem to get a plot similar to the one shown in Figure 3.4.

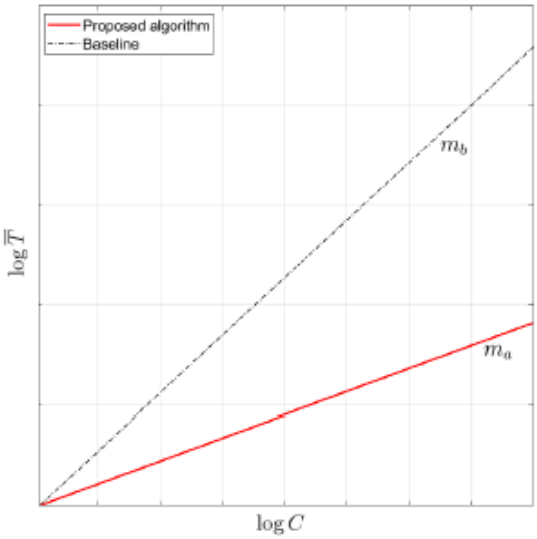

Figure 3.4: A logarithmic plot of the normalized computational time versus the size of the design problem [2].

The degree of effectiveness of the blending algorithm can then be computed using the slopes of both the baseline extrapolation m_b and the actual performance of the algorithm m_a:

$$\text{Degree of effectivity} = \frac{m_b}{m_a}$$

3.5.2. Effectivity of proposed method

To demonstrate the effectivity of the proposed method, Van den Oord [2] used the a newly proposed benchmark of a square panel with a varying large number of sections that is under uni-axial compressive loading. By using this benchmark, Van den Oord [2] managed to demonstrate that the computational time of the proposed CA blending method increased linearly with increasing the problem size. The normalized computation time of the proposed algorithm and the extrapolated baseline are shown in Figure 3.5. The degree of effectivity of the proposed method for the new benchmark is 27.37 and was measured in the domain $3700 > \log(C) > 3000$ [2].

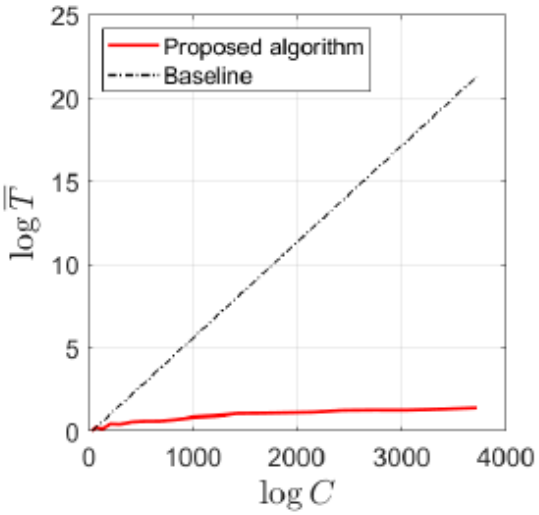

Figure 3.5: Effectivity of the proposed method for the new square benchmark with a varying amount of sections [2].

3.6. Discussion

The method proposed by Van den Oord [2] uses a GA to optimize the stacking sequence of each section in a multi-sectional laminate. The locally optimized sections are then passed on to a CA which evolves them into a blended configuration. The method was then tested using the horseshoe benchmark, and its results were very comparable to that of the other state-of-the-art blending methods in terms of the total laminate weight. However, the number of patches was higher due to the small number of sections and the layout of the horseshoe benchmark pattern. Therefore, Van den Oord [2] proposed the square laminate benchmark with a varying larger number of section and managed to demonstrate that the computational time of the proposed blending algorithm increases linearly with increasing the problem size, this proves the high effectivity of the method. The key to the high effectivity of this method lies in the nature of the CA's paradigm which was use to implement a straightforward set of rules based on local dependencies derived form the global blending constraints.

The proposed algorithm utilized a GA as a stacking sequence optimizer. However, this worked in the horseshoe benchmark only because the loads per section were pre-determined for the sake of simplicity. In reality, it is necessary to take into account the load redistribution due to the altering of local stacking sequences. When the stacking sequence or the thickness of one section in the laminated is changed, the load distribution across the entire laminate also varies. Therefore, the use of lamination parameters seams more logical in that sense. In the proposed square benchmark, the stacking sequences of the local optima were obtained from Van Campen [10], and their optimization was based on the lamination parameters. However it was assumed that the effect of blending on the local optima was minimal. This still has to be investigated. It would be ideal to hook up the local optima optimization from Van Campen [10] to the proposed algorithm to take the place of the GA optimizer used in the horseshoe benchmark. Furthermore, the global patch interpretation of the final blended results are very important for manufacturing, Van den Oord [2] performed the global patch interpretation manually, which is a tedious amount of work. This is not possible for a large number of sections.

4

Research questions

Van den Oord [2] proposed a cellular automaton (CA) based blending algorithm that effectively implements the relaxed generalized blending definition while blending laminates with a large number of sections. Authors of other state-of-the-art blending methods found in the literature demonstrated the capabilities of their blending strategies by applying them to the horseshoe benchmark. The horseshoe benchmark was first introduced by Soremekun *et al.* [15]. However, it is only limited to 18 sections, making it insufficient to test the effectivity of the CA-based algorithm which was designed to blend laminates with a large number of sections. Therefore, Van den Oord [2] proposed a new benchmark to test the effectivity of their algorithm. The proposed benchmark was a square laminate with a large number of sections subjected to a uni-axial compression load. They also established a method to determine the effectivity of the blending algorithm when applied to the new benchmark. With that measure, they managed to show that the computational time of their algorithm increases linearly with increasing the number of sections in the laminate.
In this chapter the research objective of this thesis work is described in section 4.1. Furthermore, the research questions established to achieve this objective are presented in section 4.2. The hypothesis of this research can be found in section 4.3.

4.1. Research objective

The main objective of this research is to validate the theoretical blending algorithm that Van den Oord [2] proposed by using it to design and manufacture a blended laminate demonstrator and executing an experimental campaign to test its performance. This demonstrator would also serve as a proof of concept for blended laminates that follow the relaxed generalized blending definition and should serve as the new benchmark for the laminate blending problem. To realize this objective, it is split into sub-objectives. The first is to design a blended laminate with multiple sections using the proposed CA-based algorithm. The second sub-objective is to manufacture the designed laminates and test them for defects by making use of the Delft Aerospace Structures and Materials Laboratory (DASML) lamination and non-destructive testing facilities. The final objective is to test the manufactured laminates under the compressive buckling load for which they were designed by utilizing the DASML mechanical testing machines. The research shall also include an extensive description of all the conducted activities . The results of this research effort will be used to reflect on the theoretical findings of Van den Oord [2] and, if necessary, improve the proposed laminate blending algorithm.

4.2. Research questions

A set of research questions were established to help satisfy the objective of this research. These questions were further refined using the literature study and are presented below:

Design

- What are the dimensions of the laminates?
- What are the boundary conditions and the loading case?
- How many number of sections are there in the blended laminate?

- What is the optimum stacking sequence of the conventional laminate?
- What are the optimum stacking sequences of the blended configuration laminate?
- What are the necessary modifications to the blended configuration to guarantee manufacturability?

FEM verification
- What are the necessary models to build to achieve the objective of this research?
- What are the effects of the blending modifications on the critical buckling load of the local optima?
- How sensitive is the buckling load of the laminates towards the boundary conditions?

Testing
- What is the experimental test setup?
- Which testing machines are needed to perform the tests?
- Which data acquisition equipment are necessary to obtain the required measurements?
- What are the necessary fixtures to simulate the boundary conditions?

Validation
- How do the theoretical improvements compare to the experimental results?
- Is laminate blending a useful tool for variable stiffness design?

4.3. Research hypotheses

The main hypotheses tested in this thesis are:

- It is possible to manufacture a fully blended laminate with a large number of sections according to the relaxed generalized blending definition using the CA-based blending algorithm proposed by Van den Oord [2]
- It is possible for a blended laminate with a large number of sections, which satisfies the relaxed generalized blending definition, to sustain a higher buckling load than a conventional laminate of the same global dimensions and weight

II

Thesis work

5

Problem definition and methodologies

In this chapter, a new benchmark is proposed for the laminate blending problem. The benchmark along with its boundary conditions and loading scenario are discussed in section 5.1. Furthermore, an overview of the different phases of the experimental campaign is given in section 5.2. After that, the methodology followed to obtain the optimum stacking sequence of the conventional laminate and the final blended configuration of the demonstrator is discusses in section 5.3. Moreover, the methodology followed to characterize the material used during this experimental campaign is elaborated upon in section 5.4. The methodology followed to construct the finite element (FE) models that were used to predict the buckling behavior of the laminates is then discussed in section 5.5. The analytical model used to verify the FE models is presented in section 5.6. Finally, the experimental setups used in the material characterization experiments and the compression buckling tests are discussed in section 5.7.

5.1. The proposed benchmark

To test and validate the theoretical blending algorithm proposed by Van den Oord [2], a new benchmark for the laminate blending problem is introduced. It is based on a realistic design problem and is aimed to replace the theoretical horseshoe benchmark introduced by Soremekun *et al.* [15]. Furthermore, the new benchmark should not be limited in the number of its sections as the blending algorithm proposed by Van den Oord [2] can blend a large number of sections while satisfying the relaxed generalized blending definition introduced by Van Campen *et al.* [3]. This allows for maximum utility of the tailoring capability of fiber-reinforced composites.

The new benchmark can be seen in Figure 5.1 and is representative of the top stiffened skin sections in a wing box assembly. The loading case is based on a takeoff scenario where the top skin panels are loaded in compression which is induced by the upward bending of the wing. The simply supported edges resemble the stiffeners support, and the clamped edges resemble the connections to the ribs of the wings

The cellular automaton (CA) blending algorithm which will be used to blend this benchmark is capable of handling laminates with a large number of sections. However, the demonstrator will be manufacture using a hand lay-up technique, and therefore, a reasonable number of sections had to be chosen such that it is manufacturable and at the same time can demonstrate the potential of blending. For a square laminate of 10 layers, Van den Oord [2] demonstrated that increasing the number of sections would increase the buckling performance of a given laminate as depicted in Figure 5.2. For that particular case, a 5×5 number of sections yields a 54% improvement in the buckling load when compared to a constant stiffness laminate of the same dimensions. Since the loading case is symmetric, the blended configuration is expected to be symmetric in both the longitudinal and lateral directions. Therefore, proceeding with 5×5 sections means that there will be 9 unique stacking sequences to blend in the laminate. In addition to that, the number of layers had to be determined. This was done by considering

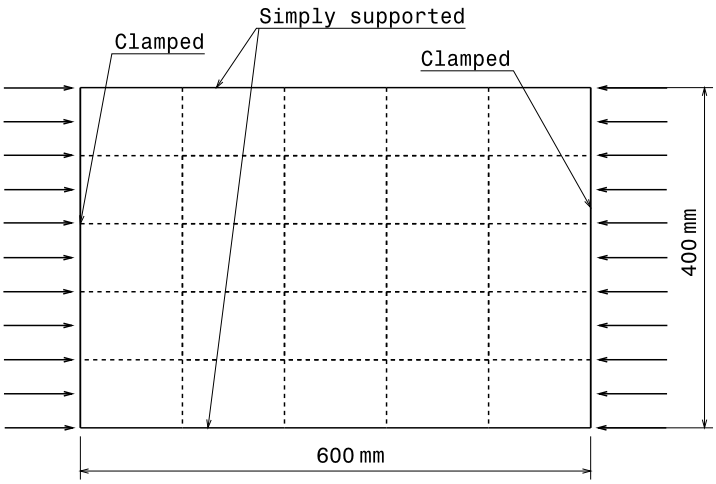

Figure 5.1: The proposed benchmark (the dashed lines represent the boundaries of the different sections).

multiple factors. For instance, the laminates were to be cured in an autoclave, and according to the supplier of the material used in this campaign, the laminate thickness was caped at 5mm [16]. Moreover, the laminates had to also be symmetric and balanced, hence the total number of layers had to be divisible by 4. The total number of layers chosen was 32, which meant that there were 8 layers to be optimized. The size of the proposed benchmark is 600mm $\times$ 400mm, with a 1.5 aspect ratio. The same laminate dimensions were chosen by Peeters *et al.* [17] during their experimental campaign on non-conventional laminates.

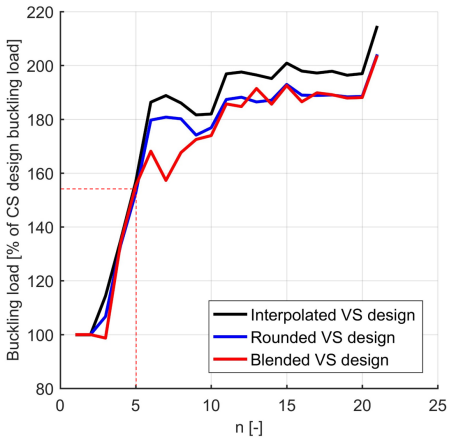

Figure 5.2: Critical buckling load for a varying amount of n $\times$ n sections [2].

5.2. Experimental campaign overview

To satisfy the objective of this thesis, a blending demonstrator had to be designed, manufactured and tested in an experimental campaign. In addition to that, a constant stiffness laminate of a conventional configuration had to also be designed, manufactured and tested to serve as a reference. In this section, an overview of the different phases of the campaign are discussed.

The main 4 phases of this campaign can be seen in Figure 5.3. Firstly, the optimum blended configuration of the different sections in the blended demonstrator was determined during a design phase along with the optimum stacking sequence of the conventional laminate. This phase also included the designing of the testing fixture that was used to simulate the boundary conditions of the newly proposed benchmark during testing. This phase was followed by a manufacturing one, where a detailed

manufacturing plan for both laminate types was devised and executed. The manufactured laminates were then tested for their pre-buckling stiffness and critical buckling load. Finally, the results of the experimental campaign were processed and conclusions were made in the final phase of this research work.

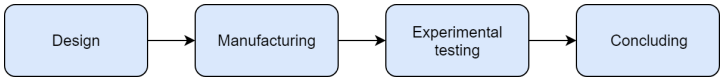

Figure 5.3: The main phases of this thesis work.

5.3. Designing the laminates

The design methodology that was exercised to obtain the optimum stacking sequence for the conventional laminate, and the optimum blended configuration for the blended demonstrator is presented and explained in this section.

The inputs for the design process of the laminates are the number of layers, the number of sections, the laminate dimensions, boundary conditions, and the mechanical properties of the material used. The number of sections of the conventional laminate and the blended laminate are 1 and 25 respectively as determined in section 5.1. The mechanical properties of the material were obtained by conducting a set of material characterization experiments which are discussed in section 5.4. Initially, the material properties found in the literature were used until the characterization experiments were conducted and processed. Once all inputs were ready, they were inputted into the lamination parameters (LP) based genetic algorithm (GA) by Van Campen [10]. The GA computed the local optima for the given design problem. For the blended laminate, the optima lacked continuity and therefore could not be manufactured. The local optima were then inputted into the blending CA proposed by Van den Oord [2]. This CA algorithm was used to blend the local optima according to the relaxed generalized blending definition introduced by Van Campen *et al.* [3]. However, the output configuration of the CA is only locally blended and therefore was not guaranteed to be manufacturable [2]. This was indeed the case and to solve this issue, a global patch interpretation step was necessary. This step was executed manually by the author.

After the configurations of both laminates were achieved, FE models of the laminates were constructed. The models were used to compute the pre-buckling stiffness and the critical buckling load of the laminates. The FE models are described in more details in section 5.5. It is important to mention, that the GA optimizer of Van Campen [10] is probabilistic and non-deterministic, which means that multiple local optima can be achieved on different runs for the same design problem. This was favorable in this situation since the global patch interpretation is executed manually. So one optimum might blend better than the other. The optimum easiest to blend was chosen. In addition to that, for every locally blended optima, there could be multiple global patch interpretations. This is why FE simulations of the different global patch interpretations were necessary to be able to choose the one with the highest buckling load as the final design to be manufactured and tested. The FE models were also necessary to verify the buckling load of the GA optimization step, and to study the knock-down effect the blending modifications of the CA has on the buckling load of the local optima. This entire design process of the blended demonstrator is depicted in Figure 5.4. The design procedure of the conventional laminate is identical to that of the blended laminate except that the number of sections was only one, and the blending steps were disregarded.

5.4. Material characterization

The material to manufacture the laminates is a uni-directional (UD) carbon fiber pre-impregnated with epoxy resin manufactured by DELTA TECH® and is often referred to as M30SC/DT120. The details of the roll used can be found in Table 7.1. Even though the mechanical properties of this material can be found in literature, it was necessary to characterize it for the roll used since the properties can vary from one patch to another. Furthermore, considering that the main focus of this thesis is on the buckling behavior of laminates under a compressive load, it made sense to only characterize the compressive

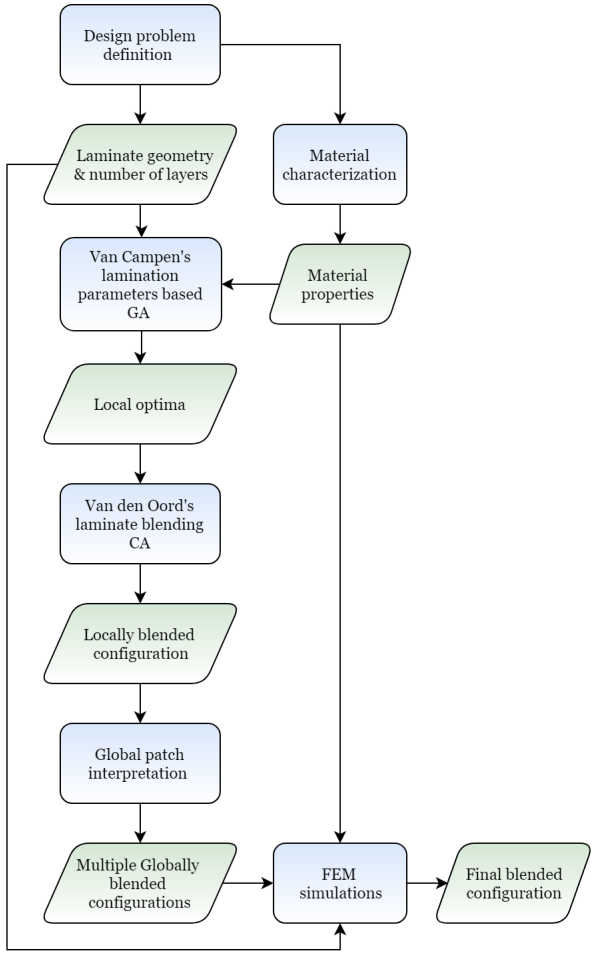

Figure 5.4: An illustrative overview of the blended laminate design procedure.

mechanical properties of the material. The mechanical properties under consideration are:

- The compressive elastic modulus along the 0°
- The compressive elastic modulus along the 90°
- The shear modulus
- The compressive Poisson's ratio
- The compressive failure strength along the 0°
- The compressive failure strength along the 90°

To calculate the compressive modulus and the in-plane shear properties, ASTM standards D6641/D6641M-16 and D3518/D3518M-18 were followed respectively [18, 19]. A total of 8 compressive specimens were manufactured, 4 with 0° and 4 with 90° fiber orientations. In addition to that, 3 specimens were manufactured for the in-plane shear characterization with $\pm 45°$ fiber orientation. The dimensions and strain gauge locations of the compressive and the in-plane shear specimens can be found in Figure 5.5 and Figure 5.6 respectively. The stacking sequences of the compressive specimens are 16 layers of 0° and 16 layers of 90°, and the stacking sequence of the in-plane shear specimens is $[\pm 45]_{8s}$.

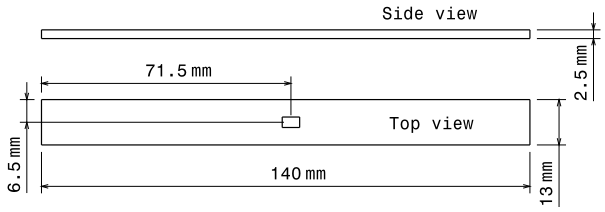

Figure 5.5: The dimensions and the strain gauge location of the compressive specimens.

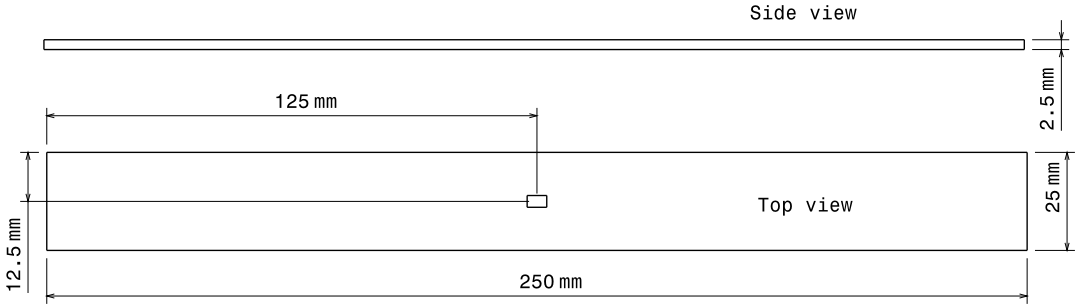

Figure 5.6: The dimensions and the strain gauge location of the in-plane shear specimens.

5.5. FE modeling and simulation

FE models of both the conventional and the blended laminates were constructed and used to help predict the buckling behavior of the laminates. They were also used to study the effect of the blending modification of the critical buckling load. As discussed earlier in section 5.3, both the CA of Van den Oord [2] and the general patch interpretation step modify the local optima to guarantee a manufacturable design. Even though the modifications are minimized during these steps, it still affects the buckling load and behavior of the final design compared to the local optima computed by GA optimizer. In this section, the construction of the FE models is discussed. The models were constructed and analysis using ABAQUS 2017. The modeling strategy is discussed in subsection 5.5.1, then the model construction of the conventional and the blended laminates were discussed in subsection 5.5.2 and subsection 5.5.3 respectively. The method used to verify both models is elaborated upon in subsection 5.5.4, and finally, general remarks are given in subsection 5.5.7.

5.5.1. Modeling strategy

To model the buckling behavior of both the conventional and blended laminates, the same modeling strategy was followed. An illustrative overview of the FE modeling strategy can be seen in Figure 5.7.

Firstly, the models were constructed then an eigenvalue buckling analysis was executed. This is a linear perturbation step which was used to estimate the critical bifurcation load of the laminates. During this step, a perfect laminate is considered, and the outputs are the first buckling mode shapes and their corresponding eigenvalues. Even though the response of the laminate structure is non-linear before buckling, this analysis provided an estimate of the critical buckling load. Following this step, a scaled version of the appropriate buckling modes shape was used as a base for the non-linear analysis step. To do so, the nodal locations of the chosen buckled shape were extracted from the linear analysis step, and then a magnitude was assigned to them. This model with imperfections was then submitted for a non-linear general static analysis, and the outputs of this analysis were the following:

- Load versus end-shortening curves
- Load versus out-of-plane deflection
- Load versus side displacement

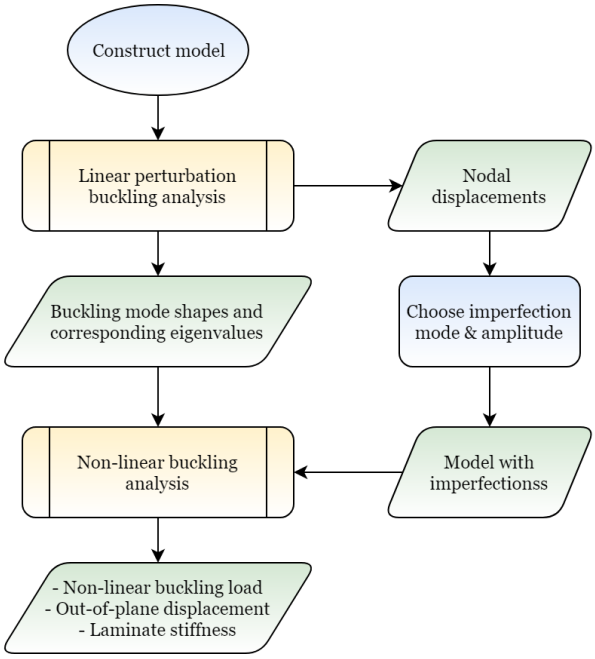

Figure 5.7: An illustrative overview of the FE modeling procedure conducted.

5.5.2. Model construction: conventional laminate

The FE model of the conventional laminate consists of three main partitions which belong to the two resin blocks and the laminate itself as depicted in Figure 5.9a. The laminate was modeled with 3850 continuum shell elements (SC8R). This is a general-purpose 8-node hexahedron element with reduced integration [20]. On the other hand, each resin block was modeled with 1860 general-purpose linear brick elements with reduced integration (C3D8R) [20]. After the element types were assigned to the partitions, a composite stacking sequence was assigned to the laminate with the corresponding material model. This was followed by meshing the partitions and ensuring that the mesh quality is uniform. For the model to produce adequate results within a reasonable computational time, especially when executing the non-linear analysis, a mesh convergence study was important. After the meshing step, the loads and boundary conditions were applied on the laminate. To introduce the load to the laminate a kinematic coupling constraint was used to couple the outermost set of nodes of the resin block and laminate to reference points as shown in Figure 5.8. On both of these reference points, the clamped boundary conditions were then applied by restricting all their degrees of freedom. However, one of the points was allowed to translate in the longitudinal direction of the laminate, and on that same point, the compressive load was simulated by applying a concentrated force in the longitudinal direction of the laminate. As for the simply supported edges, two sets of nodes were created at the same locations where the knife edges will be in contact with the laminate. These sets of nodes were then restricted

from translating in the out-of-plane direction of the laminate. It is important to note that since the laminates will be shortening during the compressive buckling tests, it will not be possible to simply support the entire edges. Therefore, it was important to perform a boundary condition sensitivity analysis to see how the length of the simply supported edges affects the buckling load of the laminate. This sensitivity analysis was then used to size the test fixture adequately.

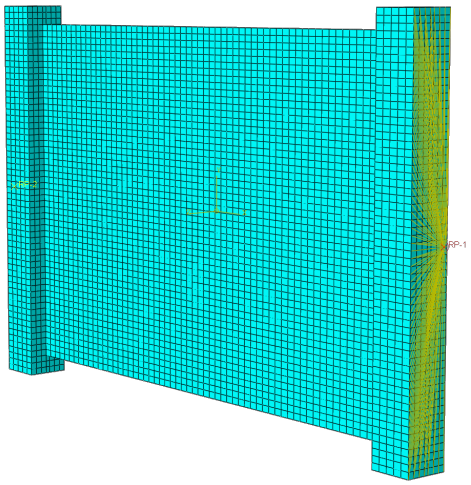

Figure 5.8: Model meshing and kinematic coupling between a point and the outermost set of nodes.

5.5.3. Model construction: blended laminate

The main difference between the construction of the blended laminate FE model and the conventional one is the partitioning of the laminate itself. In the blended FE model, the laminate was partitioned into 25 sections and each was assigned its corresponding composite stacking sequence. It was also necessary to re-mesh the model such that no elements were shared between different sections. As a result, the laminate was modelled using 3500 elements each of 8.75mm $\times$ 10mm $\times$ 5mm. The number of elements used to model each resin block was 1710. The element types for the laminate and the resin blocks were identical to ones used in the conventional model.

Furthermore, the ply drops and the transitions between the sections were not modeled as this was outside the scope of this thesis work. In addition to that, the manufactured blended laminates had severe geometrical imperfections of a saddle shape which did not match any of the buckling mode shapes of the linear perturbation analysis. Therefore the method used to introduce the laminate imperfections in the blended FE model also different. To do so, a general static step was executed before the non-linear analysis. In this step, the initial out-of-plane imperfections recorded by the digital image correlation (DIC) system were imposed on the laminate using displacement boundary conditions. This helped regenerate the imperfect geometry of the actual laminate which can be seen in Figure 5.10.

5.5.4. Verification of the FE models

The verification of the FE models was done using an analytical model which is further discussed in section 5.6. The conventional laminate model was verified by directly comparing the critical buckling load of the eigenvalue analysis with the analytically computed one. The blended laminate model was verified by changing the stacking sequence of all its 25 partitions to the same stacking sequence of its conventional counterpart, and then an eigenvalue buckling analysis was executed. The result of this analysis was then compared to that of the conventional model and its analytically computed critical buckling load.

The buckling load computed using the linear buckling analysis performed on the preliminary FE model of the conventional laminate is compared to that of the analytical model in Table 5.1. Where m and n are the number of half-waves in the longitudinal and lateral directions respectively. It should be noted that the preliminary FE model used in this verification step did not include the resin blocks. The

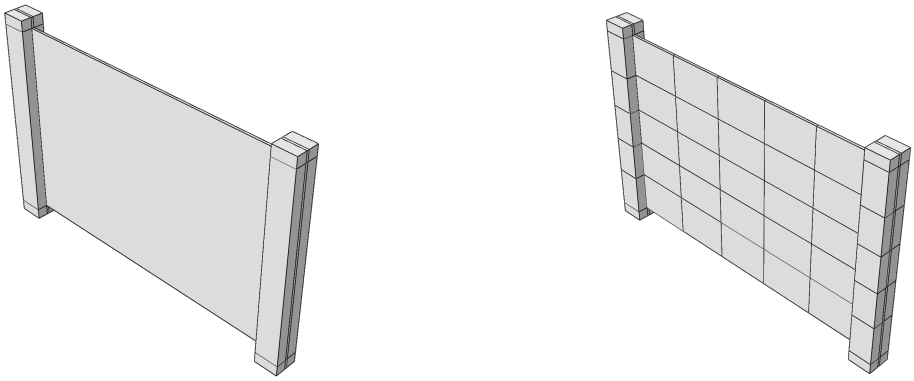

(a) Conventional laminate (b) Blended laminate

Figure 5.9: The laminates partitioning FE models

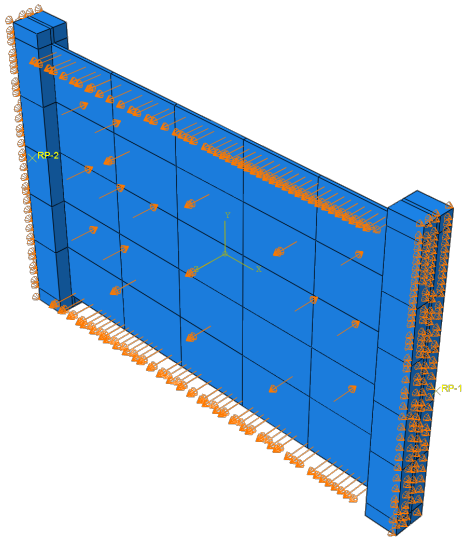

Figure 5.10: Imperfections boundary conditions step.

model also utilized the material properties reported by Rodi [21] because the material characterization experiments were not yet conducted. As for the FE model of the blended laminate, when all sections were assigned the same stacking sequence of the conventional laminate, it gave the same results. As a conclusion, the FE models were considered to be valid.

Boundary condition	Model	Buckling load [kN]		Deviation from the analytical model for the critical case [%]
		m=2, n=1	m=1, n=1	
SSSS	FE preliminary model	86.70	91.39	-1.16
	Analytical model	87.72	92.01	-
CCSS	FE preliminary model	-	99.1	-2.27
	Analytical model	-	101.4	-

Table 5.1: The verification results of the preliminary FE model of the conventional laminate.

5.5.5. Mesh convergence analysis

A mesh convergence was conducted on the preliminary FE model of the conventional laminate to determine if the mesh size and hence the number of elements used were adequate. The results of this mesh convergence study can be seen in Figure 5.11 where the buckling load of the conventional laminate is plotted against the mesh size used. It must be noted that this is the preliminary model where the material model used was obtained from literature and the resin blocks were not taken into account. As a result of this study, the size of the mesh used in the detailed FE models was 10mm or lower. The percentage change in the buckling load when changing the mesh size can be seen in Table 5.2.

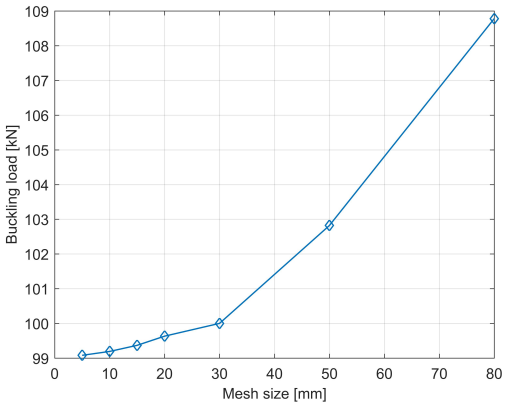

Figure 5.11: Mesh convergence analysis graph.

Mesh size [mm]	Buckling load [kN]	Error [%]
80	108.78	-
50	102.82	-5.47895
30	100	-2.74266
20	99.632	-0.368
15	99.368	-0.26498
10	99.192	-0.17712
5	99.08	-0.11291

Table 5.2: Mesh convergence results.

5.5.6. Boundary condition sensitivity analysis

In Figure 5.12, a sensitivity analysis is presented where the length of the simply-supported boundary condition was equally varied for both side edges of the laminate. The analysis demonstrates the effect of the simply-supported boundary condition on the critical buckling load. This analysis was conducted using a linear perturbation step and was conducted on the detailed FE model of the conventional laminate. As can be seen in the figure, reducing the size of the simply-supported boundary condition by 100mm only reduced the critical buckling load by around 0.05% which is not significant. The results of this sensitivity analysis were used to determine the dimensions of the knife edges used in for the test fixture as it is not physically possible to apply the knife edges on the entire length of the laminate. More information on the test fixtures can be found in Appendix A.

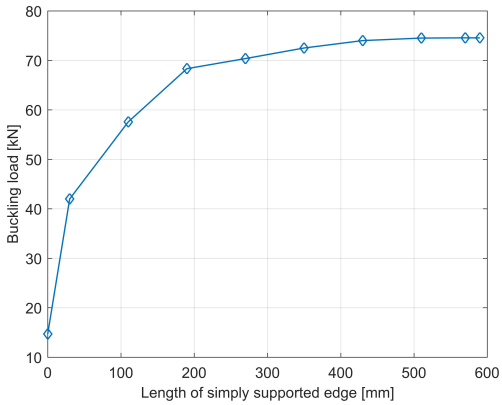

Figure 5.12: simply-supported edges sensitivity analysis.

5.5.7. General remarks

Prior to the construction of the detailed FE models of the laminates discussed earlier in this section, preliminary models were first constructed. The preliminary models did not include the resin blocks, and made use of the S4R element which is a 4-node quadrilateral shell element with reduced integration [20]. Furthermore, during the construction of these preliminary models, the results of the material characterization were not yet ready. Therefore, the material properties which can be seen in Table 5.3 and reported by Rodi [21] were initially used. An illustration of these preliminary models can be seen in Figure 5.13. It is worth mentioning that these preliminary models were the ones used to conduct the mesh convergence analysis and the verification step with the analytical model. In these models, the clamped boundary conditions were simulated by restricting the

Material property	Value
E_{11}	155
E_{22}	7.8
G_{12}	5.5
ν_{12}	0.27
t_{ply}	0.156

Table 5.3: The MS30/DT120 material properties as reported by Rodi [21].

5.6. Analytical model

An analytical model was developed and utilized to verify the FE models. In addition to that, it was used to give an initial failure load estimation to make sure that the laminates would not fail before buckling. The analytical model is based on the Classical laminate theory (CLT) which was discussed in section 2.2. The required inputs to the analytical model are the material properties, the geometrical dimensions of the laminate and its stacking sequence. Firstly, the ABD-matrix of the laminate is computed, then the critical buckling load is determined analytically. The critical buckling load of a composite laminate that

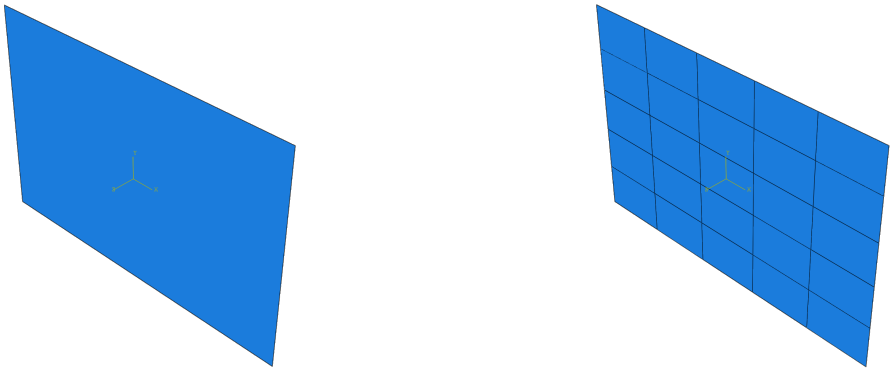

(a) Conventional laminate (b) Blended laminate

Figure 5.13: The preliminary models of the laminates.

is simply supported supported along all its edges and is under bi-axial loading is given by Equation 5.1 [4], and for a laminate that is clamped on two edges but simply supported on the other two, it is given by Equation 5.2 [4].

$$N_o = \frac{\pi^2 \left[D_{11} m^4 + (D_{12} + 2D_{66}) m^2 n^2 (AR)^2 + D_{22} n^4 (AR)^4 \right]}{a^2 \left[m^2 + k n^2 (AR)^2 \right]} \tag{5.1}$$

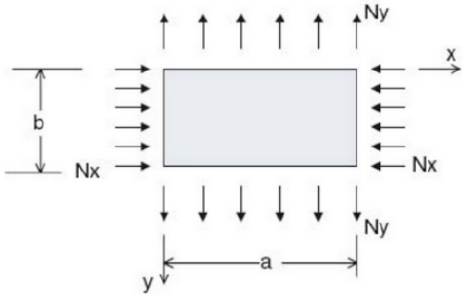

Figure 5.14: Composite plate under bi-axial loading as depicted by Kassapoglou [4].

$$\begin{aligned} N_o &= \frac{\pi^2}{b^2} \sqrt{D_{11} D_{22}}\,(K) \\ K &= \frac{4}{\lambda^2} + \frac{2\,(D_{12} + 2D_{66})}{\sqrt{D_{11} D_{22}}} + \frac{3}{4}\lambda^2 \quad \text{For} \quad 0 < \lambda < 1.662 \\ K &= \frac{m^4 + 8m^2 + 1}{\lambda^2\,(m+1)} + \frac{2\,(D_{12} + 2D_{66})}{\sqrt{D_{11} D_{22}}} + \frac{\lambda^2}{m^2 + 1} \quad \text{For} \quad \lambda > 1.662 \end{aligned} \tag{5.2}$$

Where m and n are the numbers of half waves in the x and y directions respectively, AR is the aspect ratio of the laminate, and k is the loading ratio, which is given by N_y/N_x. For the clamped case, λ is a parameter that satisfies the boundary conditions of the problem and can be calculated by Equation 5.3 [4]. A schematic representation of a composite plate under bi-axial loading is shown in Figure E.2.

$$\lambda = \mathrm{AR} \left(\frac{D_{22}}{D_{11}} \right)^{\frac{1}{4}} \tag{5.3}$$

5.7. Experimental setup

In this section, the experimental setups of the experiments conducted during this thesis are elaborated upon. Firstly, the material characterization experimental setup is discussed in subsection 5.7.1. Then the experimental configuration of the buckling experiments is explained in subsection 5.7.2.

5.7.1. Material characterization experiments

The material characterization experiments were conducted using the ZwickRoell machines in the DASML. The test arrangement used for the compressive and tensile specimens can be seen in Figure 5.15 and Figure 5.16 respectively. The strain gauge readings from the specimens were amplified using the PICAS amplifier from PEEKEL Instruments, and the testing bench was operated using the testXpert II Testing Software.

Figure 5.15: The material characterization test arrangement for the compressive specimens.

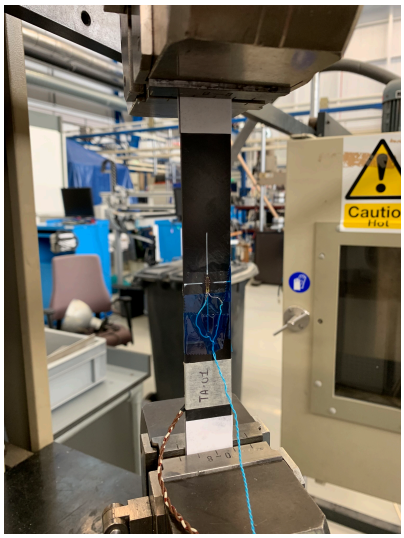

Figure 5.16: The material characterization test arrangement for the in-plane shear specimens.

5.7.2. Buckling experiments

To simulate the boundary conditions and loading scenario on the laminate during the tests, a test fixture was designed and is discussed in more details in Appendix A. The laminates and test fixture arrangement in the testing machine can be seen in Figure 5.17. The testing machine used is the MTS 311.51S four column fatigue bench with a load capability of 3500kN. To accurately measures the displacement of the machine head and therefore the edge-shortening of the laminate, two linear variable differential transformers (LVDT) are used and can be seen in Figure 5.17. The LVDTs in this setting could be used to measure the load introduction imperfection if necessary. However, the edge-shortening was taken as the average of the readings from these two LVDTs. Furthermore, each laminate was equipped with 4 strain gauges in a back to back setting to measure the longitudinal and transverse strains at the center. The data from the strain gauges, the LVDTs and the MTS were recorded using the Keithley 2701 data acquisition system. Additionally, the out-of-plane deformation and a full field strain and deformation measurement of each laminate was executed using a DIC system which can be seen in Figure 5.18. The contactless optical technique required the use of two cameras and a lighting system which were controlled with the Vic-Snap software package [22]. The post-processing of the images was conducted using the Vic-3D software package [22].

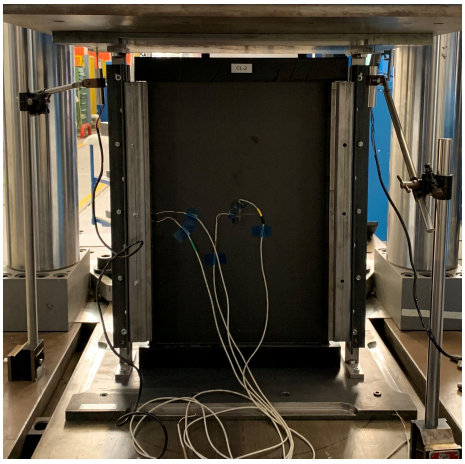

Figure 5.17: The laminate test configuration.

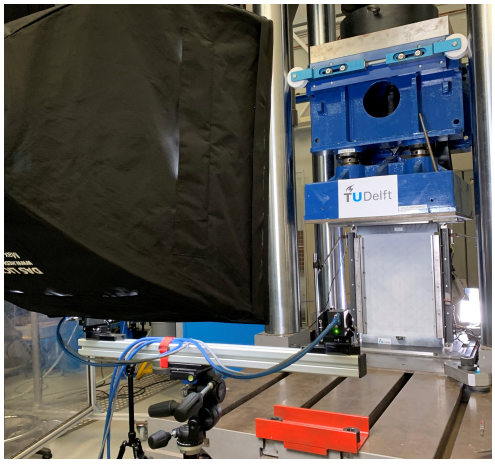

Figure 5.18: The DIC camera system setup.

6

Laminates designs

In this chapter, the design results of the blending demonstrator are firstly presented in section 6.1, and then finally in section 6.2, the optimum stacking sequence of the constant stiffness laminate is presented.

6.1. Blended laminate design

To achieve the final configuration of the blending demonstrator, three main design steps were executed as discussed in section 5.3. First of all, the local optima which were obtained using the lamination parameter (LP) based genetic algorithm (GA) optimizer of Van Campen [10] can be found in subsection 6.1.1. The local optima were then blended by the cellular automaton (CA) based blending algorithm proposed by Van den Oord [2]. The locally blended stacking sequences of that step are presented in subsection 6.1.2. Subsequently, the results of the global patch interpretation step are presented in subsection 6.1.3. The numbering scheme of the sections in the blended laminate is depicted in Figure 6.1a. Even though the laminate was segmented into 25 sections, it has only 9 unique stacking sequences because it was constrained to be symmetric about all its lines of symmetry. This also makes sense because the loading scenario is symmetric. In this section, the unique stacking sequences are called: guides and labeled with roman numerals.

1	2	3	4	5
6	7	8	9	10
11	12	13	14	15
16	17	18	19	20
21	22	23	24	25

(a) The numbering system of the sections in the blended laminate.

I	II	III	II	I
IV	V	VI	V	IV
VII	VIII	IX	VIII	VII
IV	V	VI	V	IV
I	II	III	II	I

(b) The guide stacking sequence ID of each section in the blended laminate.

Figure 6.1: The blended laminate nomenclature.

6.1.1. Local optima

The local optima of the newly proposed benchmark as computed by the LP based GA of Van Campen [10] are presented in Table 6.1. An illustrative visualization of the local optima can be seen in Figure 6.2. The critical buckling load of the local optima which was verified using a FE model is 160.74kN. This is a 115.61% improvement over the constant stiffness laminate which was optimized for the same

loading scenario and has a predicted buckling load of 74.55kN. However, at this stage, the design lacks continuity and therefore is not manufacturable.

Guide ID	**Stacking sequence**	**Section number** (see Figure 6.1b)
I	$[\pm 45_3/\pm 30/0_8]_s$	1, 5, 21, 25
II	$[\pm 45/\pm 60_2/0_{10}]_s$	2, 4, 22, 24
III	$[\pm 45_4/\pm 15/0_6]_s$	3, 23
IV	$[\pm 45/\pm 60_7]_s$	6, 10, 16, 20
V	$[\pm 45/\pm 60_7]_s$	7, 9, 17, 19
VI	$[\pm 60_8]_s$	8, 18
VII	$[\pm 60_8]_s$	11, 15
VIII	$[\pm 45/\pm 60_7]_s$	12, 14
IX	$[\pm 60_8]_s$	13

Table 6.1: The stacking sequence of the local optima.

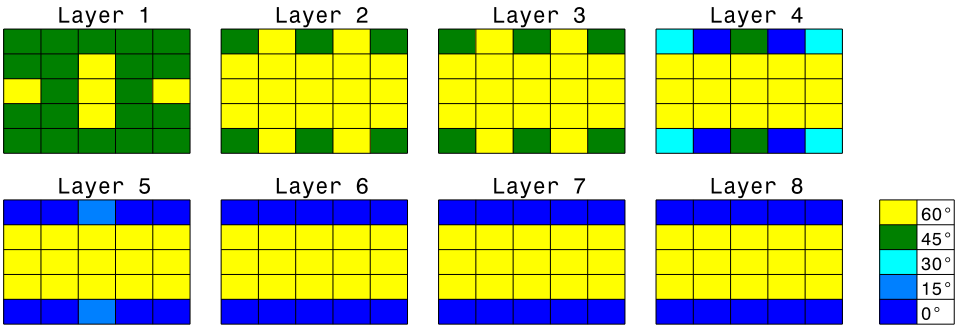

Figure 6.2: Visualization of the local optima.

6.1.2. Locally blended configuration

The CA-based blending algorithm proposed by Van den Oord [2] was used to blend the local optima locally. The locally blended configuration is presented in Table 6.2 and visualized in Figure 6.3. The term "locally blended" means that in each cross-section of the laminate in both the longitudinal and lateral directions, the algorithm guarantees a blended transition between the sections. However, it does not guarantee a blended design at a global 3D level. The critical buckling load of this configuration is 146.74kN, reducing the improvement in buckling performance to 96.83% relative to the constant stiffness panel.

Guide ID	**Stacking sequence**	**Section number** (see Figure 6.1b)
I	$[\pm 45/\pm 60/\pm 45/\pm 30/\pm 60/0_6]_s$	1, 5, 21, 25
II	$[\pm 45/\pm 60_2/\pm 30/0_8]_s$	2, 4, 22, 24
III	$[\pm 45/\pm 60/\pm 45/\pm 30/\pm 60/0_6]_s$	3, 23
IV	$[\pm 45/\pm 60_7]_s$	6, 10, 16, 20
V	$[\pm 45/\pm 60_4/0_2/\pm 60_2]_s$	7, 9, 17, 19
VI	$[\pm 45/\pm 60_7]_s$	8, 18
VII	$[\pm 45/\pm 60_7]_s$	11, 15
VIII	$[\pm 45/\pm 60_7]_s$	12, 14
IX	$[\pm 45/\pm 60_7]_s$	13

Table 6.2: The stacking sequence of the locally blended design.

6.1.3. Globally blended configuration

The results of the globally blended configuration are presented in Table 6.3 and visualized in Figure 6.4 and Figure 6.6. The buckling load of the final blended configuration is 132.28kN. This is a 77.44%

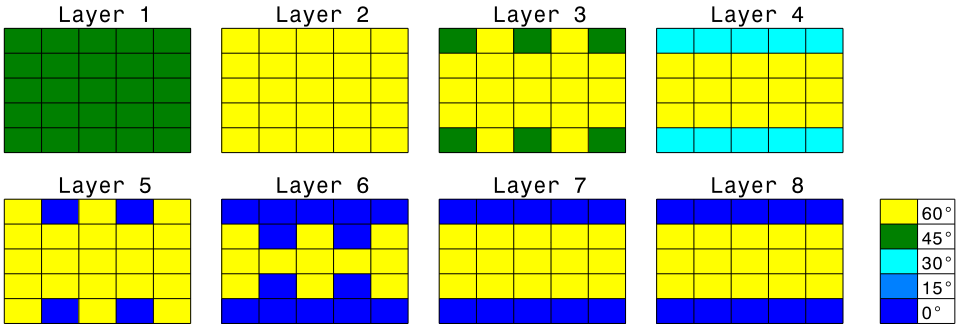

Figure 6.3: Visualization of the locally blended configuration.

higher buckling load than that of the constant stiffness panel. However to achieve this final configuration multiple manual modifications were performed by the author on the locally blended configuration. Firstly, in layer 4, section 2 and hence also 3, 22 and 24 were changed from 30° to 60°. This was necessary to ensure no butted edges existed between sections 1 and 2 in layer 3. This modification step knocked down the bucking load from 146.74 kN to 145.02kN. In addition to that, the CA-based algorithm seems to miss a series of butted edges in the y-direction in the two last layers of the laminate. This can be seen in layer 7 and 8 in Figure 6.3. In layer 7, out of the sections 1:5 and 21:25 only sections 2, 4, 22, 24 are locally blended in the y-direction. As for layer 8, none of the sections 1:5 and 21:25 are blended in the y-direction. To solve this issue, another modification step was conducted. The first possibility was to replace sections 6:10 and 16:20 in layer 8 with 0° plies, however doing that would knock down the critical buckling load of the laminate to 117.32kN which would reduce the improvement in buckling performance to 57.37%. The other solution was to replace sections 1:5 and 21:25 in layer 7 with 60° plies, this only reduced the buckling load to 132.28kN.

The global patch interpretation process was done manually starting with the outermost layer of the laminate to the innermost one. It was important to ensure that the outer most layer is fully continuous over all the section and that none of its plies were dropped as this would result in stress concentrations which could cause delaminations during loading. The blended configuration of the demonstrator is composed of 15 patches and the process of determining them can be seen in Figure 6.5. In this figure, sections with the same shading mean that they share the same patch. It was not possible to follow all the laminate design guidelines summarized in subsection 2.4.3. The rule limiting the number of ply drops per location was not enforced because of the limited number of sections and the relatively large number of layers to blend. It is also important to mention that because of the balanced constraint each patch is composed of two layers, one of a positive fiber orientations and another of a negative one. This means that when one patch is transitioning from one layer to another, there will be two plies dropping at the same location.

Guide ID	**Stacking sequence**	**Section number** (see Figure 6.1b)
I	$[\pm 45/\pm 60/\pm 45/\pm 30/\pm 60/0_2/\pm 60/0_2]_s$	1, 5, 21, 25
II	$[\pm 45/\pm 60_3/0_4/\pm 60/0_2]_s$	2, 4, 22, 24
III	$[\pm 45/\pm 60/\pm 45/\pm 30/\pm 60/0_2/\pm 60/0_2]_s$	3, 23
IV	$[\pm 45/\pm 60_7]_s$	6, 10, 16, 20
V	$[\pm 45/\pm 60_4/0_2/\pm 60_2]_s$	7, 9, 17, 19
VI	$[\pm 45/\pm 60_7]_s$	8, 18
VII	$[\pm 45/\pm 60_7]_s$	11, 15
VIII	$[\pm 45/\pm 60_7]_s$	12, 14
IX	$[\pm 45/\pm 60_7]_s$	13

Table 6.3: The stacking sequence of the final blended configuration after a global patch interpretation.

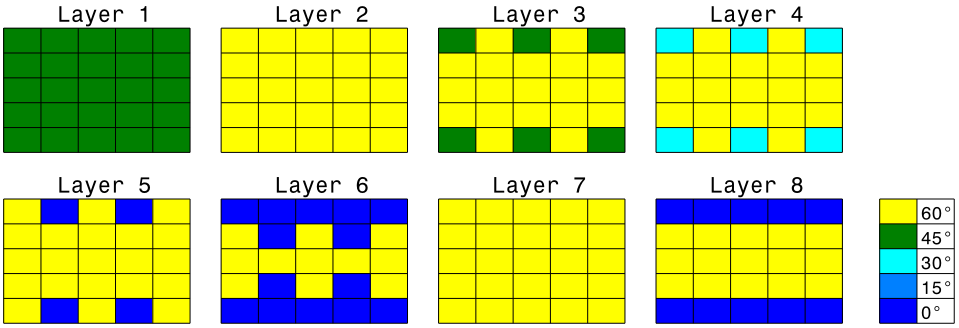

Figure 6.4: Visualization of the globally blended configuration.

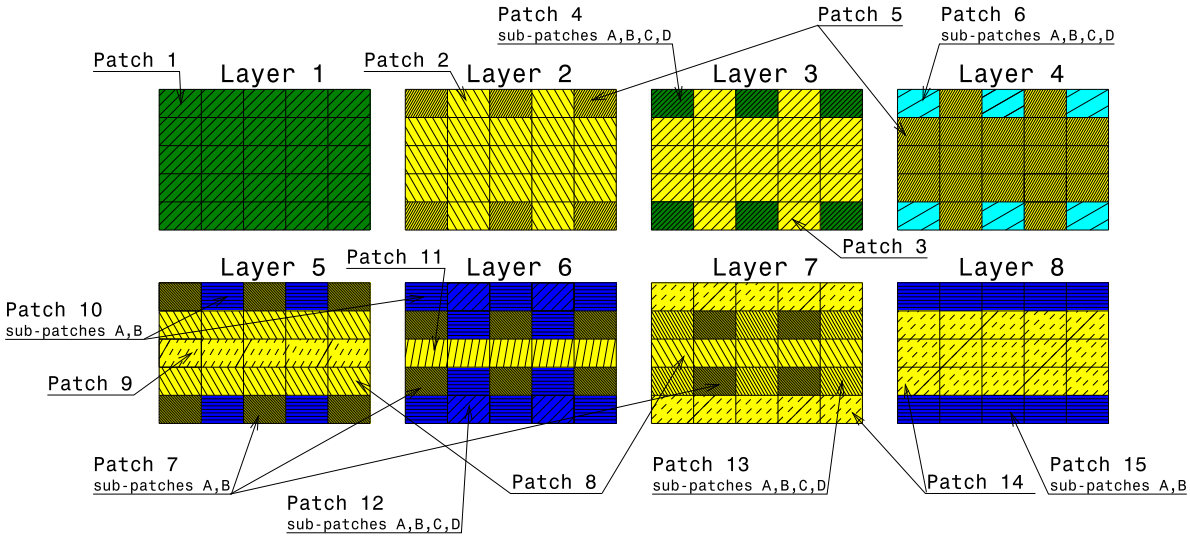

Figure 6.5: Global patch interpretation process visualization.

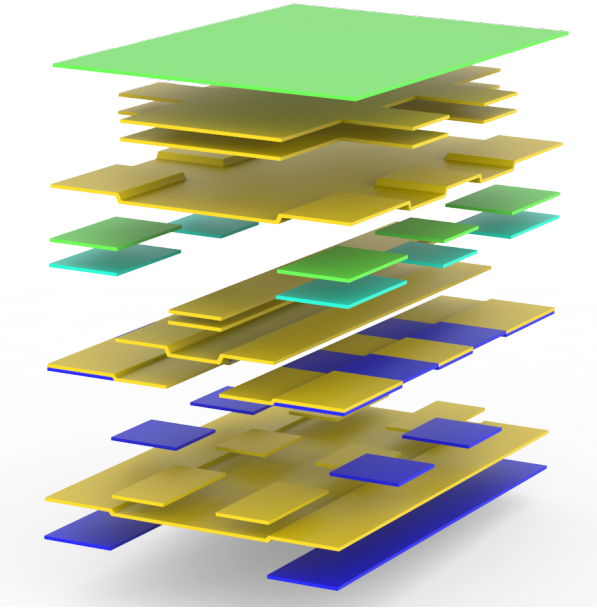

Figure 6.6: 3D visualization of the globally blended configuration that was built.

6.2. Conventional laminate design

The stacking sequence of the conventional laminate is:

$$[\pm 45_8]_s$$

7

Manufacturing of the laminates

The manufacturing procedure of both the conventional and the blended laminates is segmented into five main steps starting with cutting the necessary patches, then laying-up which is then followed by curing, post processing and finally resin potting. In this chapter, an overview of theses steps is provided. The procedure followed was based on the ASTM standard for preparation of flat composite panels [23]. It is important to mention that even though all sections of the optimized laminate had the same dimension, that was not the case for the manufactured laminates. The reason for that was to account for the partitions of the laminate that are potted in resin blocks and the others that are sticking out of the knife-edges. However, between the boundary conditions the dimensions did not change. The added dimensions can be seen in Figure 7.1. In that figure, the dimensions of the sections are only applicable to the blended laminates, but the outer general dimensions apply to both the blended and the conventional laminates.

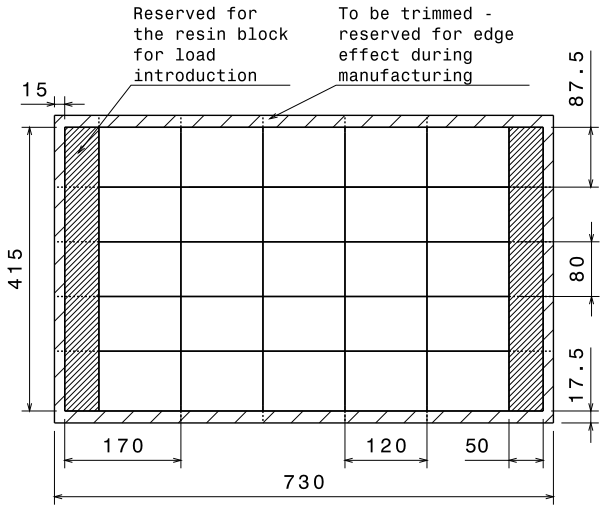

Figure 7.1: The dimensions [mm] of the manufactured laminates.

7.1. Patch cutting

For both the conventional and the blended laminates the GERBER® cutting machine at the Delft Aerospace Structures and Materials Laboratory (DASML) was used to cut the required patches from the prepreg roll. The cutting bench can be seen in Figure 7.4 and the details of the roll used can be found in Table 7.1. The width of the roll used was only 600mm and therefore large patches with fiber orientations larger than 0° had to be constructed out of smaller sub-patches which were then aligned side by side along the fiber orientation during the lay-up procedure. After designing the necessary patches and sub-patches needed to manufacture both laminates, the patches were imported in the

nesting software of the GERBER® cutting machine. The nesting software picks the most optimum cutting nest to minimize the amount of material wasted based on the width of the roll and the length of the cutting table. This was especially important for the blended laminates as the patches and sub-patches were smaller and sometimes had a complex geometry. The patches and sub-patches of the blended laminate can be seen in Figure 7.5. After the cutting step was conducted, the sub-patches were assembled to form the necessary patches. The conventional laminate was composed of only 45° layers and therefore all its patches were identical. However, the blended laminates required a total of 15 patches which can be seen Figure 7.6.

It is important to point out that half of the patches were cut in positive fiber orientations, and the other half was cut in negative ones. Moreover, before the laying up process, every patch was balanced by stacking it with its negative version. This helped prevent stacking errors, especially in the already complex design of the blended laminate. The patches at this stage can be seen in Figure 7.3.

Lot No	H18-1353
Length [m]	150
Width [mm]	600
Material	M30SC-150-DT120-34 F
Date	03/10/2018

Table 7.1: The details of the prepreg roll used.

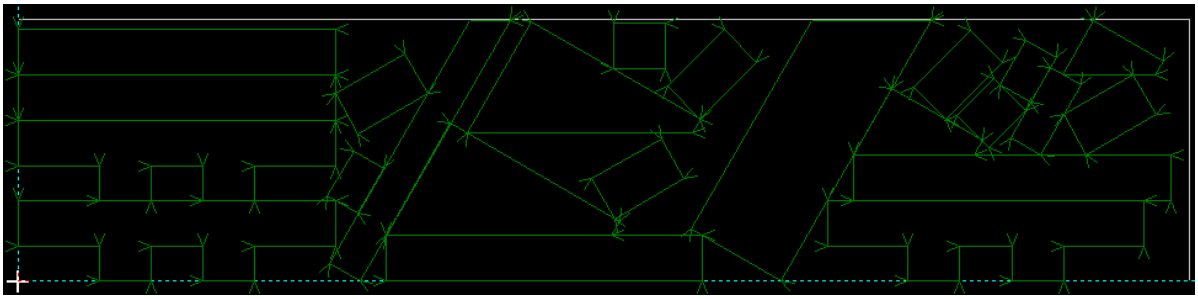

Figure 7.2: An example of the sub-patches nesting done by the GERBER® cutting software.

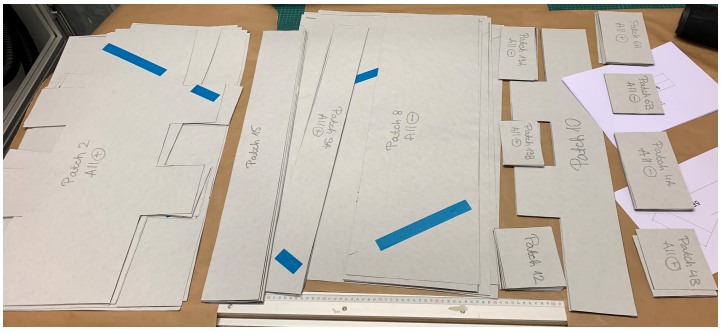

Figure 7.3: The patches of the blended laminate ready for laying-up.

7.2. Laying-up

After cutting the layers/patches, they were moved to the laminating cleanroom facility at the DASML where the laying-up was conducted. For the conventional laminate, this was a straight forward procedure because each patch was a single layer. After every 4 layers, a debulking step was conducted in a vacuum debulking table. This was necessary to reduce the air bubbles trapped between the layers. However, for the blended laminate debulking was done after each patch and each debulking run lasted from 5 to 10 minutes. A schematic representation of the laying-up plan of the blended laminate can

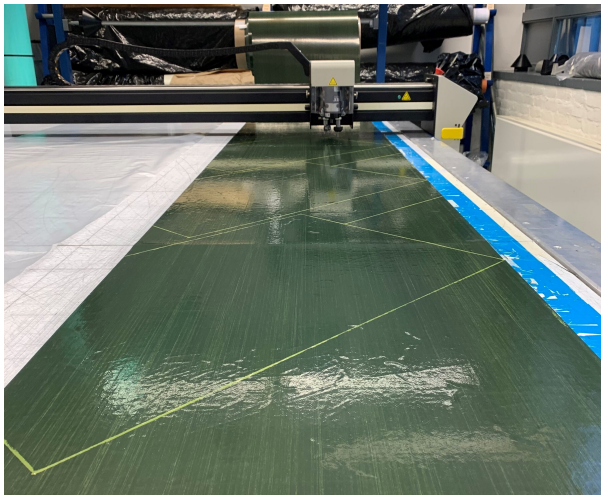

Figure 7.4: The GERBER® cutting bench at the DASML.

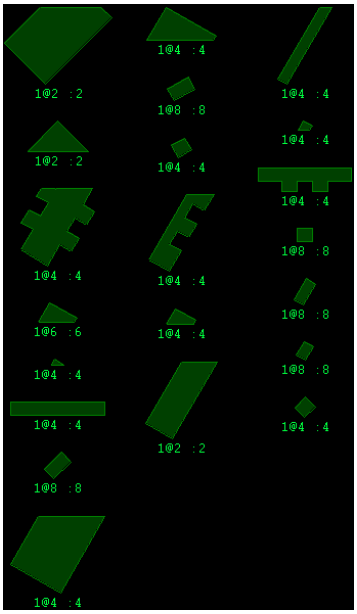

(a) The patches and sub-patches needed to manufacture the blended laminate.

(b) Some of the patches and sub-patches of the blended laminate after cutting.

Figure 7.5: The patches and sub-patched of the blended laminate.

be seen in Figure 7.6 and pictures of the actual laying-up can be seen in Figure 7.8. Furthermore, a detailed view of patches 7 and 10 of the blended laminate can be seen in Figure 7.7, these patches were the most complex to bring together as they had to be weaved. After laying up all the patches, the laminates were vacuum bagged to be cured in the Autoclave. A schematic illustration of the bagging assembly can be seen in Figure 7.9.

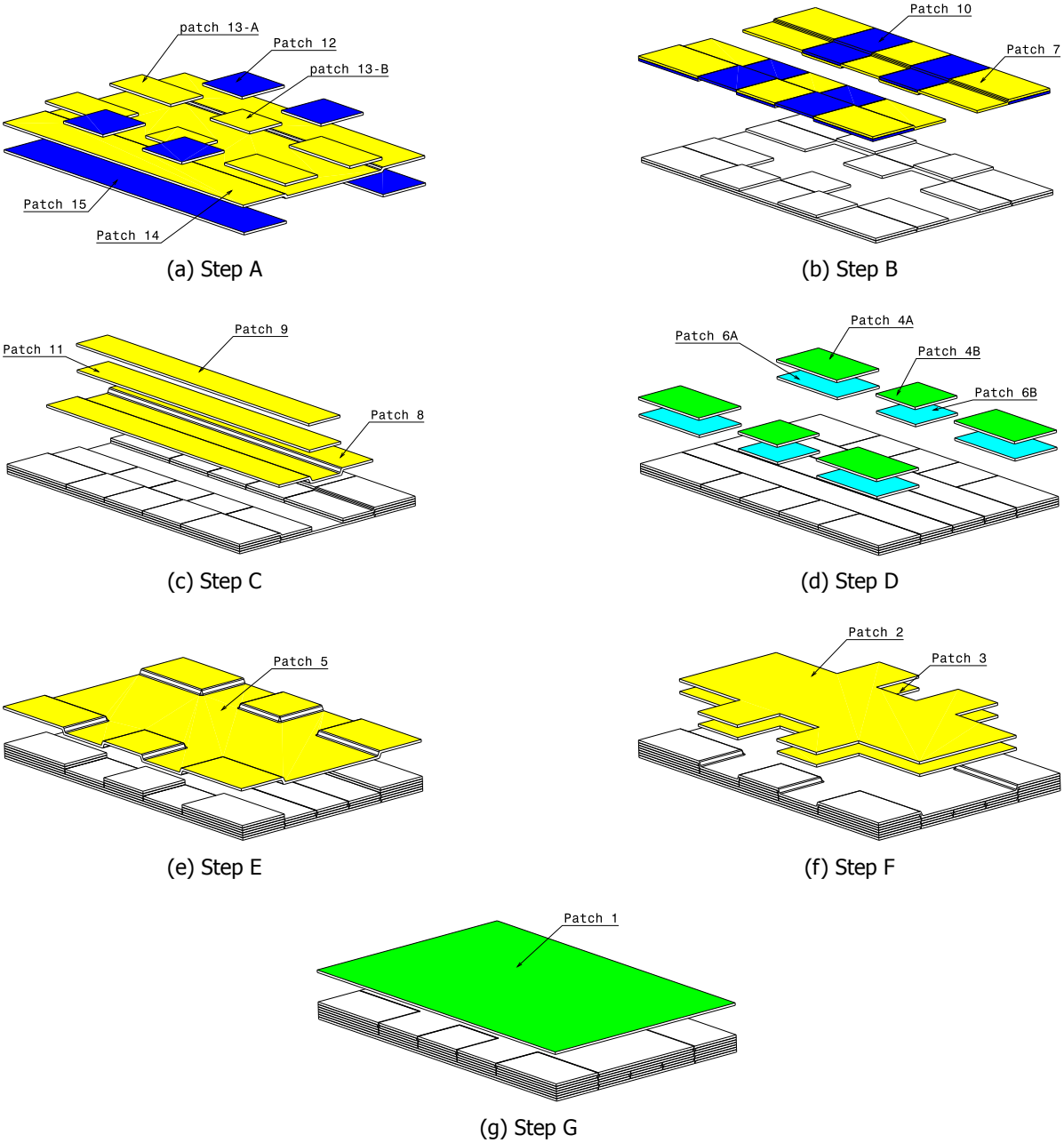

Figure 7.6: A schematic representation of the lamination plan of the blended configuration.

7.3. Autoclave cure cycle

Following the lamination procedure, the laminates had to be cured in an Autoclave as recommended by the material supplier [16]. The Autoclave cycle used to cure both, the conventional and blended laminates can be seen in Figure 7.10.

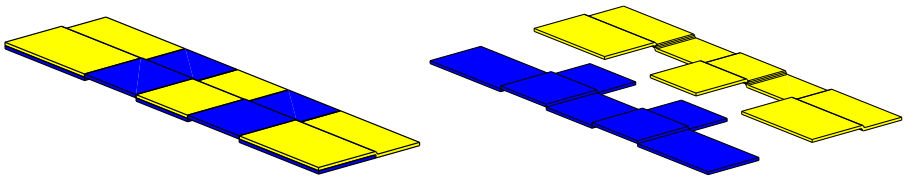

(a) Patches weaved. (b) Exploded view.

Figure 7.7: Detailed view of patches 7 and 10.

7.4. Resin-potting

After the laminates were cured, they were trimmed to their final dimensions using a diamond saw at the DASML. Then the laminates were potted in their resin blocks. A resin block mold with special guides was designed and manufactured for that purpose. The mold which can be seen in Appendix B featured guides that would center the laminate and make sure it stays perfectly vertical while the resin cures. For the conventional laminate that was straight forward as they were perfectly flat. However, the blended laminates had severe geometrical imperfections. To pot the blended laminates in resin, their multi-stable behavior was utilized. The laminates had three equilibrium states out of which one was flat but unstable. To stabilize the laminate in that state, the majority of the laminate was clamped between two steel plates and then the free section was potted first. The potting process can be seen in Figure 7.11.

7.5. General remarks

- All laminates were manufactured out of the same roll
- The same Autoclave cycle was used for all laminates, except for the third blended laminate BL-03, where the cooling rate was slowed down from 4°C/min to 1°C/min to see if this would have any effects on the final curvature of the blended laminates.
- For all laminates, extra 20mm in the width and length directions were added to account for the edge effect after curing
- As mentioned earlier, the length of the roll was only 600mm so sometimes patches or layers had to be divided into sub-patches. This was mainly an issue for the conventional laminate as the layers were all made up of 45°. Because all sub-patches were identical, the location where these sub-patches meet was repeated every 4 layers and at the end they could be detected in the c-scans as can be seen in Figure 8.6. However, this partitioning was always done along the fiber direction and no overlaps between sub-patches were allowed
- A total of four manufacturing cycles were conducted. The two conventional laminates were manufactured together at the same cycle, then two blended laminate were manufactured together and finally a third blended laminate (BL-03) was manufactured alone.
- To eliminate or at least minimized the chances of errors during laying-up, a manufacturing document for every laminate was devised. The document included an extensive description of every patch and a quality checking protocol which required a minimum of two people to be present during all manufacturing steps

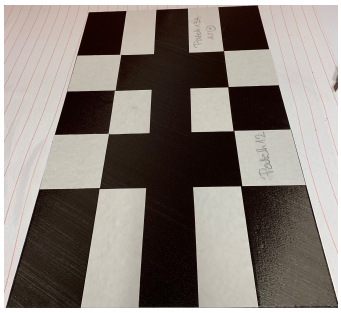

(a) Step A

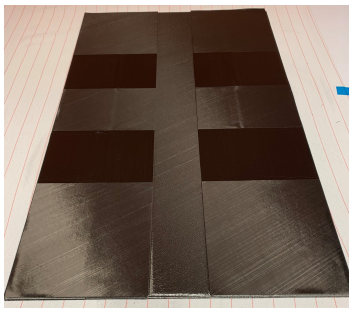

(b) Step B

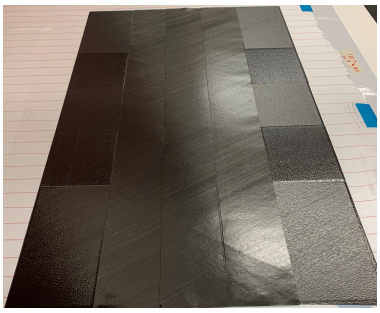

(c) Step C

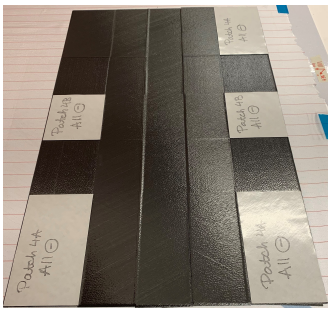

(d) Step D

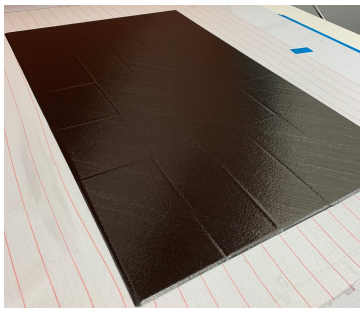

(e) Step E

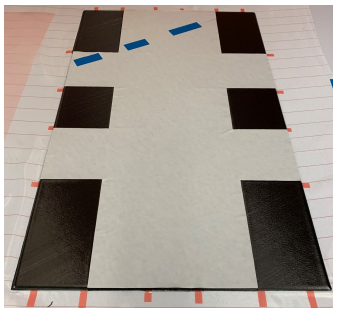

(f) Step F

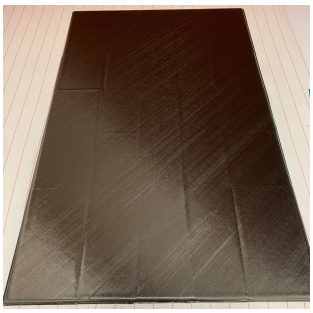

(g) Step G

Figure 7.8: Blended laminate hand lay-up manufacturing.

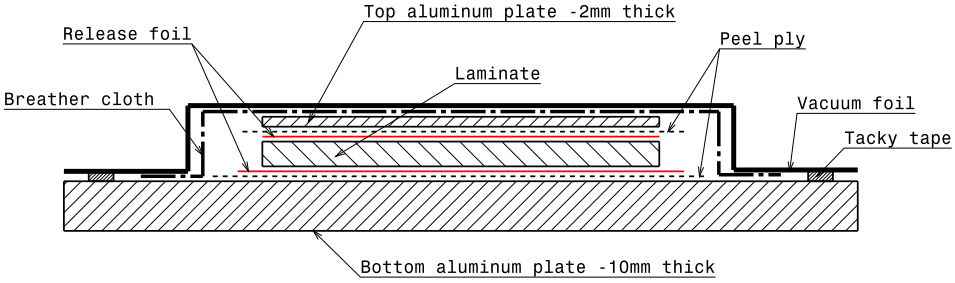

Figure 7.9: A schematic illustration of the vacuum bagging of the laminates for curing.

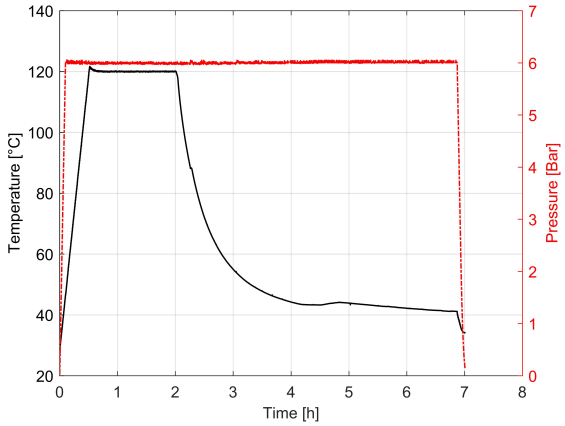

Figure 7.10: The autoclave cycle used to cure the laminates.

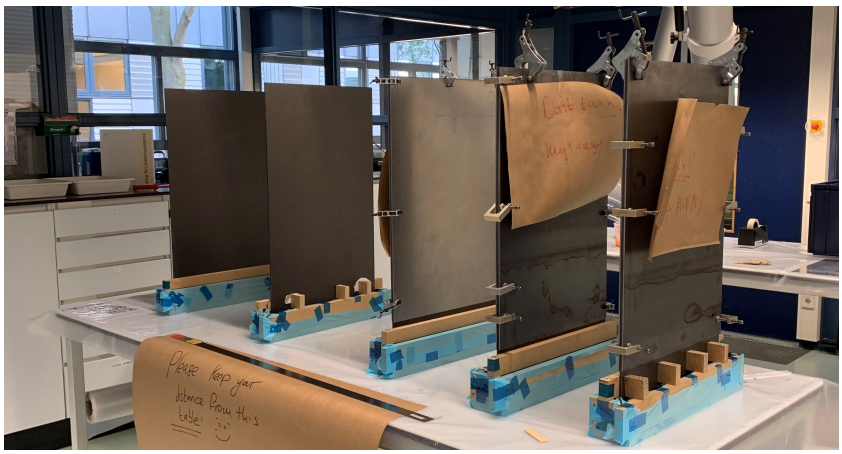

Figure 7.11: The laminates during the resin potting process.

8

Results and discussion

In this chapter, the results of the work done during this thesis are reported and discussed. The results of the material characterization experiments are presented in section 8.1. The inspection results of the manufactured laminates are presented and discussed in section 8.2. The results of the finite element (FE) simulations and the experimental buckling tests are presented and discussed in section 8.3 and section 8.4 respectively. Finally, both, the predicted results and the experimental ones are compared in section 8.5.

8.1. Material characterization

In this section, the results of the material characterization experiments are presented and analyzed. Firstly, the results of the compressive specimens with the 0° and 90° fiber orientations are discussed in subsection 8.1.1 and subsection 8.1.2 respectively. Then the results of the in-plane shear specimens are discussed in subsection 8.1.3. The results of these experiments which are summarized in subsection 8.1.4 were used to update the material models used in the FE simulations.

8.1.1. Compressive specimens - 0°

The compressive specimens with 0° fiber orientation were equipped with two strain gauges each in a back-to-back configuration. One was oriented in the longitudinal direction of the specimen and the other in the transverse direction. The ratio of the strains recorded by these two gauges was used to compute the compressive Poisson's ratio. The compressive modulus was calculated over a range of axial strain between 1000 to 3000 microstrain. The stress-strain curve of these specimens can be seen in Figure 8.2a. It is obvious that the curves are not smooth, that is a result of slipping between the clamps and the specimens. The slipping does not affect the computation of the compressive modulus because it is stress-strain related. However, the slipping caused the specimens to fail in the clamped section and not the strain gauge area as can be seen in Figure 8.1. The failure mode codes of the specimens according to the ASTM standard are either "CIT" or "CIB", which stand for end-crushing inside the grip at top or bottom respectively [18]. These failure modes are unacceptable according to the standard because they underestimate the compressive strength of the material, and hence the compressive strength of the material was not computed. However, since only stiffness analyses were performed in this thesis work, that was not problematic. The results of these compressive specimens are summarized in Table 8.1.

8.1.2. Compressive specimens - 90°

The 90° compressive specimens were equipped with one strain gauge each in the longitudinal direction. Similar to the 0° specimens, the compressive modulus was calculated over a range of 1000 to 3000 microstrain. The stress-strain curves of these specimens are presented in Figure 8.2b. Unlike the 0° specimens, all the 90° failed in the gauge section of the fixture, and hence the compressive strength of the material could be computed. The results of the tests are presented in Table 8.2.

Figure 8.1: The 0° compressive specimens after testing.

Specimens set	**Specimen ID**	$\mathbf{E_{11}}$ **[GPa]**	ν_{12}
CA	CA-01	125.89	0.34
	CA-02	128.98	0.33
	CA-03	127.12	0.40
	CA-04	128.85	-
Average		127.71	0.38
Standard deviation		1.48	0.06
Coefficient of Variation [%]		1.16	15.37

Table 8.1: The results of the 0° compressive specimens for material characterizations.

Specimens set	**Specimen ID**	$\mathbf{E_{22}}$ **[GPa]**	**Compressive strength [MPa]**
CB	CB-01	7.20	137.17
	CB-02	7.20	136.76
	CB-03	7.57	136.22
	CB-04	7.22	140.74
Average		7.30	137.72
Standard deviation		0.18	2.05
Coefficient of Variation [%]		2.50	1.49

Table 8.2: The results of the 90° compressive specimens for material characterizations.

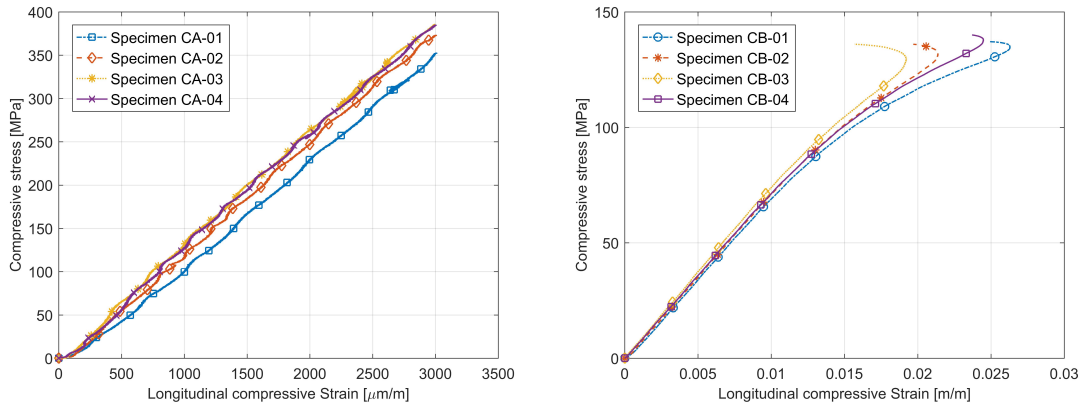

(a) 0° specimens (b) 90° specimens

Figure 8.2: The stress-strain measurement of the compression specimens for material characterization.

8.1.3. In-plane shear specimens

The in-plane shear specimens were equipped with two strain gauges in a back-to-back configuration where one was measuring longitudinal strain and the other was measuring transverse strain. The shear strain is the difference between the readings of these two strain gauges and is plotted against the shear stress in Figure 8.3. The shear stress at a given instance was computed by dividing the force by twice the cross-sectional area of the specimen. The final results of the in-plane shear specimens are presented in Table 8.3.

Specimens set	Specimen ID	G_{12} [GPa]	Compressive strength [MPa]
TA	TA-01	3.04	51.30
	TA-02	3.10	49.60
	TA-03	3.16	53.30
Average		3.10	51.40
Standard deviation		0.06	1.85
Coefficient of Variation [%]		1.83	3.60

Table 8.3: The results of the in-plane shear specimens for material characterization.

8.1.4. Summary of material properties

The results of the material characterization experiments are summarized in Table 8.4. In addition to the material properties derived from the experiments, the transverse shear modulus was calculated. This was done by using Equation 8.1 which is based on the Saravanos-Chamis micromechanical model [24, 25]. It was also assumed that $E_{22} = E_{33}$, $G_{12} = G_{13}$ and $\nu_{12} = \nu_{13} \approx \nu_{23}$.

$$G_{23} = \frac{E_{33}}{2\,(1 + \nu_{23})} \tag{8.1}$$

8.2. Inspecting the manufactured laminates

After all the laminates were manufactured, they were thoroughly inspected for defects and geometrical imperfections as this could have an effect on their buckling behavior during the experimental campaign. Firstly, the laminates were inspected visually for defects and abnormalities. As a result, no visual manufacturing defects nor geometrical imperfections were observed for the conventional laminate. However, the blended laminates seemed to show a multi-stable behavior. Out of the oven, the blended laminates stayed flat on the oven bench, but when disturbed or touched they snap through into a saddle mode shape as can be seen in Figure 8.4. However, when flipped and pushed into the other direction, the laminate snapped through to acquire another saddle mode shape that is negative to the original one. To quantify the extent of these geometrical imperfections, the blended laminates were

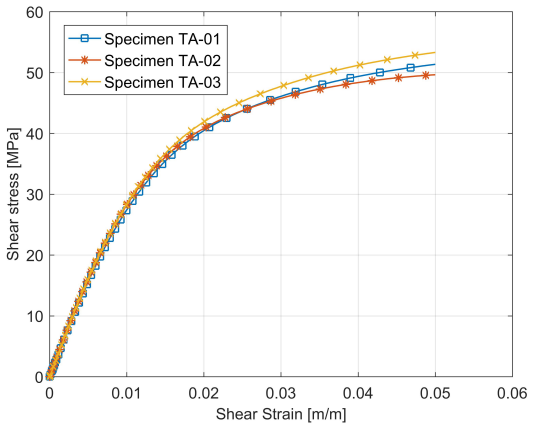

Figure 8.3: Shear stress-strain measurements of the in-plane shear specimens for material characterization.

Material property	**Value**
Compressive E_{11} [GPa]	127.71
Compressive E_{22} [GPa]	7.30
G_{12} [GPa]	3.10
G_{23} [GPa]	2.69
Shear strength [MPa]	51.40
Compressive strength $(0°)$ [MPa]	-
Compressive strength $(90°)$ [MPa]	137.72
ν_{12}	0.36
t_{ply} [mm]	0.155

Table 8.4: Summary of material properties characterized in this chapter.

laser scanned and the results can be seen in Figure 8.5. As can be seen in the figures, the magnitude of the imperfection is consistent between the three blended laminates. Furthermore, the laminates were analyzed for internal defects by c-scanning them. The c-scans of the conventional laminates can be seen in Figure 8.6 and the c-scans of the blended laminates can be seen in Figure 8.7. The laminates were c-scanned twice, once just after manufacturing and once after testing. As can be seen in the c-scan figures of the blended laminates, there are resin-rich areas along the boundaries of the sections. As for the conventional laminates, something similar can be seen near the corners of the laminates. This is because the 45° layers of the conventional laminates were larger than the material roll width would allow, and thus each layer had to be constructed of two sub-patches. The dimensions of the two sub-patches were identical for the entire laminate, and even though the location where these two sub-patches meet was alternated every layer it still showed on the c-scan. A smarter but more tedious solution to this would have been to vary the sizes of the sub-patches. As for delaminations, non were detected after testing except for laminates CL-02 and BL-02 as they were tested till failure.

Figure 8.4: Laser scanning the blended laminate for geometrical imperfections.

8.3. FE simulations results

This section describes the results of the FE simulations for both the conventional and blended laminates. Firstly, the eigenvalue buckling analysis results are shown in subsection 8.3.1 then the results of the non-linear analysis are presented in subsection 8.3.2. In addition to that, the results of the simply supported boundary condition sensitivity analysis are discussed in subsection 5.5.6.

8.3.1. Eigenvalue buckling analysis

The main outputs of this linear perturbation analysis are the critical buckling load and its corresponding buckling mode shape. The results for the conventional laminate can be seen in Figure 8.8. The first eigenvalue which is the critical one is 74.55kN, and the laminate is predicted to buckle with a one-half wave in the longitudinal direction and a one-half wave in the transverse direction. For a perfectly flat blended laminate with no imperfections, the eigenvalue buckling analysis results can be seen in Figure 8.9. The critical buckling load is 132.28kN, and the buckling modes shape is two-half waves in the longitudinal direction and one-half wave in the lateral direction. However, since the manufactured blended laminate came out with severe geometrical imperfections they had to be taken into account. The initial imperfections capture by the DIC before the buckling experiments were used to update the nodal locations in the blended laminate model. The eigenvalue buckling analysis results for the manufactured plate can be seen in Figure 8.9. In that case, the critical buckling load does not change, but the critical buckling shape is one-half wave in both the longitudinal and lateral directions. Unlike the conventional laminate, the initial buckled shape seems to be more localized in the inner sections of the laminate. The results of this linear analysis step are summarized in Table 8.5. In the same table, the predicted pre-buckling stiffnesses of both laminates are presented. The blended laminate

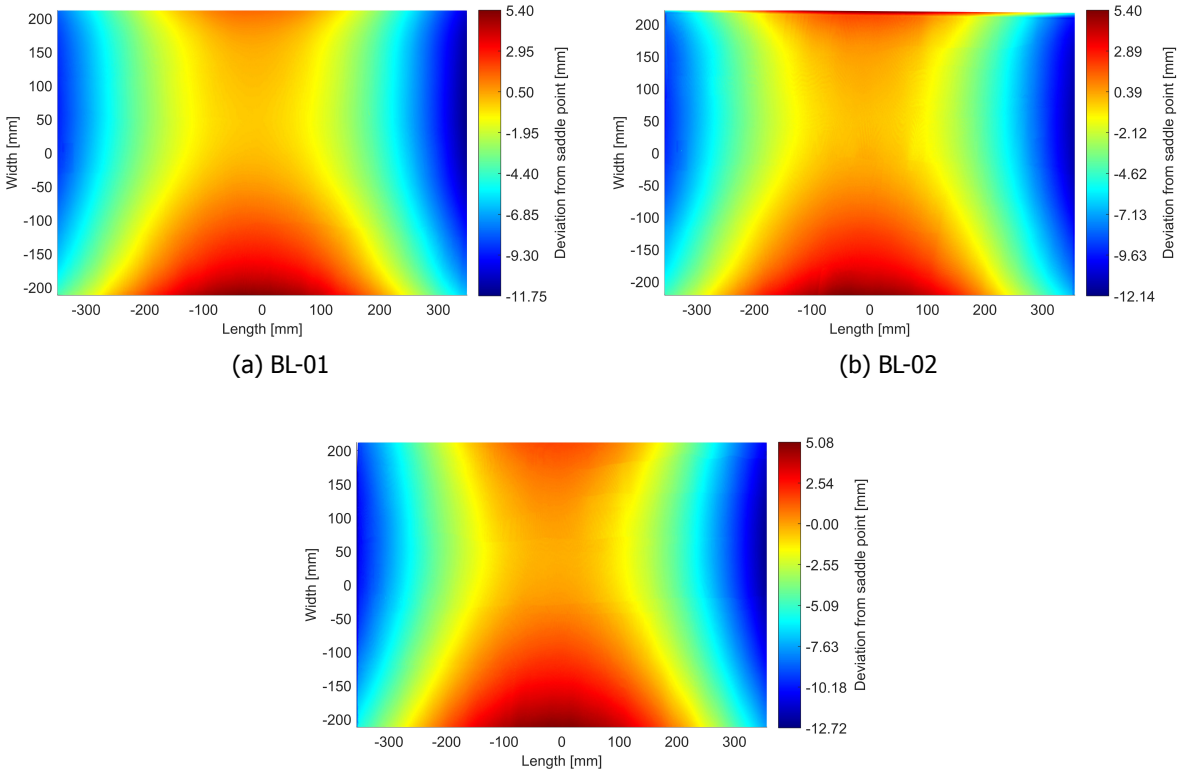

(a) BL-01

(b) BL-02

(c) BL-03

Figure 8.5: The geometrical imperfections of the manufactured blended laminates.

was predicted to be a 101.5% stiffer than the conventional laminate, and its critical buckling load is expected to be 78.0% higher.

Laminate type	**Conventional**	**Blended**
Buckling load [kN]	74.55	132.73
Critical edge-shortening [mm]	1.63	1.44
Stiffness [kN/mm]	45.74	92.17

Table 8.5: The FE eigenvalue buckling analysis results.

8.3.2. Non-linear analysis

The results of the non-linear analysis for the blended laminate and its conventional counterpart can be seen in Figure 8.12 and Figure 8.11 respectively. For the conventional laminate, three FE models were created. The first model labeled as 0.01mm imperfection is the closest to a perfect laminate. The 0.01mm is the amplitude of the eigenmode imperfection used to run the non-linear analysis. The other two models have higher amplitudes of imperfection being 0.1mm and 0.5mm. The eigenmode used for these three models can be seen in Figure 8.8a.As for the blended laminate, only two models were created. The first is a near-perfect one with 0.01mm amplitude of the eigenmode imperfection that can be seen in Figure 8.9b. The second model utilizes the saddle imperfections recorded by the DIC system of one of the blended laminates during testing, which can be Figure 8.18.

The results of the blended laminate models are discussed first. In Figure 8.11a, it can be seen than the pre-buckling stiffnesses of both the near-perfect model and the one with the DIC imperfections are identical. In addition to that, the transition into post-buckling happens at almost the same instant. However, the out-of-plane displacement response to the compressive force of both models was different. For the near-perfect laminate, there is barely any out-of-plane displacement up until the critical

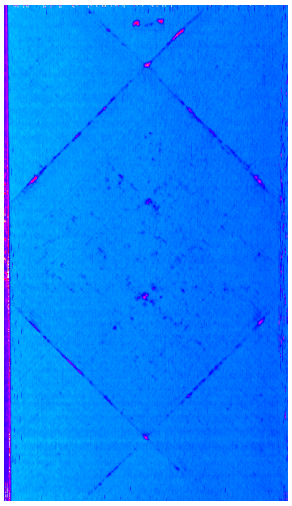

(a) CL-01 before testing.

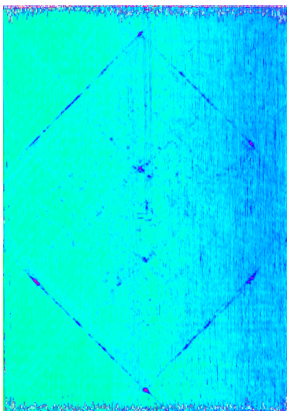

(b) CL-01 after testing.

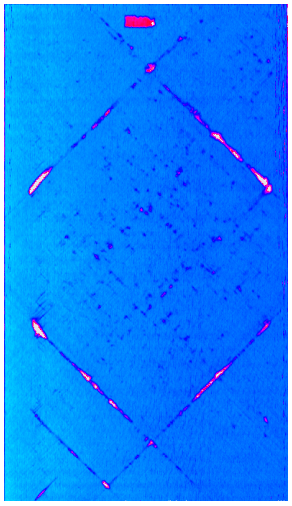

(c) CL-02 before testing.

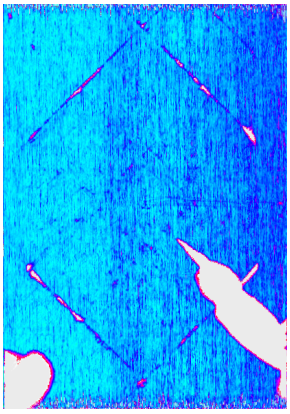

(d) CL-02 after testing.

Figure 8.6: The c-scans of the conventional laminates before and after testing.

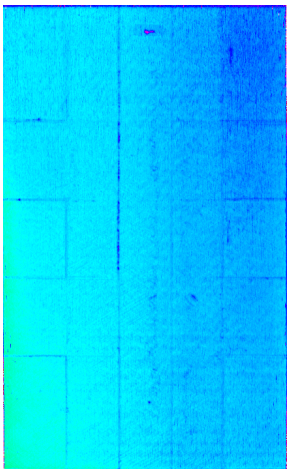

(a) BL-01 before testing.

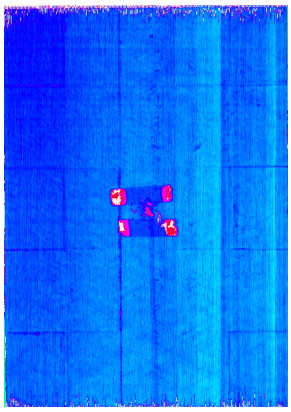

(b) BL-01 after testing.

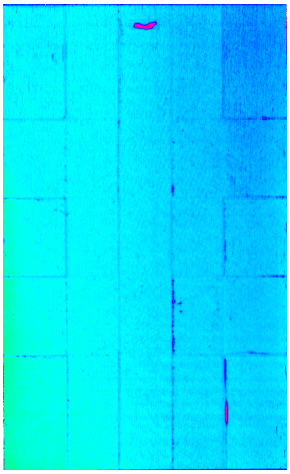

(c) BL-02 before testing.

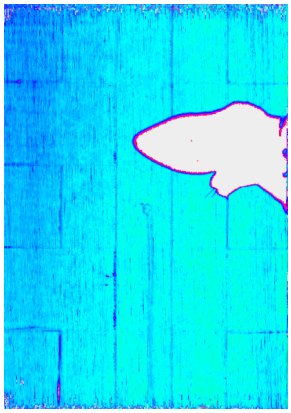

(d) BL-02 after testing.

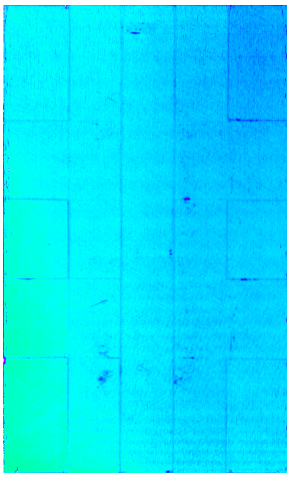

(e) BL-03 before testing.

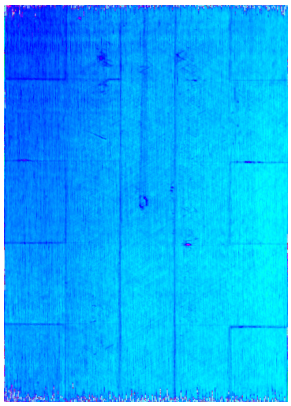

(f) BL-03 after testing.

Figure 8.7: The c-scans of the blended laminates before and after testing.

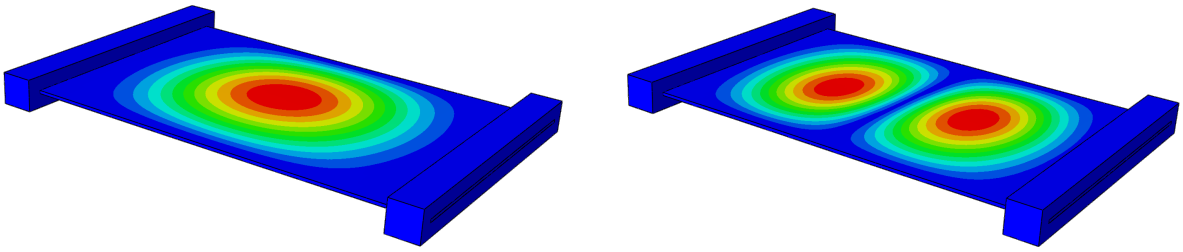

(a) First buckling mode, eigenvalue: 74.55kN. (b) Second buckling mode, eigenvalue: 77.40kN.

Figure 8.8: The first two buckling mode shapes and their eigenvalues of a perfect conventional laminate.

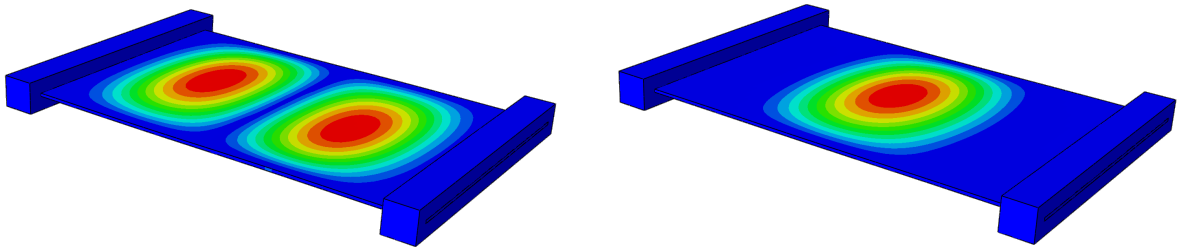

(a) First buckling mode, eigenvalue: 132.28kN. (b) Second buckling mode, eigenvalue: 132.41kN.

Figure 8.9: The first two buckling mode shapes and their eigenvalues of a perfect blended laminate.

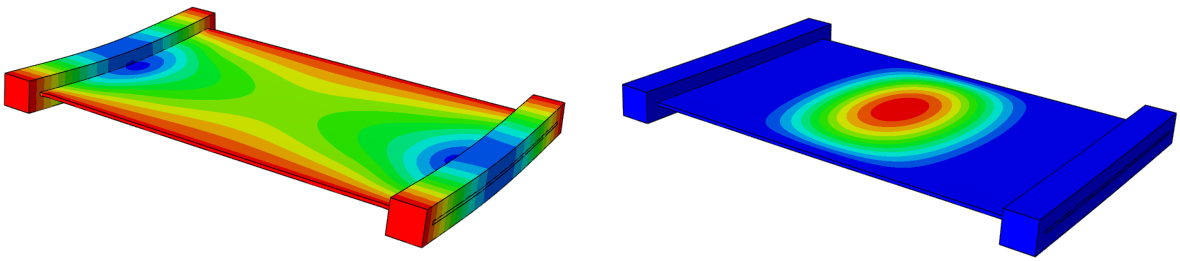

(a) Initial imperfections imported from DIC. (b) First buckling mode, eigenvalue: 132.73kN.

Figure 8.10: The FE eigenvalue buckling analysis results for the blended laminate with initial imperfections.

buckling load of 132kN, but for the model with the DIC imperfections, the out-of-plane displacement increases instantly when the loading starts. This can be seen in Figure 8.11b. Secondly, the results of the conventional laminate models are discussed. Similar to the blended laminate models, the pre-buckling stiffnesses of the conventional laminate models are identical to one another. However, the deviation of the out-of-plane displacement response of the three models from one another is less severe than the case for the blended laminate. The reason for that is that initial imperfection of the imperfect blended laminate is of a different mode shape (saddle configuration) than that of the almost perfect blended model. Also, the magnitude of the imperfection was much larger for the blended laminate model. In addition to the graph plots presented in this section, there were more graphs generated as a result of this non-linear analysis step that can be found in Appendix C.

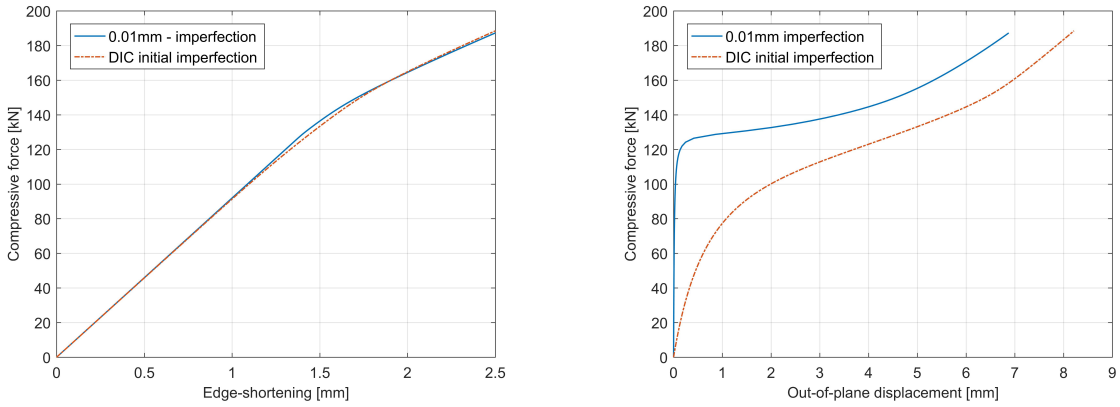

(a) Force versus end-shortening.

(b) Force versus out-of-plane displacement.

Figure 8.11: The non-linear analysis results of the FE simulations for the blended laminate.

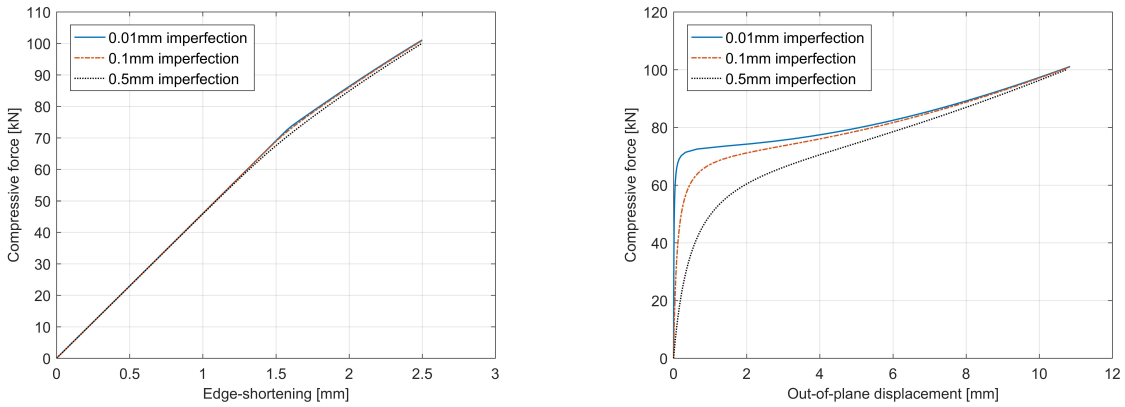

(a) Force versus end-shortening.

(b) Force versus out-of-plane displacement.

Figure 8.12: The non-linear analysis results of the FE simulations for the conventional laminate.

8.4. Experimental buckling tests

A total of 5 laminates were manufactured out of which 3 are of the same blended configuration, and the other 2 are conventional constant stiffness laminates serving as a benchmark. All laminates were tested for their pre-buckling stiffness and critical buckling load and the results of these tests are presented in this section. Firstly, the load versus edge-shortening and out-of-plane displacement results are presented in subsection 8.4.1 and subsection 8.4.2 respectively. Then, the load versus strain readings from the strain gauges on laminates are the presented in subsection 8.4.3. The digital image correlation (DIC) results can be seen in subsection 8.4.4. Following the presentation of the experimental results,

the critical buckling load is computed using 5 different methods in subsection 8.4.5.

8.4.1. Load versus edge-shortening

In these displacement controlled experiments, the compressive load and edge-shortening of all the laminates were recorded and plotted against each other. These plots can be seen in Figure 8.13. As can be seen in the figures, the graphs seem to start at a pre-load, this is just a result of shifting the curves such that the interpolation of pre-buckling stiffness would intersect with the origin of the axis. This was done because all laminates demonstrated a settling behavior at the beginning of the loading cycle which is irrelevant in this study. It can be also be seen from the figures how the results of the different specimens for a specific laminate type match one another. Especially for the blended laminate, this is an important finding that can be used to derive conclusions on the consistency of performance even though it was hand-laid up. The initial linear segment of the load vs edge-displacement curve was used to compute the pre-buckling stiffness of the laminates. The stiffness results and the computed average for both the conventional and the blended laminates can be found in Table 8.6. The pre-buckling stiffness of the blended laminates is 93.75% higher than that of the conventional ones. Also, their transition to the non-linear region of the curve occurs at around 150kN which is 100% more than the loading of which this occurs for the conventional laminate (around 75kN).

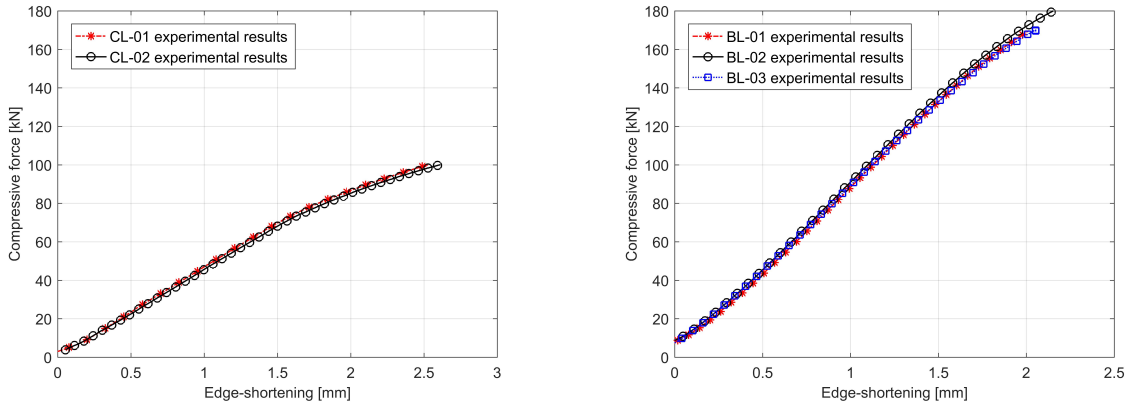

(a) Conventional laminates (b) Blended laminates

Figure 8.13: The load versus edge-shortening measurements of the laminates.

Laminate type	**Conventional**		**Blended**		
Laminate	**CL-01**	**CL-02**	**BL-01**	**BL-02**	**BL-03**
Stiffness [kN/mm]	46.96	45.21	87.85	90.79	89.26
Average [kN/mm]	46.09		89.3		

Table 8.6: The Experimental stiffness results.

8.4.2. Load versus out-of-plane displacement

The load versus out-of-plane displacement curves of both laminate types can be seen in Figure 8.14. Similar to the load versus edge-shortening curves, the measurements of the out-of-plane displacements of the different specimens of the same type match one another very well. The effects of the initial severe imperfections of the blended laminates can be seen on the out-of-plane displacement results. Buckling is a more gradual phenomenon for the blended laminate.

8.4.3. Load versus strain

The longitudinal and transverse strains at the center of the laminates were measured using strain gauges during testing. The strains on both faces of the laminates were then plotted against the compressive load and can be seen in Figure 8.15. However, the readings from the strain gauges on the second conventional laminate (CL-02) were not recorded successfully. For this laminate, the connection

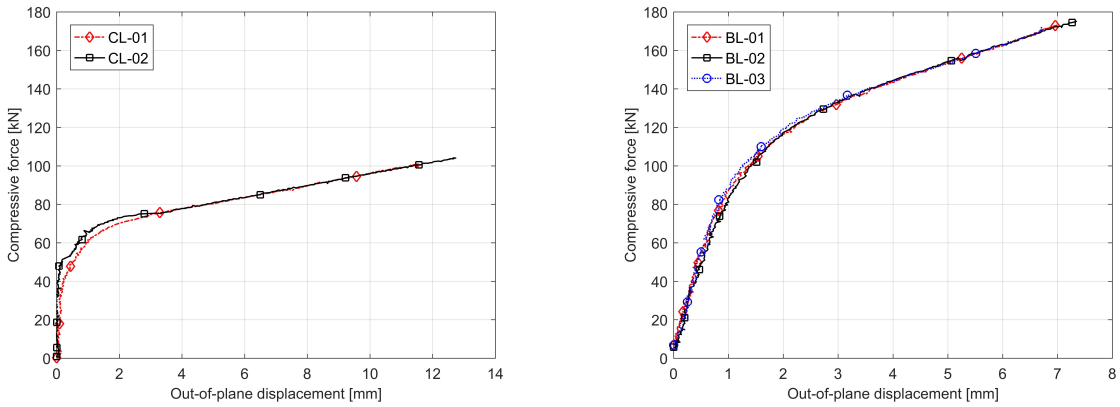

(a) Conventional laminates (b) Blended laminates

Figure 8.14: The load versus out-of-plane displacement measurements of the laminates.

wires to the strain gauges were cut by the knife-edges during testing. It can be seen from these figures that the separation of the strain readings from the two faces of the laminate is more sudden for the conventional laminate, and is much more gradual for the blended laminate. This is because of the much more severe initial geometrical imperfection of the blended laminate.

8.4.4. DIC results

The DIC system was used to measure the out-of-plane displacement of the laminate during the buckling tests. Figure 8.16 presents the out-of-plane displacement recorded by the DIC system for both laminate types at 72kN which is close to the predicted buckling load of the conventional laminate. On the other hand, Figure 8.17 shows the out-of-plane displacements for both laminates at 132kN which is predicted buckling load of the blended laminate. In addition to that, the DIC system was used to record the initial imperfection of the laminates in the testing fixture before the loading. This was more important for the blended laminates as they had severe geometrical imperfection while the conventional ones had no visually obvious imperfections. The recorded imperfection of one of the blended laminates can be seen in Figure 8.18. These imperfection readings were used to update the FE model of the blended laminate as discussed in subsection 8.3.2.

8.4.5. Experimental critical buckling load

To compute the experimental critical buckling load of all the specimens, 5 methods were used and their results are summarized in Table 8.7. The detailed plots of all the methods used per laminate can be found in Appendix D. It was not possible to apply the strain reversal method to the conventional laminates because there was no distinct point where the strain on the convex side of the buckle crest stopped decreasing and started increasing as can be seen in Figure 8.15d. Also, the average compressive strain method could not be applied to the conventional laminates for two reasons, the first being that the strain gauge readings of the second conventional specimen (CL-02) were lost due to their wires being severed by the knife edges during the test. The DIC system could have been used to recover the strains from the laminate's side facing it, however, there was no way to recover the strain measurements of the other side, and this method requires both strain readings. The second reason is when this method was applied to the first conventional specimen (CL-01) there was not a distinct flipping point as there was for the blended laminates which can be seen in Figure D.1. The rest of the methods, when applied to the conventional laminates, gave results within the same range between 71.66kN and 79.40kN. However according to Singer *et al.* [26], the most reliable method in the absence of strain data is the load vs deflection (out-of-plane displacement) method, and hence the average critical buckling load for the conventional laminate is 71.87kN. As for the blended laminates, the load vs deflection method was not possible to utilize because there was not enough data available in the post-buckling region. Furthermore, because of the severe initial geometrical imperfections of the blended laminates pinpointing down a critical buckling load is not realistic. However, the methods used gave a range for the average critical buckling load between 130.03kN to 170.51kN. The lower

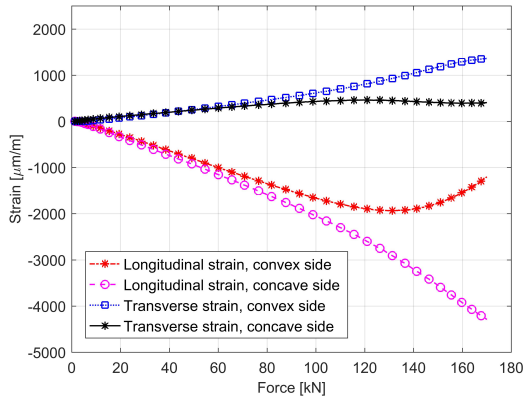

(a) BL-01

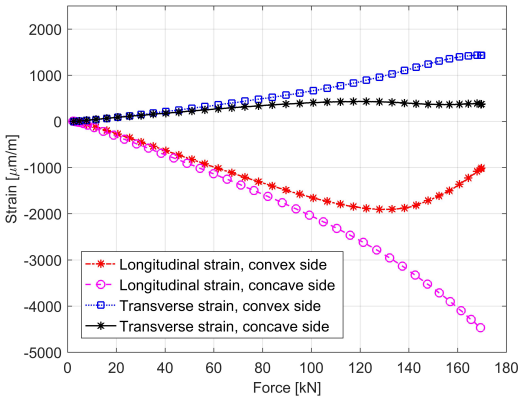

(b) BL-02

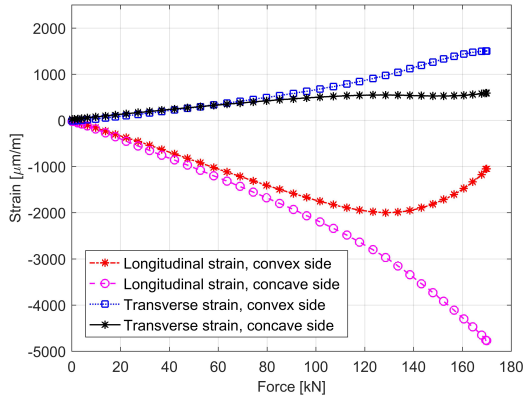

(c) BL-03

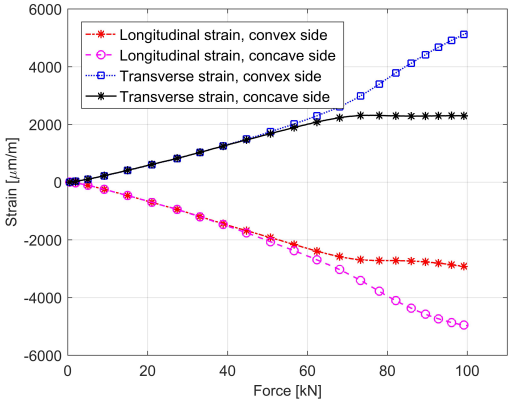

(d) CL-01

Figure 8.15: Strain measurements from the strain gauges.

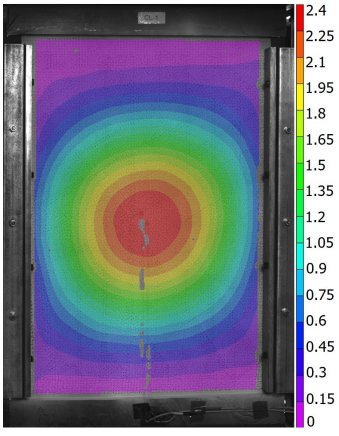

(a) Conventional laminate

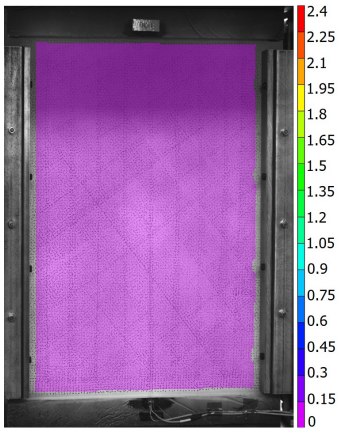

(b) Blended laminate

Figure 8.16: Comparison of the out-of-plane displacement [mm] using DIC at 72kN.

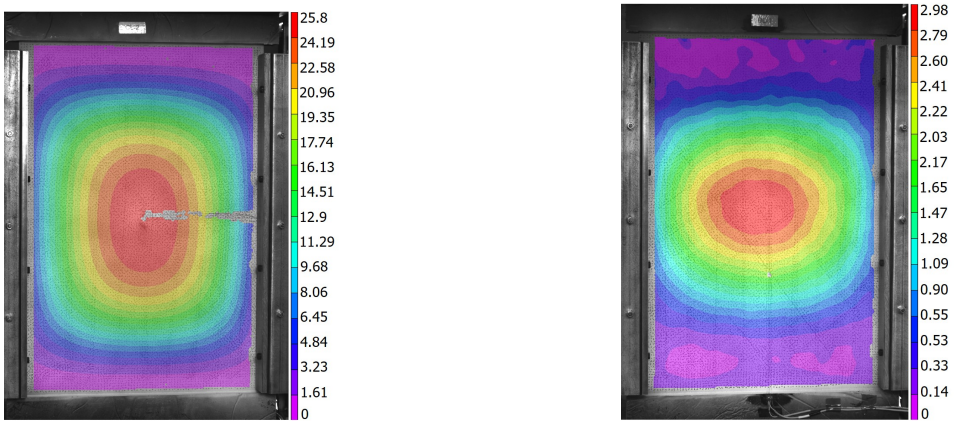

(a) Conventional laminate (b) Blended laminate

Figure 8.17: Comparison of the out-of-plane displacement using DIC at 132kN.

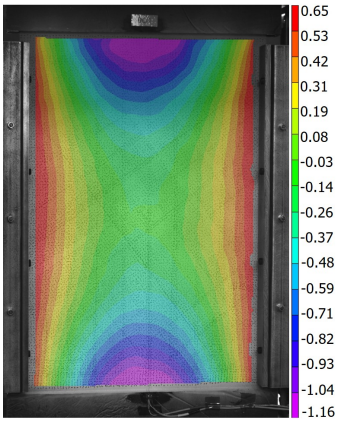

Figure 8.18: The initial imperfection of BL-01 calculated using DIC.

bound is given by the strain reversal method which is evaluated by Singer *et al.* [26] to be the least reliable but most conservative method. This conservative method gives a buckling load which is still in the linear region of the load versus edge-shortening curved as can be seen in Figure 8.13b. The upper bound is calculated using the average compressive strain method which is evaluated by Singer *et al.* [26] to be the simplest and most effective method as it shows a distinctive and very clear flipping point at the buckling load.

Laminate type	**Conventional**		**Blended**			
Laminate	**CL-01**	**CL-02**	**BL-01**	**BL-02**	**BL-03**	**Method**
Buckling load [kN]	76.20	78.42	154.83	150.73	149.81	Load vs. end-shortening
	76.11	79.40	132.17	133.51	132.31	Load vs. deflection squared
	72.07	71.66	-	-	-	Load vs. deflection
	-	-	167.37	174.5	169.65	Average compressive strain
	-	-	130.53	129.71	129.84	Strain reversal

Table 8.7: The experimental critical buckling load per laminate and the corresponding method used.

8.5. Results summary and discussion

In this section, the results of the experimental tests are compared to the predictions of the FE simulations. Not only that but the results are summarized to give an overview of how the blending demonstrator compares to the conventional constant stiffness laminate. Firstly, the pre-buckling stiffness is discussed. For both, the conventional and the blended laminates, the predicted stiffnesses match the experimentally calculated ones. As can be seen in Table 8.9, the deviation from the FE prediction is only 0.76% for the conventional laminate and -3.21% for the blended laminate. Secondly, the buckling mode shapes of the experiments were identical to the predicted ones for both the conventional and the blended laminates. This can be seen when comparing Figure 8.16a and Figure 8.8a for the conventional laminate, and Figure 8.17b and Figure 8.10b for the blended one. Furthermore, the transition from the linear region to the non-linear post-buckling region is discussed. For the conventional laminate, the transition happens at the same instant for both the experiments and the predicting FE simulations as can be seen in Figure 8.19a. In addition to that, the predicted buckling load matches the experimental one with a minor deviation of 3.73% as summarized in Table 8.8. However, for the blended laminate, the transition into the non-linear post-buckling region is delayed for the experimental case as can be seen in Figure 8.19b. A possible explanation for this is that the laminate is pre-stressed in tension before loading. This pre-load is a result of securing the laminate in the test fixture between the knife edges which suppress the amplitude of geometrical imperfections but also introduces tensile stresses into the laminate. This could also explain the deviation of the out-of-plane response of the tested laminates from the predicted one as can be seen Figure 8.20b. As for the conventional laminates, their out-of-plane displacements matches closely the simulation with the 0.1mm as amplitude for its eigenmode imperfection. As for the buckling load of the blended laminate, the manufactured laminates had severe imperfections which makes pinpointing a single critical buckling load not realistic. However, the experimental buckling load was computed using 4 different methods and the computed results vary from 130.03kN for the most conservative strain reversal method to 170.51kN for the average compressive strain method.

Laminate [-]	**Predicated buckling load [kN]**	**Average experimental buckling load[kN]**	**Deviation from predicted buckling load [%]**	**Experimental Deviation from conventional laminate [%]**	**Predicted deviation from conventional laminate [%]**
Conventional	74.55	71.87	-3.59	-	-
Blended	132.73	130.03	-2.03	80.92	78.04

Table 8.8: Overview of the buckling results.

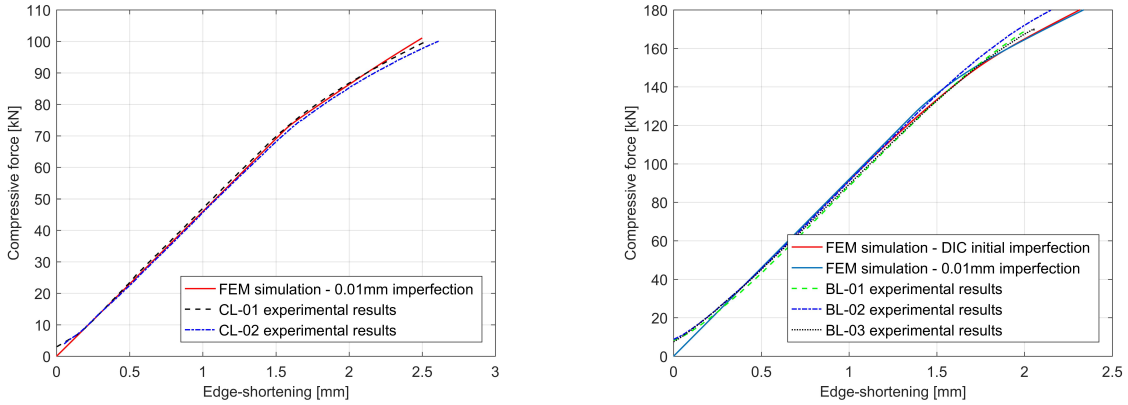

(a) Conventional laminates (b) Blended laminates

Figure 8.19: The load versus edge-shortening results of the experiments compared to FE simulations.

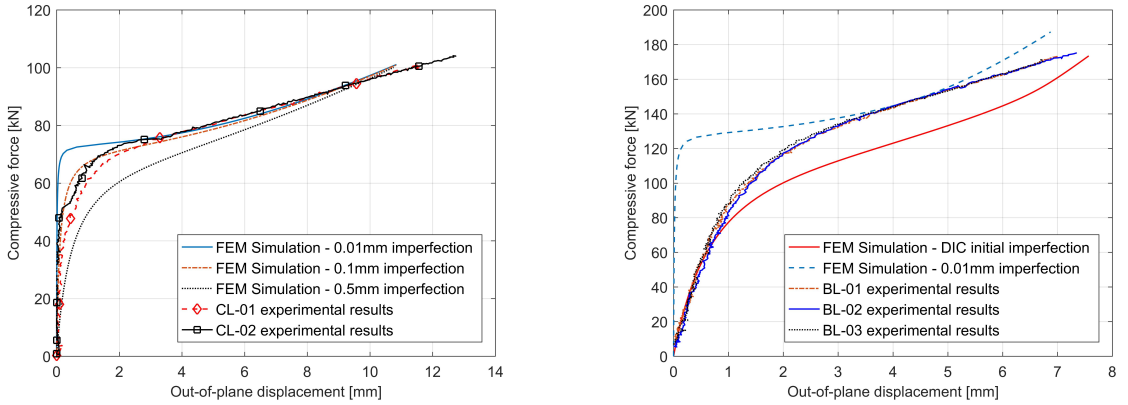

(a) Conventional laminates (b) Blended laminates

Figure 8.20: The load versus out-of-plane displacement results of the experiments compared to FE simulations.

Laminate [-]	**Predicted stiffness [kN/mm]**	**Experimental stiffness [kN/mm]**	**Deviation from predicted stiffness [%]**
Conventional	45.74	46.09	0.76
Blended	92.17	89.3	-3.21

Table 8.9: Overview of the stiffness results.

9

Conclusions and recommendations

Van den Oord [2] proposed a laminate blending algorithm that can blend laminates with a large number of sections while satisfying the relaxed blending definition proposed by Van Campen *et al.* [3]. Furthermore, Van den Oord [2] theoretically demonstrated the potential of using laminate blending to achieve a significant improvement in the buckling performance of a square laminate. The main objective of this research was to validate the findings of Van den Oord [2] by designing and manufacturing a physically blended demonstrator, and in addition to that, executing an experimental campaign to test its buckling performance. In this chapter, the conclusions and recommendations that resulted from this thesis work are presented in section 9.1 and section 9.2 respectively.

9.1. Conclusions

A blended configuration for a laminate of dimensions 600mm $\times$ 400mm that is segmented into 5×5 sections with 9 unique guide stacking sequences and 32 layers was achieved using the cellular automaton (CA) based algorithm proposed Van den Oord [2]. However, few modifications had to be manually performed on the output of the algorithm because a series of 2D butted edges were detected in the last two layers of the laminate. These were different from the modifications performed to achieve a 3D global patch interpretation. Therefore, it was concluded that the algorithm fails to detect 2D butted edges at the last two layers of the laminate and thus requires further developments.

A total of three blended laminates were successfully manufactured using a hand lay-up technique. In addition to that, a total of two constant stiffness laminates with the same number of layers and global dimensions were successfully manufactured and used as a reference. All laminates were inspected visually and using a c-scan technique to detect external and internal defects after manufacturing but none were found. The laminates were also c-scanned after the buckling tests and no difference between the after and before tests scans were detected. The only visible anomalies from the c-cans were the resin-rich areas along the boundaries of the sections. It was therefore concluded that it is possible to manufacture a blended laminate that satisfies the relaxed generalized blending definition using a hand lay-up technique. It was also concluded that the blended laminate maintained its structural integrity after being loaded to its critical buckling load.

The blended laminates had phenomenal geometrical imperfections of a saddle configuration. Furthermore, they exhibited a multi-stable behaviour that is often associated with laminates that have an asymmetric stacking sequence. It was therefore concluded that the blended laminates had thermal pre-stresses in them.

A FE sensitivity analysis was performed to study the effect of reducing the length of the knife edges on the buckling load of the laminates. It was concluded that the reducing the length of the knife edges by 100mm would only reduce the buckling load by only 0.05%. A significant reduction in the buckling load was only observed after reducing length of the knife edges by more than 400mm.

As a result of the material characterization experiments performed during this thesis, it was concluded that the material properties of the patch used to manufacture the laminates were different than that reported in the literature. Especially the Poisson ratio and the shear modulus as they varied by a 33% and -43.4% respectively.

Both the blended and the conventional laminates were tested for their pre-buckling stiffness and their critical buckling load. The results were also compared to predictions by finite element (FE) simulation. The stiffness of the blended laminate was 93.75% higher than its conventional counterpart and the critical buckling load was 80.92% higher. It was therefore concluded that is possible for a manufactured blended laminate to have a significantly improved pre-buckling stiffness and critical buckling load when compared to its constant stiffness counterpart. It was also concluded that the pre-buckling stiffness of the blended laminate can be perfectly predicted using FE simulations.

9.2. Recommendations for future research

9.2.1. Understanding the multi-stable behavior of the blended laminate

The blended laminates that were manufacture displayed two stable states of out-of-plane deformations of a saddle shape and an unstable flat state. This behavior is usually associate with unsymmetrical multilayered laminates, where the thermal effects, chemical shrinkage and moisture absorption cause direction expansion of the individual layers, and thus induce a residual stress field over the thickness of the laminate [27]. Even though each of the sections of the manufactured blended configuration had a symmetric stacking sequence, the transition zones between the sections could have not been perfectly symmetric given the fact that the laminate was manufactured using a hand lay-up technique. Therefore, at these transitions the B-matrix is non-zero. In addition to that, the laminate was segmented into 25 sections of different stacking sequences. During curing and cooling, each section would expand and contract with different magnitudes along the principle accesses of the laminate. These incompatibilities in the thermal-extension coupling between the different sections will build up thermal stresses in the laminate. To better understand what is causing this multi-stable behavior more studies and simulations must be conducted. The results of such research would help with either eliminating this multi-stable behavior or being able to utilize it for morphing structures for aerospace applications.

9.2.2. Improve the CA blending algorithm

The blended configuration manufactured in this thesis work is not possible to reproduce using automated fiber placement (AFP). This is because two of the patches are weaved around each other. The algorithm should be improved to be able to take into account the limitation of the manufacturing method used. This would reduce the design space which could limit the improved performance but would allow for automation and high-speed production, especially when compared to the hand lay-up technique which is tedious and less accurate.

Furthermore, the CA algorithm should be able to guarantee locally blended configurations as claimed by Van den Oord [2]. However, during this thesis work, it was noticed that the algorithm always misses a series of butted edges in the last two layers of the laminate. The algorithm needs further developments to fix this issue. In addition to that, the global patch interpretation which was manually conducted during this thesis should be automated and added to the algorithm. This algorithm should also feature a method to be able to take into account the knockdown effects caused by the blending modifications on the stiffness or strength properties of the laminates.

9.2.3. Investigating the manufacturability of blended laminates using other novel techniques and materials

The blending technology should not be limited to fiber-reinforced composites. Gantenbein *et al.* [28] demonstrated a three-dimensional (3D) printing approach of self-reinforcing hierarchical liquid-crystal-polymer structures. The self-reinforcing feature of these materials arises from the self-assembly of the liquid-crystal polymer molecules into highly oriented domains along the printing direction while being extruded from the printing head. These materials are recyclable and have mechanical properties that outperform the state-of-the-art 3D printed polymers. An extra advantage of using this technique to manufacture blended laminates is that complex geometries can be achieved.

Bibliography

[1] J. Anderson, John D., *Introduction to flight*, 6th ed. (McGraw-Hill, Boston, 2008).

[2] E. Van den Oord, *Overcoming the curse of dimensionality in composite laminate blending*, Msc. thesis (2018).

[3] J. M. J. F. Van Campen, O. Seresta, M. Abdalla, and Z. Gürdal, *General blending definitions for stacking sequence design of composite laminate structures,* in *49th AIAA/ASME/ASCE/AHS/ASC Structures, Structural Dynamics, and Materials Conference* (Schaumburg, IL, USA, 2008).

[4] C. Kassapoglou, *Design and Analysis of Composite Structures : With Applications to Aerospace Structures* (John Wiley & Sons Ltd, 2013).

[5] D. Jegley, B. Tatting, and Z. Gurdal, *Optimization of elastically tailored tow-placed plates with holes,* in *44th AIAA/ASME/ASCE/AHS/ASC Structures, Structural Dynamics, and Materials Conference*, Structures, Structural Dynamics, and Materials and Co-located Conferences (American Institute of Aeronautics and Astronautics, 2003).

[6] Z. Zabinsky, *Global optimization for composite structural design,* in *35th Structures, Structural Dynamics, and Materials Conference*, Structures, Structural Dynamics, and Materials and Co-located Conferences (American Institute of Aeronautics and Astronautics, 1994).

[7] B. D. Agarwal, L. J. Broutman, and K. Chandrashekhara, *Analysis and performance of fiber composites*, 3rd ed. (John Wiley & Sons Ltd, 2006).

[8] S. W. Tsai and N. J. Pagano, *Invariant properties of composite materials*, Report (AIR FORCE MATERIALS LAB WRIGHT-PATTERSON AFB OHIO, 1968).

[9] S. W. Tsai and H. T. Hahn, *Introduction to composite materials* (Technomic Pub, 1980).

[10] J. M. J. F. Van Campen, *Optimum lay-up design of variable stiffness composite structures*, Thesis (2011).

[11] D. B. Adams, L. T. Watson, Z. Gürdal, and C. M. Anderson-Cook, *Genetic algorithm optimization and blending of composite laminates by locally reducing laminate thickness,* Advances in Engineering Software **35**, 35 (2004).

[12] F. X. Irisarri, A. Lasseigne, F. H. Leroy, and R. Le Riche, *Optimal design of laminated composite structures with ply drops using stacking sequence tables,* Composite Structures **107**, 559 (2014).

[13] J. Bailie, R. Ley, and A. Pasricha, *A summary and review of composite laminate design guidelines,* Langley RC, Hampton (1997).

[14] S. Setoodeh, Z. Gürdal, and L. T. Watson, *Design of variable-stiffness composite layers using cellular automata,* Computer Methods in Applied Mechanics and Engineering **195**, 836 (2006).

[15] G. Soremekun, Z. Gürdal, C. Kassapoglou, and D. Toni, *Stacking sequence blending of multiple composite laminates using genetic algorithms,* Composite Structures **56**, 53 (2002).

[16] D. Tech, *DT120 Versatile High Toughness Epoxy Matrix*, Technical data sheet 10 (2015).

[17] D. M. J. Peeters, F. X. Irisarri, C. Groenendijk, and R. Ruzek, *Optimal design, manufacturing and testing of non-conventional laminates,* Composite Structures **210**, 29 (2019).

[18] A. International, *Astm d6641/d6641m-16e1 standard test method for compressive properties of polymer matrix composite materials using a combined loading compression (clc) test fixture,* (2016).

[19] A. International, *Astm d3518/d3518m-18 standard test method for in-plane shear response of polymer matrix composite materials by tensile test of a ±45° laminate,* (2018).

[20] A. Documentation and U. Manual, *Version 6.10,* Dassault systemes (2010).

[21] R. Rodi, *The Residual Strength Failure Sequence in Fibre Metal Laminates*, Thesis (2012).

[22] C. solutions, *Vic-3d software manual,* (2019).

[23] A. International, *Astm d5687/d5687m-95 standard guide for preparation of flat composite panels with processing guidelines for specimen preparation,* (2015).

[24] C. C. Chamis, *Mechanics of composite materials: Past, present, and future,* Journal of Composites Technology and Research **11**, 3 (1989).

[25] D. A. Saravanos and C. C. Chamis, *Mechanics of damping for fiber composite laminates including hygrothermal effects,* AIAA Journal **28**, 1813 (1990).

[26] J. Singer, J. Arbocz, and T. Weller, *Buckling experiments : experimental methods in buckling of thin-walled structures. Vol. 1, Basic concepts* (Wiley, Chichester, 1998).

[27] W. Hufenbach, M. Gude, and L. Kroll, *Design of multistable composites for application in adaptive structures,* Composites Science and Technology **62**, 2201 (2002).

[28] S. Gantenbein, K. Masania, W. Woigk, J. P. W. Sesseg, T. A. Tervoort, and A. R. Studart, *Three-dimensional printing of hierarchical liquid-crystal-polymer structures,* Nature **561**, 226 (2018).

[29] Huntsman, *RenCast CW 2418-1 / Ren HY 5160-61-62*, Technical data sheet (2014).

[30] O. Seresta, M. Abdalla, and Z. Gurdal, *A genetic algorithm based blending scheme for design of multiple composite laminates,* in *50th AIAA/ASME/ASCE/AHS/ASC Structures, Structural Dynamics, and Materials Conference* (American Institute of Aeronautics and Astronautics, 2009).

[31] S. T. IJsselmuiden, M. M. Abdalla, O. Seresta, and Z. Gürdal, *Multi-step blended stacking sequence design of panel assemblies with buckling constraints,* Composites Part B: Engineering **40**, 329 (2009).

[32] F.-X. Irisarri and R. Le Riche, *Multiscale composite optimization with design guidelines,* in *Journée d'étude : Optimisation des composites* (2014).

III

Appendix

A

Test fixture

A test fixture was designed and manufactured to validate the predicated buckling behavior of the designed laminates. The fixture had to fit in the MTS 3500kN fatigue bench at the DASML (Delft Aerospace Structures and Materials Laboratory). The designed fixture can be seen in Figure A.1. The fixture was made of out of steel because it is significantly stiffer than the material used in the test specimens. The fixture also featured two flat support plates which were designed to be attached to the testing bench and at the same time offer mounting points for the knife edges. The knife edges which can be seen in Figure A.1c, and as their name suggests, they are two sharp edges per set that simulate the simply supported boundary conditions on the vertical edges of the laminate during the test.

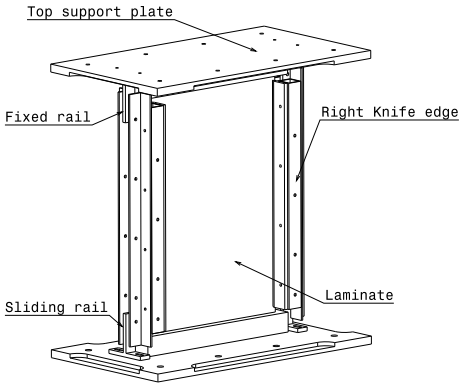

(a) An isometric view of the test fixture.

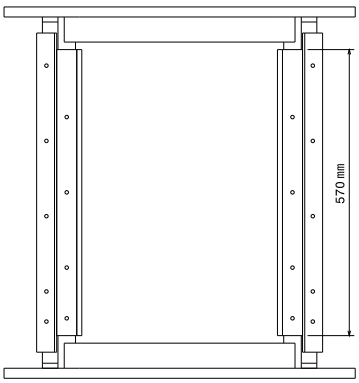

(b) A front view of the test fixture.

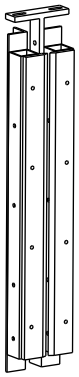

(c) An isometric view of the left set of knife edges.

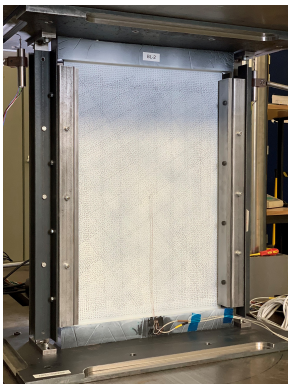

(d) The test fixture during testing.

Figure A.1: The test fixture designed and used during the experimental campaign.

B

Resin block and mold

To create a clamped boundary conditions on both sides where the load is introduced to the laminates, they had to be potted in resin blocks. To be able to do that a mold had to be designed and manufactured. A schematic representation of the mold can be seen in Figure B.1. The mold was manufactured out of MDF (Medium-density fibreboard) wood due to its availability at the time. After manufacturing the mold, its components were wrapped with Teflon foil before assembling them. This step is important and necessary for demolding. The mold also features two free edges along the longitudinal wall for gripping during demolding. In addition to that, the mold is equipped with guiders that help center the laminate in the center with respect to the edges but also hold the laminate in a straight-up position during the curing hours of the resin. A total of 5 molds were manufactured since only one edge of the laminates could be potted at the same time as can be seen in Figure 7.11.

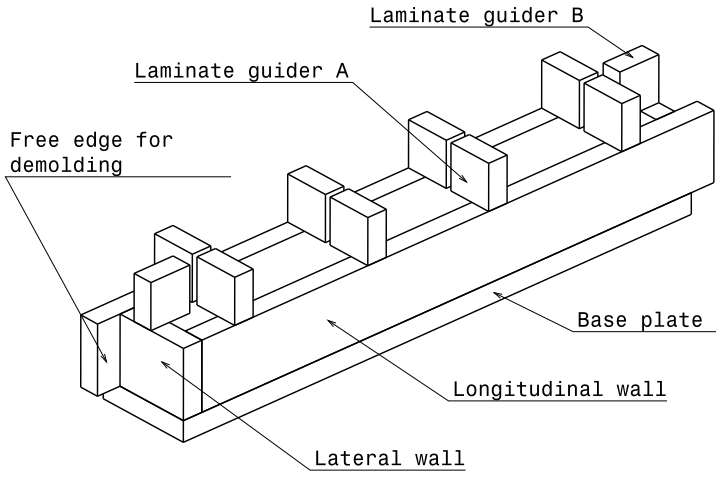

Figure B.1: An isometric view of the resin mold designed.

As for the blocks themselves, the RenCast CW2418-1 metal-filled epoxy resin was used in combination with the hardner Ren HY5160 by Huntsman [29]. The mixture cured at room temperature and had a maximum casting thickness of 80mm which sufficient for the 50mm thick blocks needed. The final mechanical properties of the resin can be found in Table B.1.

Compressive modulus [GPa]	4.5 - 5.5
Compressive strength [MPa]	80 - 90
Poisson's ratio [-]	0.3

Table B.1: The mechanical properties of the resin block material.

C

Extra Simulation results

The maximum in-plane lateral displacement of the simply supported edges of each laminate was plotted against the edge-shortening to make sure that they were not going to slip from the testing fixture. In addition to that, the out-of-plane displacement was plotted against the edge-shortening. These plots can be seen in Figure C.1 and Figure C.2 for the conventional and the blended laminate respectively.

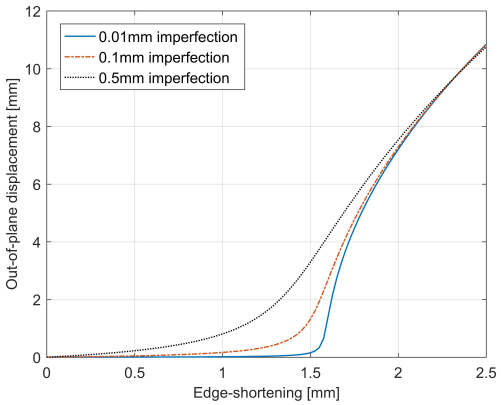

(a) Out-of-plane displacement versus end-shortening.

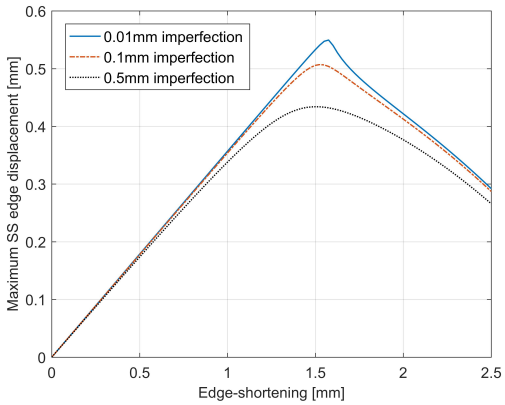

(b) Side-displacement versus end-shortening.

Figure C.1: Extra results of the FE simulations for the conventional laminate.

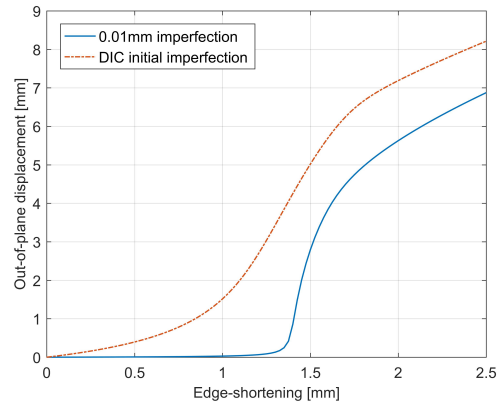

(a) Out-of-plane displacement versus end-shortening.

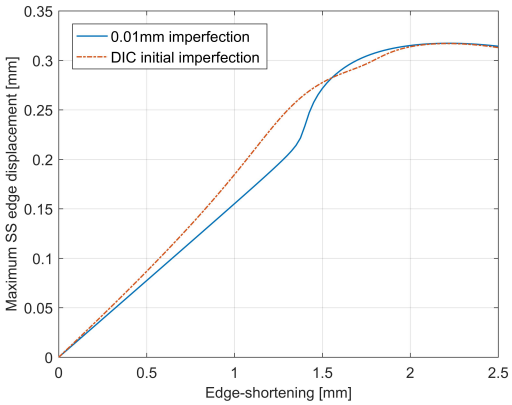

(b) Side-displacement versus end-shortening.

Figure C.2: Extra results of the FE simulations for the blended laminate.

D

Experimental buckling load determination

The experimental critical buckling load of the tested laminates was computed using 5 different methods. The graphs of the load versus average compressive strain, load versus edge-shortening, strain reversal, load versus defelction and load versus defelction squared methods can be seen in Figure D.1, Figure D.2, Figure D.3, Figure D.4 and Figure D.5 respectively.

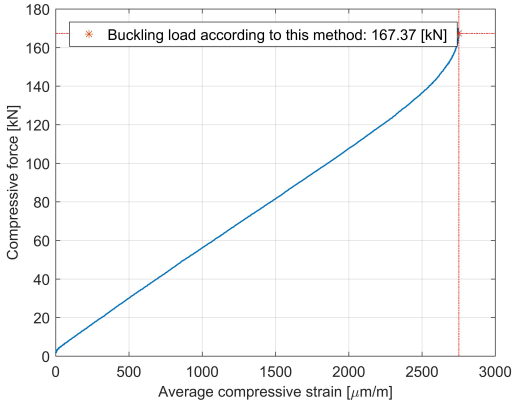

(a) BL-01.

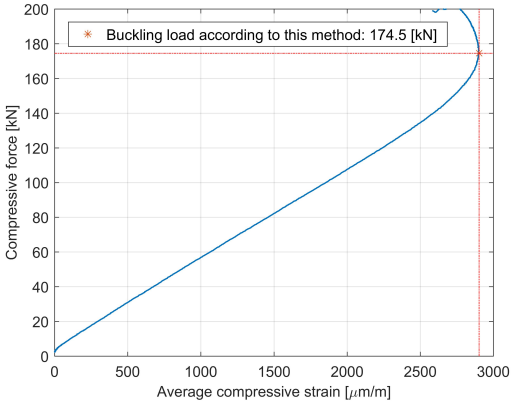

(b) BL-02.

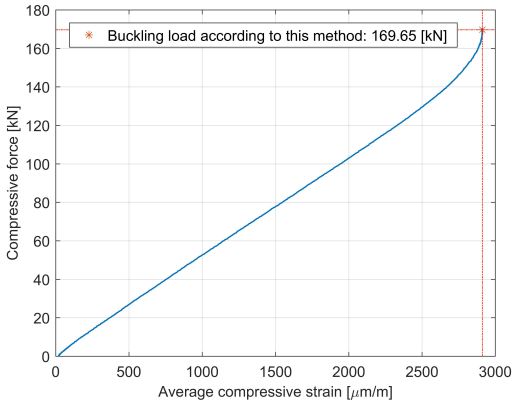

(c) BL-03.

Figure D.1: Load versus average compressive strain method plots.

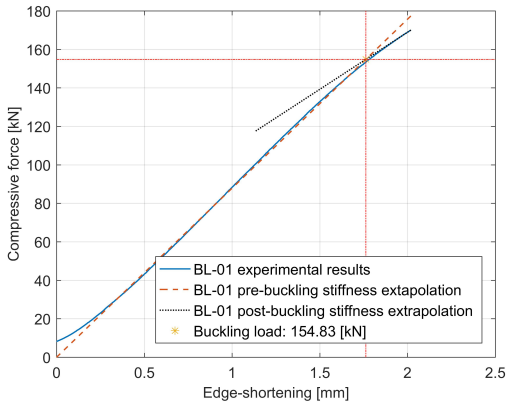

(a) BL-01.

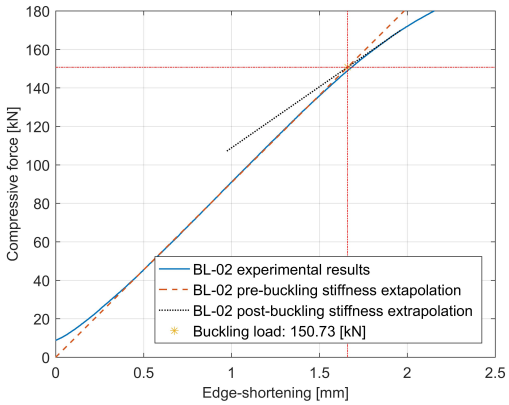

(b) BL-02.

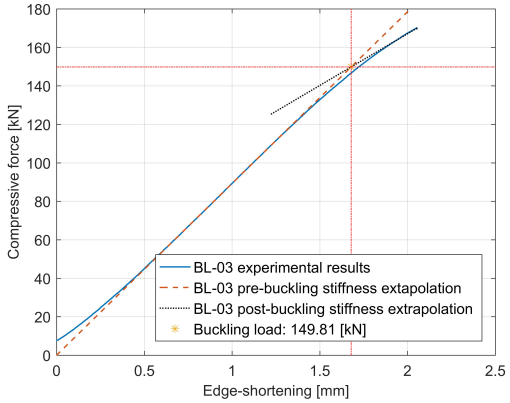

(c) BL-03.

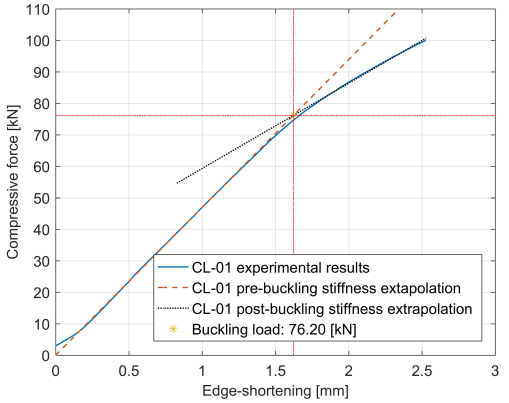

(d) CL-01.

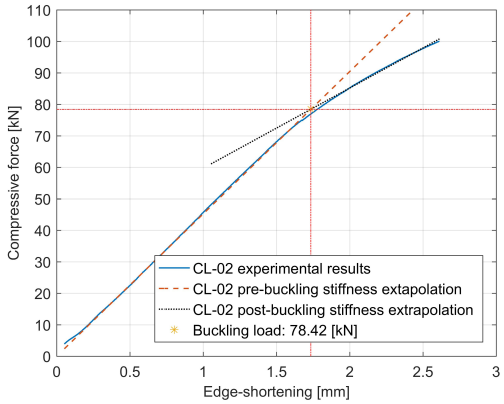

(e) CL-02.

Figure D.2: Load versus edge-shortening method plots.

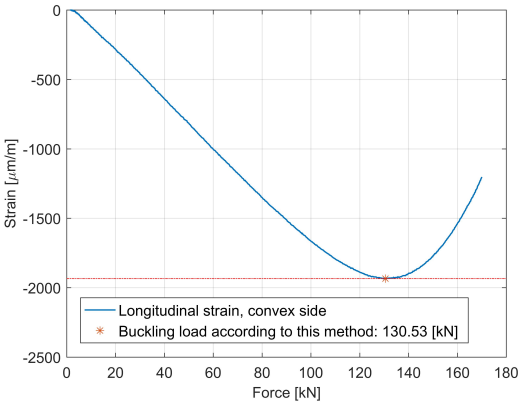

(a) BL-01.

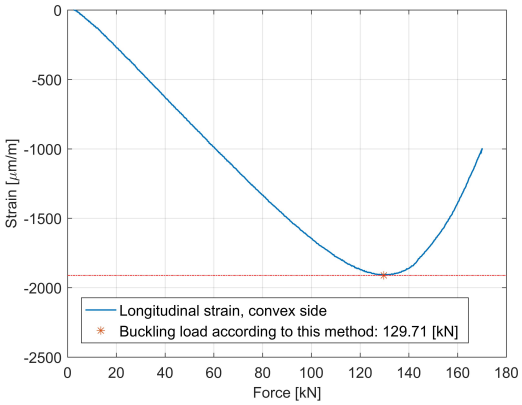

(b) BL-02.

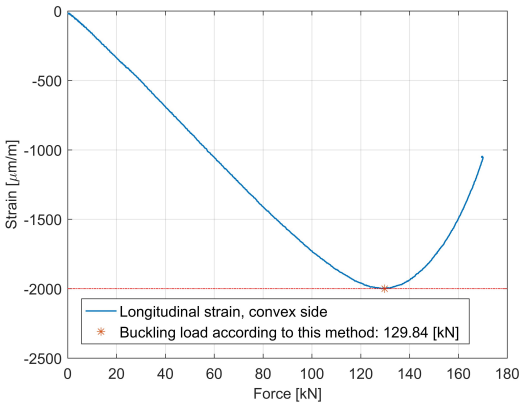

(c) BL-03.

Figure D.3: Strain reversal method plots.

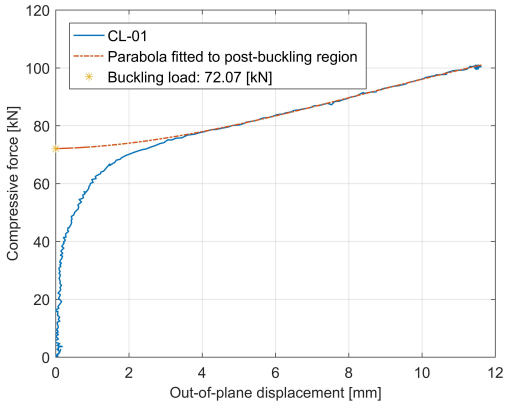

(a) CL-01.

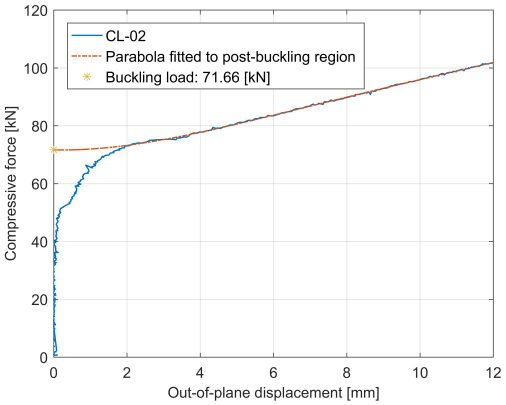

(b) CL-02.

Figure D.4: Load versus defelction method plots.

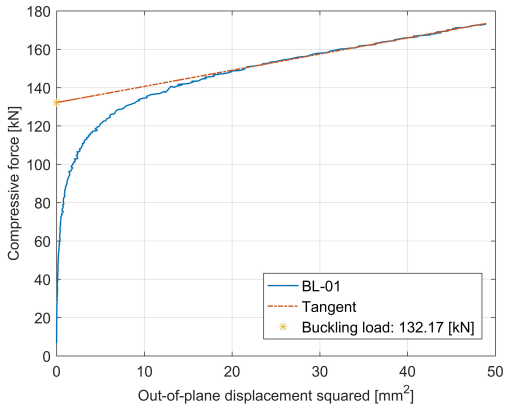

(a) BL-01.

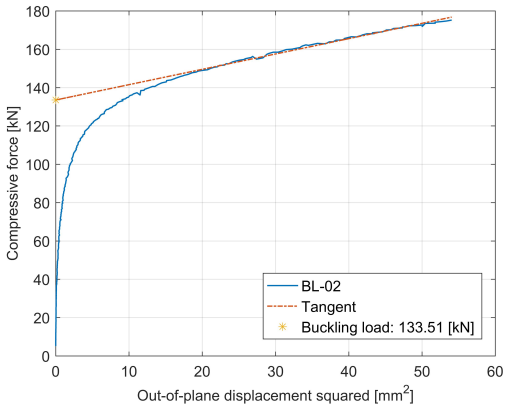

(b) BL-02.

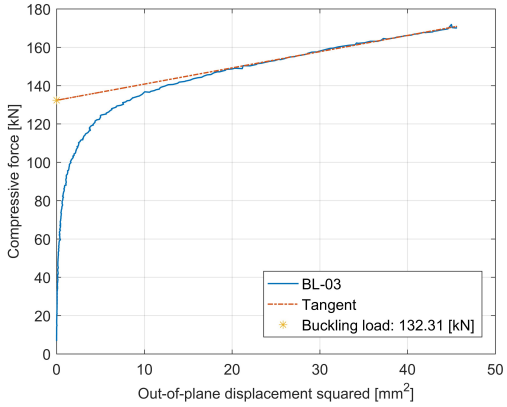

(c) BL-03.

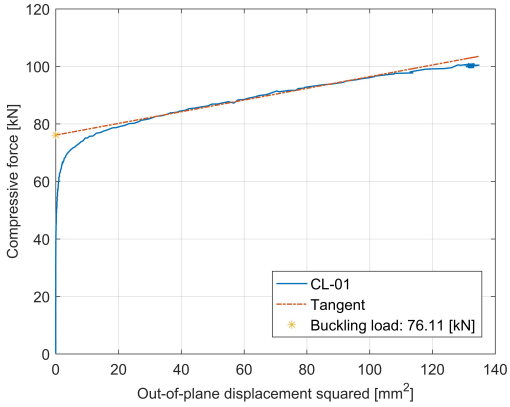

(d) CL-01.

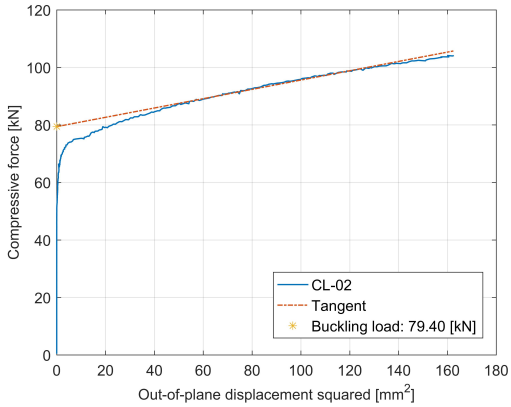

(e) CL-02.

Figure D.5: Load versus defelction squared method plots.

E

Horseshoe benchmark case

Soremekun *et al.* [15] introduced an 18-panel horseshoe configuration that resembles a section of a helicopter floor panel, and since then, it has been used in the literature by many researchers [2, 11, 15, 30–32] to illustrate the effectiveness of their blending methods. In this appendix chapter, the problem definition of the horseshoe benchmark is described. The horseshoe configuration, its dimensions and in-plane loads per section are shown in Figure E.1.

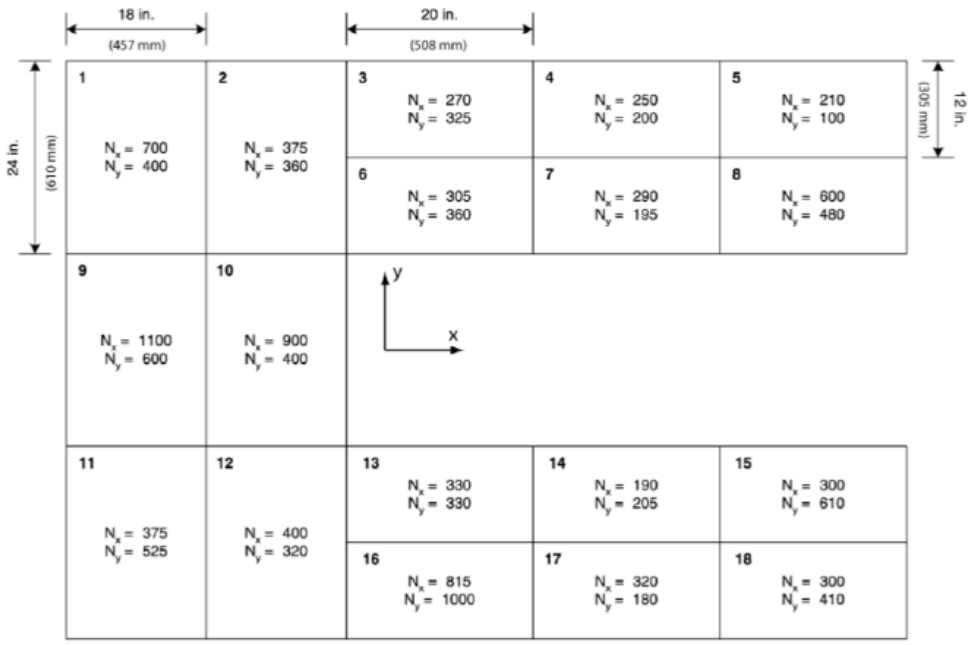

Figure E.1: The horseshoe benchmark according to Soremekun *et al.* [15].

E.1. Objective and constraints

All the sections in the horseshoe configuration are under bi-axial compression loading, and each section is assumed to be simply supported along all its edges. The objective of the optimization is to minimize the weight W of each section without violating its mechanical constraint, which is the critical buckling load. The critical buckling load of a composite laminate that is simply supported at all edges and is under bi-axial loading can be calculated using Equation E.1 [4]. It is important to note that this benchmark completely ignores the load redistribution caused by updating the layup of individual sections during the optimization process [15].

$$N_o = \frac{\pi^2 \left[D_{11} m^4 + (D_{12} + 2D_{66}) m^2 n^2 (AR)^2 + D_{22} n^4 (AR)^4 \right]}{a^2 \left[m^2 + k n^2 (AR)^2 \right]} \tag{E.1}$$

Where m and n are the numbers of half waves in the x and y directions respectively, AR is the aspect ratio of the laminate, and k is the loading ratio, which is given by N_y/N_x. A schematic representation of a composite plate under bi-axial loading is shown in Figure E.2.

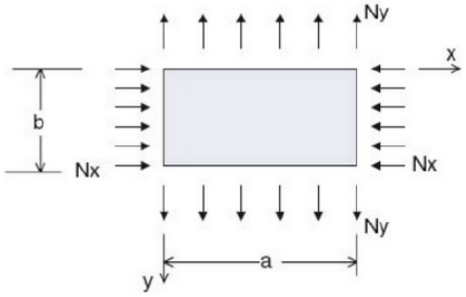

Figure E.2: Composite plate under bi-axial loading as depicted by Kassapoglou [4].

The buckling constraint is formulated such that a possible design has a positive margin. This formulation is shown in Equation E.2.

$$g_{min} = \frac{N_0}{N_x} - 1 \tag{E.2}$$

The objective function of the laminate stacking sequence optimization is thus:

$$\begin{aligned} &\text{Minimize } W \\ &\text{while } g_{min} \geq 1 \end{aligned}$$

The objective function was enforced using an augmented fitness function that rewards and penalizes laminate designs according to how well they satisfy the objective of the optimization. A laminate is awarded a score θ which is computed using Equation E.3.

$$\theta = \begin{cases} W + \beta g_{min}, & \text{if } g_{min} < 0 \\ W + \varepsilon g_{min}, & \text{if } g_{min} > 0 \end{cases} \tag{E.3}$$

Where W is the normalized weight of the laminate, ε is a bonus parameter, and β is a penalty parameter. The fitness function is designed to award feasible designs that satisfy the buckling constrain a higher fitness value and penalize ones that fail to do so.